UNIVERSITY OF KWAZULU-NATAL

A STUDY OF THE ELECTRICAL ENVIRONMENT BELOW HVDC TRANSMISSION LINES

BY

DHEVANDHRAN GOVENDER,
BSc (HONS) - APPLIED SCIENCE
BTECH (ELECTRICAL ENGINEERING)

A DISSERTATION SUBMITTED IN PARTIAL FULFILMENT OF THE REQUIREMENTS FOR THE DEGREE OF MASTER OF SCIENCE IN ELECTRICAL ENGINEERING AT THE UNIVERSITY OF KWAZULU-NATAL

SUPERVISORS:

PROFESSOR N.M. IJUMBA, PHD, PRENG, CENG
ADJUNCT PROFESSOR A.C. BRITTEN, MSC, PRENG

JULY 2008

ACKNOWLEDGEMENTS

ABSTRACT

The main aim of this project was to determine the extent to which the study of electric fields and ions in a laboratory can be used to study the electrical environment below High Voltage Direct Current (HVDC) transmission lines. The focus of the study was to set up small scale laboratory experiments and to compare these results to actual line measurements and to software simulations. The laboratory tests were undertaken at the HVDC Centre at the University of KwaZulu-Natal (Westville Campus). The software simulations that were conducted as part of this study were done using EPRI TL 3.0 and Microsoft Excel.

Initially tests conducted were the measurement of the induced voltage and corona leakage current on a floating object. The next set of laboratory tests conducted was the measurement of ion current density and the electric field at ground level. The ion current density was measured with a Wilson Plate ($1m^2$) and the electric field at ground level was measured using a JCI static monitor field meter (JCI 140) and a Monroe (257D) Portable Electrostatic Fieldmeter, with an elevated earth plane.

Measurements of ion current density and electric field at ground level were also taken under an operating HVDC transmission line (Cahora Bassa to Apollo), in order to compare the laboratory measurements and simulations with real line measurements.

The results have shown that the electrical parameters (i.e. ion current, induced voltages, corona currents, electric field, ion density, space charge) are higher under the negative pole as compared to the positive pole. The results of the laboratory measurements show that the ion currents under the negative polarity are almost double the ion currents that were measured under positive polarity, while the electric field under negative polarity was 20 percent higher than under positive polarity. Measurements of the electric field show that the total electric field below the line is greatly enhanced when corona generated space charge is present. The results of the EPRI TL Workstation simulations show good correlation with the EXCEL® simulations. However, there was poor correlation between EPRI simulations and test line measurements in the laboratory. The EPRI simulations show good correlation to the measured electric field values below the Cahora Bassa line. The comparison between the actual measurements on the test line and the Cahora Bassa line showed poor correlation and this was attributed to factors such as scaling, laboratory size constraints, ion concentration in laboratory, line loading and wind speeds.

TABLE OF CONTENTS

LIST OF FIGURES

LIST OF TABLES

LIST OF ABBREVIATIONS

ABBREVIATION	DESCRIPTION
ACSR	Aluminium Conductor Steel Reinforced
AFIS	Advanced Fire Information System
AN	Audible Noise
BPA	Bonneville Power Administration
CRIEPI	Central Research Institute of the Electric Power Industry (Japan)
CSM	Charge Simulation Method
DC	Direct Current
DOE	Department of Energy
EPRI	Electric Power Research Institute
FEM	Finite Element Modelling
GMR	Geometric Mean Radius
HVDC	High Voltage Direct Current
HVTRC	High Voltage Transmission Research Centre
JCI	John Chubb Instruments
kV	Kilo Volt
LPATS	Lightning Positioning Tracking System
PVC	Poly Vinyl Chloride
RAD	Relative Air Density
RFI	Radio Frequency Interference
RH	Relative Humidity
RI	Radio Interference

UHV	Ultra High Voltage
UKZN	University of Kwa-Zulu Natal
WESTCOR	Western Corridor

CHAPTER 1

INTRODUCTION

1.1 BACKGROUND:

HVDC technology is becoming more widely used for bulk power transmission over long distances since it has been proven to be more economical and efficient over such distances. Africa has an abundance of hydro resources and these green power resources are located in the central regions of the continent. In order for the southern African countries to tap into these resources, long HVDC transmission lines need to be built between the power resources and the distant load centres.

On Eskom's only HVDC transmission line (The Cahora Bassa line); there is some evidence that some of the faults fall into an unknown category [1]. It is suspected that the electrical environment in the vicinity of the HVDC lines could be playing a part in the occurrence of these unknown faults. It is therefore essential to have a clear understanding of the electrical environment in the vicinity of HVDC lines.

The main aim of this project is to determine to what extent the study of electric fields and ions in a laboratory can be used to determine the parameters that make up the electrical environment below operating HVDC lines. It is hypothesized that the electric field environment under HVDC lines can be studied in laboratory conditions, by considering ionic currents and electric field measurements and that it is possible to correlate laboratory and actual line measurements. The laboratory measurements obtained will be compared to actual line measurements and to software simulations to verify if some correlation exists. The results will be used as a guide to anticipate the behaviour of the electrical environment for future design of HVDC transmission lines.

On completion of this research project, the following questions are expected to be answered:

- What measurement techniques can be used to quantify the electrical environment below HVDC transmission lines?
- Is there any correlation between the laboratory measurements and the actual transmission line measurements?
- Is there any correlation between the EPRI TL Workstation simulations and the actual measurements?
- What is the impact for the design of future HVDC lines?
- How can the electrical environment effects be reduced?

Once this research study has been completed, it is expected that a better understanding of the electrical environment below HVDC lines, will be gained. The research study will also add to Eskom's HVDC knowledge base and this will prove essential in the design of future HVDC schemes.

1.2 RESEARCH METHODOLGY:

- **A literature review** was carried out in order to understand the work and findings that was previously conducted in the area of electric fields and ionic currents. Literature on space charge effects, ionic coupling effects and field measurements (ion density, electric field, induced voltage) was reviewed.

- **Initial laboratory tests** were conducted to try and replicate some of the tests that were previously conducted. This gave us an understanding of the difference in coupling effects between the negative and positive polarities.

- **Design and procurement of testing equipment.** Current probes for measuring ion current density were designed and manufactured. An elevated earth plane and a screening mesh was also designed and manufactured. Electric field meters to measure the voltage (JCI field meter) and electric field (Monroe) at ground level were purchased. A Pico Scope Oscilloscope was also purchased to help with viewing and data analysis.

- **Laboratory tests** were conducted at the University of Kwa-Zulu Natal HVDC Centre.

- **Field measurements** were conducted under the Cahora Bassa HVDC Transmission line just outside Zwavelspoort in Gauteng Province, South Africa.

- **Simulations using the EPRI TL Workstation** software were carried out to verify the electric fields at ground level, on the laboratory test line. Simulations were also carried out for the Cahora Bassa transmission line and this was used to compare the calculated and measured values.

- **Analysis of results.** The results of the laboratory tests were analysed and compared to previous tests, actual line measurements and to software simulations.

Some of the important topics that were covered in the literature review were:

- Electrical parameters around HVDC lines

- The effect of space charge

- Small and large ion characteristics

- Space charge measurements on a 500 kV HVDC test line

- Measurement of ion current density, induced voltage and electric field at ground level under an HVDC line

- Corona, field effects and telecommunications requirements as factors in the design of long UHVDC lines

- An investigation into "unknown" line faults on a + 533 kV DC line in South Africa

CHAPTER 2

LITERATURE REVIEW

2.1 ELECTRICAL PARAMETERS NEAR HVDC TRANSIMSSION LINES:

The electrical environment near HVDC transmission lines is characterised by several different electrical parameters. These parameters are the electric-field strength (E), the ion current density (J), the ion current (I), and the monopolar space charge density (p). HVDC transmission lines are commonly bipolar configurations by design, with each pole (negative and positive) having a bundled conductor. Large amounts of ions are produced by these conductor bundles when they are coronating and the presence of the ions enhances the electric field strength at ground level. When convection forces are absent, these ions travel along the field lines to the conductor of opposite polarity, to the ground wires and towards the ground plane. A number of resultant ions (large ions) are formed by reactions of the primary ions (small ions) that are initially produced directly by corona. This can be seen in figure 2.1. [2]

$$i = pKE * pv_a \qquad E - E \text{ conductors} * E \text{ ton}$$
$$\text{dotal)} \quad i\text{conductive)} \quad I \text{ corrective)} \quad \text{(total)} \quad \text{(nominal)} \quad \text{(•nhancament)}$$
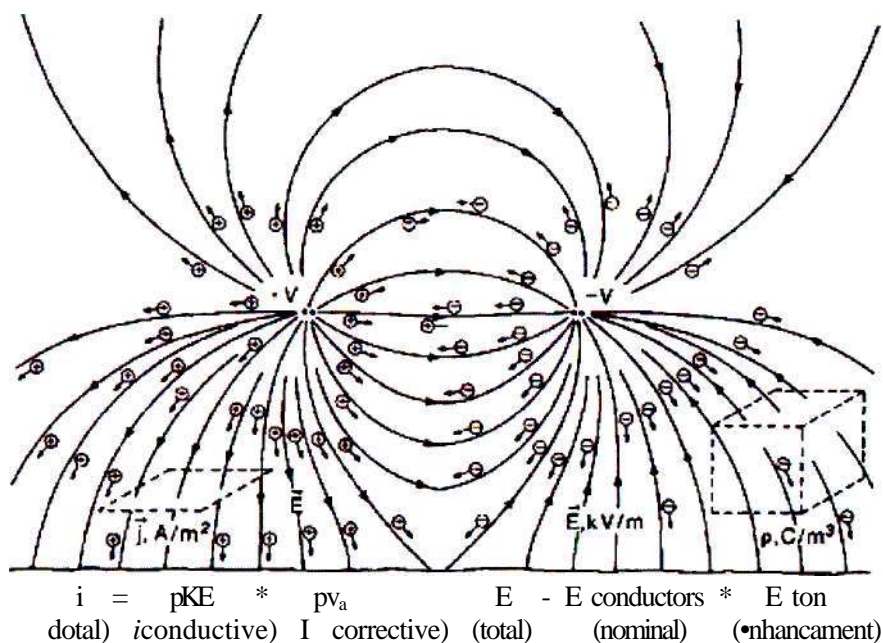
Figure 2.1: Electric Field Lines - Bipolar HVDC Transmission Line [2]

The monopolar ion current density in the presence of wind is given by [3]:

$$J = pKE + pu_a \qquad (2.\text{i})$$

where

K = average ion mobility, v_a = wind velocity

The charge density p (C / m) is given by [3]:

$$KE \qquad\qquad (2.2)$$

where

J = ion current density (A / m^2); E = electric field strength (V/m)

At ground level below the HVDC line, the ion density is given by [3]:

$$n = \frac{J}{e/jE} \qquad\qquad (2.3)$$

where

n = ion density (ions/cm^3); e = charge of an ion;
J = ion current density (A/m^2)
E = electric field strength (V/m)
$\setminus i$ = average ion mobility (m^2 / v.s)

EPRI states that the best average ion mobility, for a humidity of 70 % and ion travel time in the order of a few seconds is 1.15 x 10 $^{-4}$ m^2 / v.s for the positive polarity and 1.5 x 10 $^{-4}$ m^2 / v.s for the negative polarity [3].

2.2 THE EFFECT OF SPACE CHARGE:

Electric fields are known to be vector quantities with both magnitude and direction whereas the space charge density is a scalar quantity having only magnitude. Space charge consists of two types or two classes of charge carriers i.e.

- Small air ions and
- Large air ions or charged aerosols

The two types of ions are classified according to their mobility and their diameters. It is also known that both types of ions are present under HVDC transmission lines during corona activity. The Japanese Electrostatic Handbook defines the air ions according to their size [4].

Table 2.1: Air Ion Classification [4]

Type of Ion	Diameter
Small	About 0.001 Mm
Medium	About 0.001 - 0.01 Mm
Large	About 0.01~10 Mm

The space charge phenomenon has been described in qualitative terms by many different authors. This phenomenon can be easily visualised given the detailed descriptions of the behavioural patterns. The small air ions at conductor height, which are generated by corona, are subjected to a force that is caused by the constant polarity electric fields under HVDC conditions. These ions move away from the line and the electric field due to the line decreases as a result. Work conducted has shown that it is the large ions that move further away due to convective forces such as wind and that the large air ion densities are greater downwind from the line [4]. This work has also concluded that the small ion densities for both the positive and negative polarity are the highest directly below the conductor [4].

If the surface gradient of the conductor increases the corona activity will also increase which in turn will result in higher space charge activity. This increased corona activity causes more small ions to be directly produced. This fills the region between the conductor and ground, causing an increase in both the electric field and small ion density. When the applied voltage exceeds the corona onset voltage, unipolar DC corona in air manifests itself in the region beyond the ionisation layer as a steady unidirectional flow of charged particles emanating away from the conductor that is in corona. The flow of the charged ions is steady and is determined by the magnitude and direction of the electric field intensity vector E. The conventional methods of describing the ionised fields under DC make use of the following assumptions for simplification [5]:

• Ionic mobilities are constant (independent of electric field magnitude)
• Positive and negative ion mobilities are equal
• The diffusion of ions is neglected
• The effect of wind, humidity and aerosols is neglected

2.2.1 Bipolar and Monopolar Space Charge Effects:

There is a difference between the corona generated and corona loss performance of bipolar and monopolar DC transmission lines. On bipolar lines both the positive and the negative polarity conductors will simultaneously experience corona activity. Because of this, three space charge regions exist for the bipolar configuration viz [6].

• The positive unipolar region between the positive conductor and ground
• The negative unipolar region between the negative conductor and ground
• The bipolar region between the two conductors (positive and negative poles)

In the bipolar region, both negative and positive polarities mix and this leads to a reduction of the net space charge and also to recombination and neutralisation of ions. This mixing of ions will cause the effective space charge to be reduced and this results in a lower screening effect.

In the unipolar region, the space charge within the inter-electrodes produces a screening effect. By lowering the electric field in the vicinity of the conductor, the intensity of ionisation gets reduced and this will stabilise the discharge activity and also limit the corona current [6]. The different space charge regions are shown in figure 2.2.
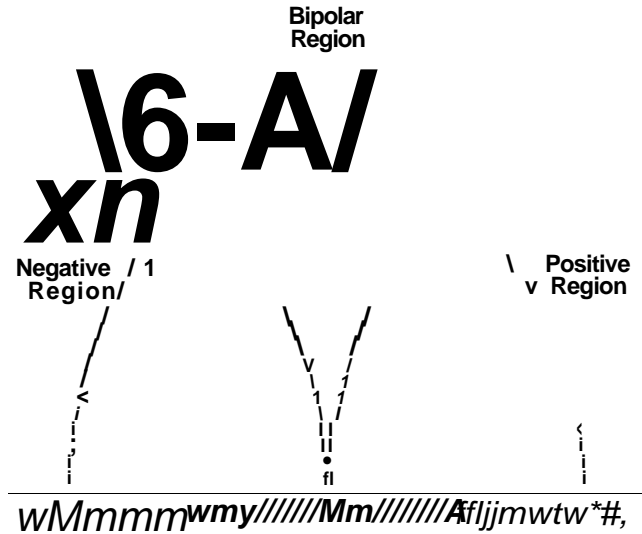
Figure 2.2: Flux Lines in a Bipolar Configuration [6]

2.3 SMALL ION MOBILITY CHARACTERISTICS:

Experimental work was carried out by the Central Research Institute of the Electric Power Industry (CRIEPI) on small ion mobility characteristics under the Shiobara HVDC test line [7]. Ion density is recognised as an important electrical environmental factor under HVDC transmission lines. For the experimental work, an aspirator type ion counter was developed to measure the ion density and ion mobility simultaneously under the Shiobara HVDC test line. The results of the experiments are described below [7].

2.3.1 Seasonal Variations:

The results of typical ion mobility spectra over a period of four months are presented. In general, it was found that most of the small ion mobilities under the HVDC test line are in a range of 0.37 - 3.7 cm^2 /V.sec for both the positive and negative ions. The seasonal variations are small.

It was found that the mean positive ion mobilities for each season were in the range of 1.2 - 1.4 cm^2 / V.sec and the mean positive ion mobility of all seasons is 1.34 cm^{2}N.sec. The best value for the average ion mobility for positive was 1.15 cm / V.sec which was estimated by EPRI. It was also found that the mean negative ion mobilities for each season was in the range of 1.4 - 1.7 cm^2 / V.sec and the mean negative ion mobility for all seasons is 1.56 cm / V.sec compared to the 1.5 cm^2 / V.sec best value for average ion mobility estimated by EPRI [3].

2.3.2 Effect of Absolute Humidity:

Work previously carried out has suggested that absolute humidity has some influence on ion mobility, however, the results presented here do not show any correlation between the two quantities for either the negative or the positive pole [7].

2.4 LARGE ION DENSITY CHARACTERISTICS UNDER THE SHIOBARA HVDC TEST LINE:

Experiments concerning the voltage characteristics and lateral profiles of large ions under the Shiobara HVDC test line were carried out by the Central Research Institute of the Electric Power Industry (CRIEPI) [8]. Air ions are classified according to their diameters as small, medium and large ions according to the Japanese Electrostatic Handbook. The large ions are formed when small ions collide with neutral aerosols.

Table 2.2 shows the density of small and large ions in clean air and polluted air [8].

Table 2.2: Ion Density in Clean and Polluted Air [8]

Kind of ion density	Clean	Highly polluted
Large ion density (ions/cm^3)	5000 ~ 6000	10^* ~ 10^s
Small ion density (ions/cm^3)	500-600	about 100

The lateral profiles for the monopolar, bipolar and the double circuit were measured. Each pole has a two conductor bundle with a subconductor diameter of 38.4 mm. The horizontal pole spacing was 22m with a minimum line height of 22m. The vertical pole spacing for the double circuit was 20m.

Figure 2.3 shows the results for the positive monopole case. The results show that the positive small ion density increases more rapidly than the corresponding large ions when the voltage is increased.
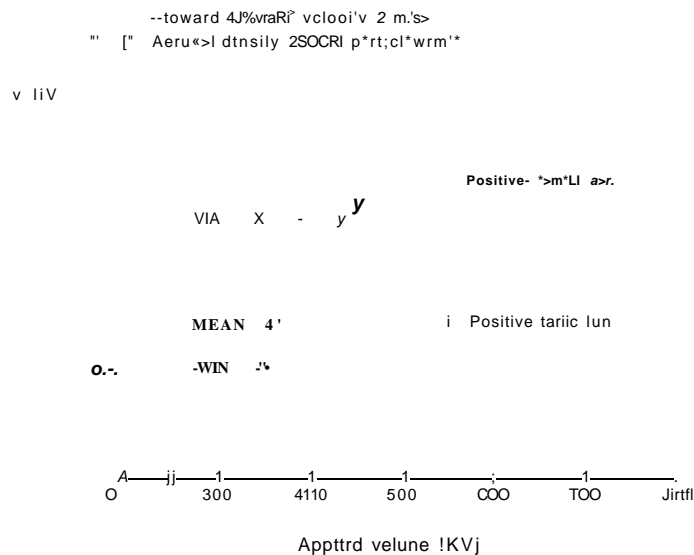
Figure 2.3: Applied Voltage versus Ion Density (Positive Monopole) [8]

Figure 2.4 and 2.5 show the effect of increasing voltage on the negative ion density for the negative monopole and horizontal bipole cases respectively.
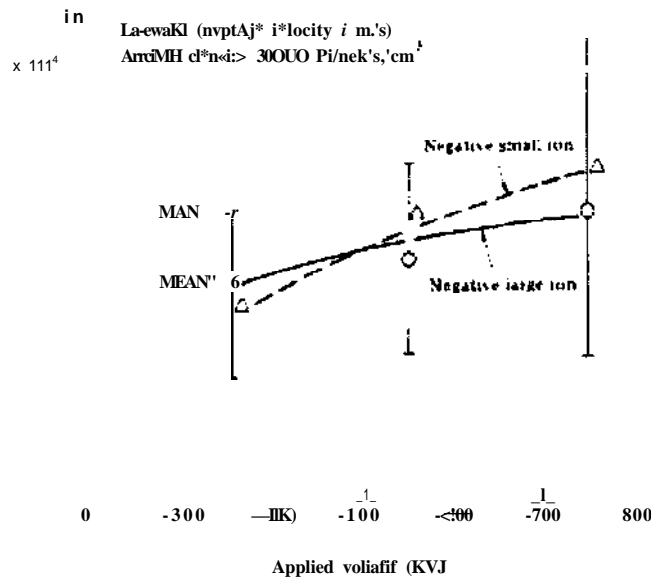
Figure 2.4: Applied Voltage versus Ion Density (Negative Monopole) [8]
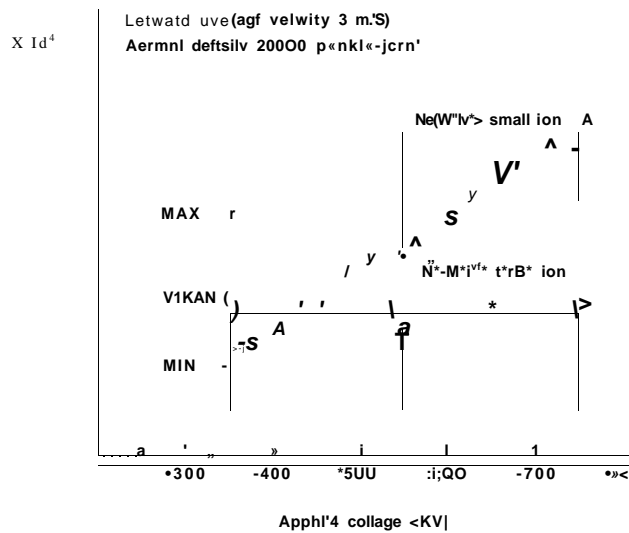
Figure 2.5: Applied Voltage versus Ion Density (Horizontal Bipole) [8]

Figure 2.6 shows the lateral profile in the vicinity of the line for the horizontal bipolar case. It can be clearly seen that the small ion density under the negative pole is a lot higher than the large ion density; the same applies for the positive pole. It can also be seen that the small ion density under the negative pole is higher than the small ion density under the positive pole.

x 10^4 Aerosol density 20000 particlcs/cm

South wind 2 m.s-
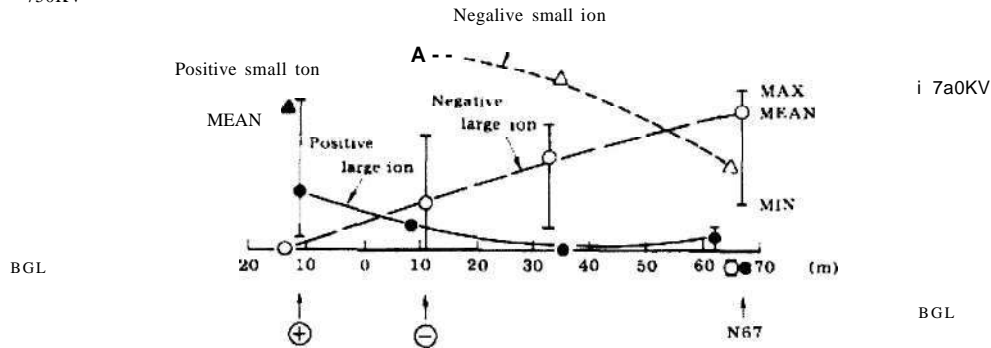
Figure 2.6: Lateral Profile under HVDC Test Line (Horizontal Bipole) [8]

The results of the experiments conducted conclude that the applied voltage has a less significant effect on large ion density, as compared to small ion density. The large ion density increases downwind and reaches a maximum value at 67m from the line centre. It then decreases gradually further away from the line. This means that convection forces blow away the large ions from under the transmission line leaving only the small ions present under the line [8].

2.5 CALCULATION OF LARGE ION DENSITIES UNDER HVDC TRANSMISSION LINES:

A method for calculation of large ion densities (charged aerosols) under HVDC transmission lines was developed by T. Suda and Y. Sunaga. The method considered both the charging mechanism of aerosols by small ions and the drifting process created by wind. Large ion densities calculated by this method agreed well with the ones measured under the Shiobara HVDC test line on the lateral profiles at ground level up to about 70m downwind from the line. Measured values decreased more rapidly than calculated ones further downwind from the line. Considering the effect of point discharge from ground cover (earth corona) improved the agreement in the further downwind region [9].

Ions suspended in air are classified into small ions and large ions, on the basis of their diameters. Large ions are also called charged aerosols. Small ions are generated directly by corona discharge of HVDC transmission lines, while large ions are produced by small ions adhering to aerosol particles [9].

Large ions are carried far from the line by wind because of their small electrical mobility and they enhance ion densities and electric fields downwind from the line. This indicates that anomalous flashovers could be caused or enhanced by small ions and not large ions.

Figures 2.7 and 2.8 show the small and large ion densities in the vicinity of a positive and negative monopolar HVDC transmission line respectively. The solid black dots represent the large ion density and the plain dots represent the density of the small ions.

Wind:>m/s   """"f 22 m
>* S y .* V

+ve large ion   +vesmalion

measurement
calculation

Distance from **the ine** centre (m)
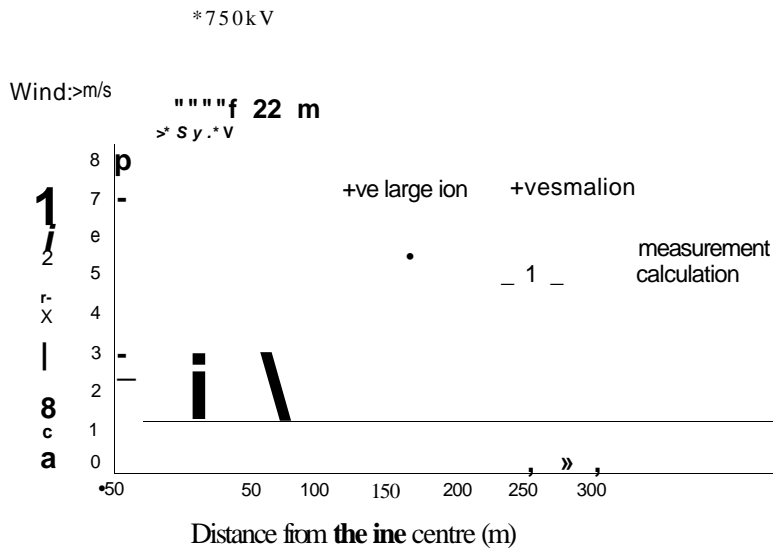
Figure 2.7: Lateral Profile of Ion Densities (Positive Monopolar) [9]

- 750 kV

,%« «".i^$_e$ Aerosol density 2x10 particles/crn'

f ?5 m

-ve large ion   -ve small ion

measurement   A   A
calculation Miithout earth corona————
calculation with earth corona ——————

ion densities (×10^4 ions/cm^3)

^   **Distance from trre** taie cecKer **(m)**
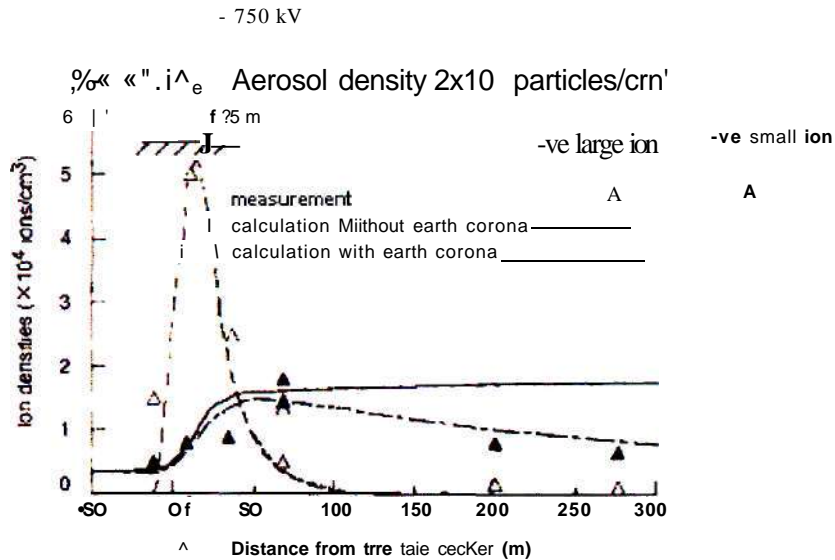
Figure 2.8: Lateral Profile of Ion Densities (Negative Monopolar) [9]

Both figure 2.7 and 2.8 show that the small ion densities for the positive and negative monopole are highest directly under the line, with the positive monopole having slightly higher densities than the negative monopole.

Figure 2.9 shows the large and small ion densities under a bipolar HVDC transmission line. It is clearly seen that the negative small ion density is slightly higher than the positive small ion density. The highest levels of ion density for both the negative and positive poles occur directly under each pole. This suggests that the negative pole experiences more interference due to space charge activity.

+-TSI.V Hoitoitel 6|»fcii

Wind 1m/s   JST Aerosol dens ity 2x 10^4 particles/cm^

T7~J~T7   large ion   smai ion
                                 +ve -ve   +ve -we
                    Measurement   •   O   +   -

. .^,   Calculation   —   ••••_____

x

•(\

fee

-SO   SO   100   ISC   SCO   250   30D   3S0

Distance from line centre (m)
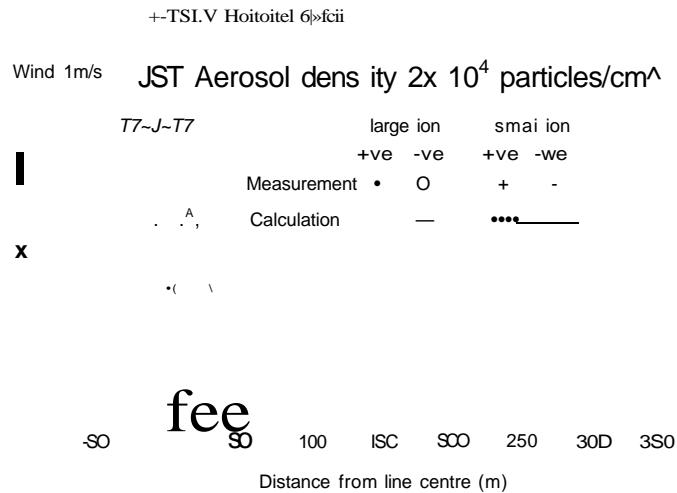
Figure 2.9: Lateral Profile of Ion Densities (Horizontal Bipolar) [9]

2.6 ACCURATE CALCULATION OF ION FLOW FIELD UNDER HVDC BIPOLAR TRANSMISSION LINES:

Ions produced by corona on overhead HVDC transmission lines drift through space under the action of the electric field and wind. Understanding the ion flow characteristics is essential for performance evaluation of existing and planned lines. Work that was conducted by Qin, Sheng, Yan and Gela presents a new, accurate, iterative numerical method for calculating the ion field flow quantities associated with HVDC bipolar lines [6]. The method can also be applied to monopolar lines by setting the appropriate quantities to zero in the equations. The recommended computational procedure pioneers the use of the Charge Simulation Method (CSM) for calculation of ion field flow and a weighted residual method for calculating the space charge densities. The method presented is a fast and accurate computational method and results compare well with experimental results.

2.6.1 Examples of Calculations:

Coaxial Cylindrical Geometry

The coaxial cylindrical geometry consists of an inner conductor 0.1 cm in radius which is energised to 25 kV with respect to a grounded outer cylinder of 1.794 cm radius. Making use of Peek's formula, the computed corona onset gradient E at the surface of the inner conductor is 58.85 kV/cm and the corona onset voltage V is 16.99 kV. The region of interest between the inner and outer electrodes is divided into 480 elements with 260 interior nodes. Figure 2.10 shows the relative errors in E when the traditional Finite Element Modelling (FEM) is used as compared to the vastly superior CSM [6].
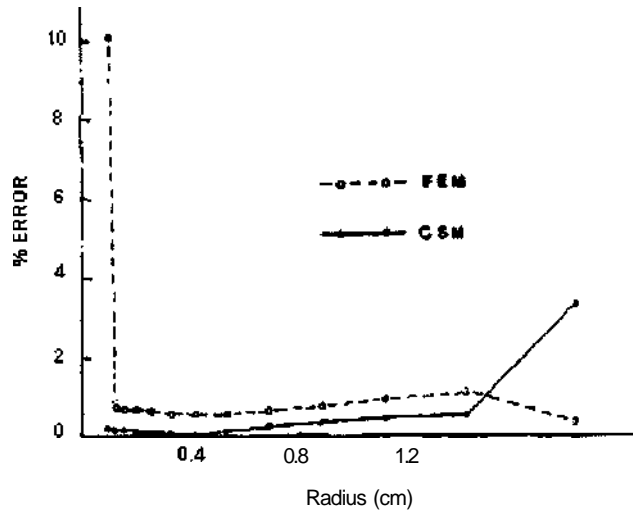
Figure 2.10: Relative Computational Errors of Different Methods [6]

Unipolar DC Line Model

The unipolar DC line model consists of a thin conductor 1.78 mm in diameter which is suspended 27.8 cm above the ground plane. With the applied voltage at +45 kV DC, the measured corona onset voltage is *Von* = 35 kV and the measured positive ion mobility is $k+ =$ 1.2 cm^2 / V.s. Separate experiments were performed with wind speeds (w) of 0 m/s and 3.1 m/s , with the wind direction being perpendicular to the model line. Figure 2.11 shows the measured and calculated lateral profiles, at ground, of the electric field strength E and the current density J [6].
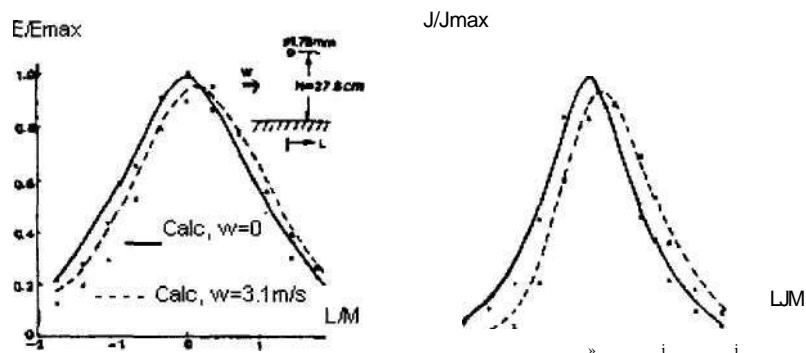
Figure 2.11: Measured and Calculated Lateral Ground Level Profiles of E and J under a Unipolar DC Line Model [6]

Full-Scale Bipolar + 400 kV DC Line

Figure 2.12 shows the computed lateral ground-level profiles of E and J (not normalized) for a + 400 kV bipolar DC transmission line. The parameters used for calculations were: ion mobilities $k+$ = 1.2cm^2/V.s and $k-$ = 1.5cm^2/V.s, ionic recombination coefficient $R,$ = 1.8 x 10-6cm^2/s, maximum conductor surface voltage gradient E = 23.99 kV/cm, wind speed $w = 0$ m/s.
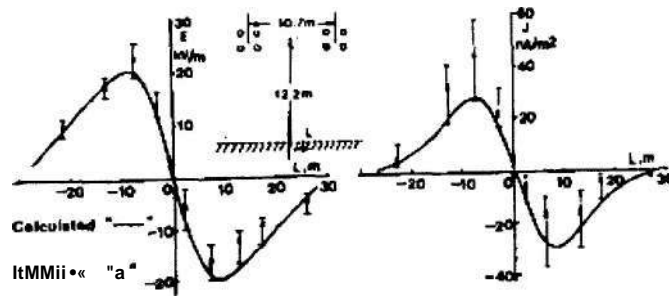
Figure 2.12: Comparison of Computed and Measured Lateral Ground Level Profdes of E and J under a + 400 kV Bipolar DC Line [6]

Full-Scale Bipolar + 600 kV DC Line

In Figure 2.13, the computed lateral ground-level profile of E is compared with available measured data and previous calculations for a + 600 kV DC transmission line. The good agreement between the results computed with this numerical method and measured data in figure 2.13 confirm the accuracy of the presented method. The corona parameters used for the calculations were obtained from the EPRI Transmission Line Reference Book for + 600 kV HVDC.
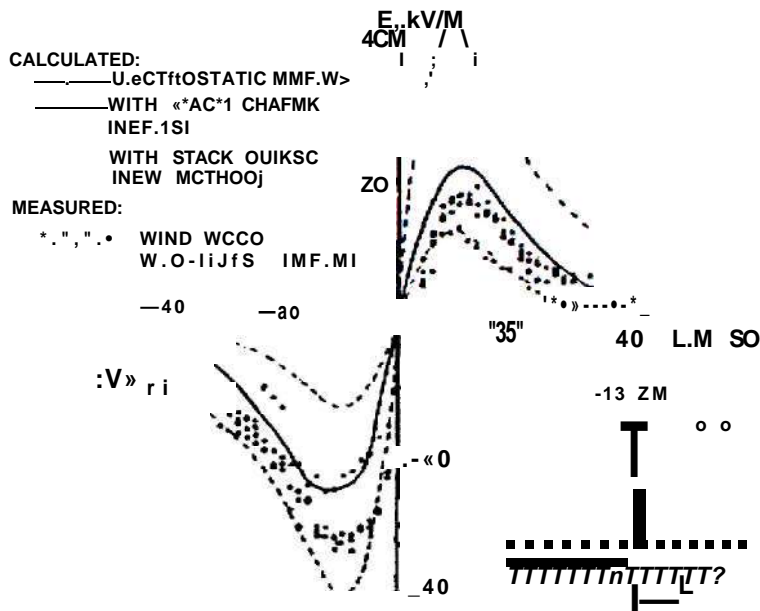
Figure 2.13: Comparison of Computed and Measured Lateral Ground Level Profiles of E under a + 600 kV Bipolar DC Line [6]

2.7 FINITE ELEMENT MODELLING OF IONISED FIELD QUANITIES AROUND A MONOPOLAR HVDC TRANSMISSION LINE:

The formation of extensive steady state space charge under a HVDC line in corona substantially alters the electric field, and the charges also drift into the inter-electrode region. Research conducted by the Indian Institute of Science (V. Jaiwal and MJ. Thomas) uses an improved Finite Element Model (FEM), to solve Poisson's equation. This describes the ionized field around an HVDC line. The method presented is used to compute the total corona current at different applied voltages (above corona onset voltage), electric field E at the ground plane with and without the presence of space charge and the ion current density J at the ground plane. The results show that there is a significant enhancement of the electric field in the ground plane in the presence of space charge. This is clearly shown in figure 2.14 [10].
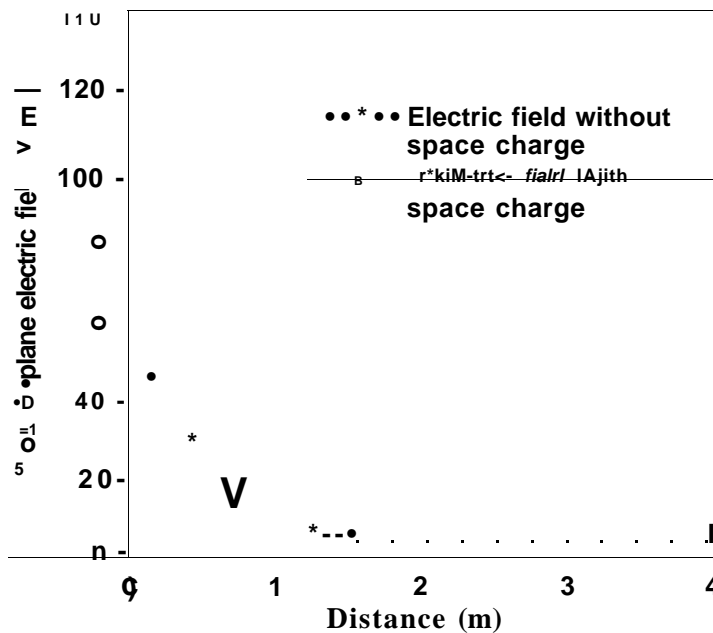
Figure 2.14: Electric Field at Ground Level for a Monopolar HVDC Line [10]

2.8 EFFECTS OF RELATIVE AIR DENSITY AND CONDUCTOR TEMPERATURE ON HVDC CORONA PHENOMENA:

Work was done by V.L. Chartier and R.D. Stearns of the Bonneville Power Administration (BPA), to determine the effects of relative air density (RAD) and conductor temperature on HVDC corona. They statistically examined the fair weather audible noise (AN), radio noise (RI), ion enhanced electric field, and ion current density from the Grizzly Mountain database. Previous measurements that were taken on the Pacific NW/SW HVDC Intertie at an altitude of 1100m above sea level showed that the negative pole had produced higher electric fields and ion activity than the positive pole [11].

2.8.1 Calculation of Conductor Temperature [11]

Conductor temperature was not measured directly on the Pacific HVDC Intertie during the initial design of the test program as this did not seem to be an important parameter at that stage. All the weather parameters that were needed (wind speed, ambient temperature, solar radiation, pressure) to calculate the conductor temperature were continuously monitored. A

simplified heat balance technique was developed to calculate the conductor temperature by using an iterative computer process.

2.8.2 Calculation of Relative Air Density [11]

The relative air density is the ratio of the air density at any given barometric pressure (B) and any temperature (T) to that at standard conditions of 20 ° C and 760 mm Hg. The RAD can be calculated by using equation 2.4.

$$RAD = 0.386 \cdot \frac{B}{273 + T} \qquad \textbf{(2.4)}$$

For the temperature (T) used in equation 2.4, V.T. Morgan suggests the use of an effective temperature in equation 2.5.

$$T = Ta + 0.8(Ti - To) \qquad (2.5)$$

where Ta and Ts are the ambient and surface temperatures respectively. The constant of 0.8 was experimentally determined for taking into account the temperature gradient through the corona sheath.

2.8.3 Results

The results of the measurements showed that the AN,RI, electric field and ion current density on the negative pole increased with an increase in ambient and conductor temperature and decreased with an increase in RAD. The electric field and ion environment on the negative side were up to 2 times higher than on the positive side. The results of the study (negative pole) are shown in figures 2.15 and 2.16. From figure 2.15, it is clear that the electric field at ground level increases with an increase in conductor temperature. It is also evident that at low conductor temperatures, the electric fields are also lower. This can be attributed to the effect that the lower conductor temperature has on the relative air density (RAD) surrounding the conductor. The lower temperature results in a higher RAD (8) and this in turn causes a higher corona inception gradient (Ec), hence corona activity is reduced. The lower corona activity results in less space charge ions being produced and the electric field at ground level is lower (64 % lower). Peeks formula can be used to calculate the corona inception gradient at the different conductor temperatures [19, page 82].
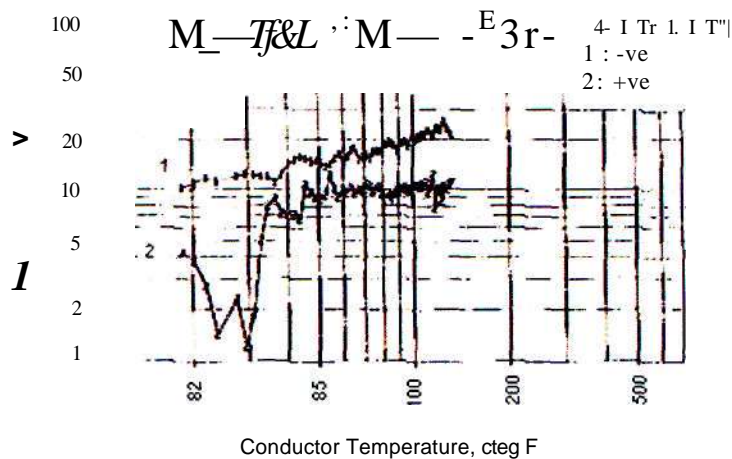
Figure 2.15: Electric Field versus Conductor Temperature   [11]

100

50

I   l8 | ».n*i*i»T*-»-*
; 2; UT |"

ID

1 i
0.78   0.82   0.86   0.9   0.94   0.98   1.0

Relative Air Density (Cond Temp)
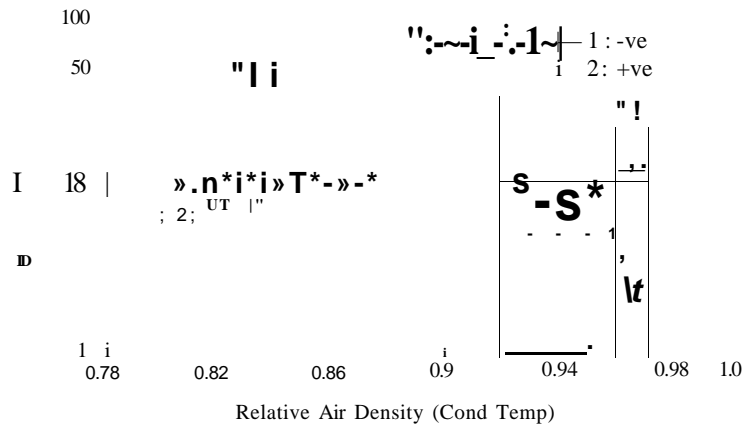
Figure 2.16: Electric Field versus Relative Air Density [11]

2.9 REDUCING THE ELECTRICAL ENVIRONMENTAL FACTORS UNDER HVDC TRANSMISSION LINES:

Studies carried out by Y. Amano and Y. Sunaga discusses the methods to reduce the electrical environmental factors below HVDC transmission lines. When designing and operating HVDC transmission lines, it is important to keep the electric field effects such as ion flow, charged voltage, electric field, ion current and ion density, at ground level in the vicinity of HVDC lines, as low as possible. Electrical environmental factors are regarded as important factors that relate to biological effects, therefore measurements have been conducted in many countries [12].

One important problem in Japan is the electric shocks which are caused by charged voltage due to ion current flowing into human beings wearing shoes of high resistance while standing under a transmission line. In order to prevent these shocks, the design of the transmission line height is considered. One of the methods to reduce the effects of the electrical environment is to make use of parallel shield wires. Several models of shield wires were tested under the Shiobara HVDC test line.

The shielding factor of an electric field is defined by equation 2.6.

$$Sf \quad \frac{Es}{Eo} \qquad (2.6)$$

Where Eo and Es represent the electric field without and with shield wires respectively [12].
The Shiobara HVDC Test line was used for the measurements. The test line is composed of a bipolar double circuit. The conductor height can be set at either 22 m or 27 m. The horizontal spacing between the poles and the vertical spacing between the upper and lower bipoles are fixed at 22 m and 16 m respectively. An inverse double circuit is used and the lines are energised to + 650 kV.

There are 3 shield wires used (Gl, G2, G3) and their height above ground are set at either 5m or 10m. Their distance from the centre of the two circuits is set at 1 lm (directly below 2 poles) for Gl, 17 m for G2 and 23m for G3. Figure 2.17 shows the set up of the test line including the shield wires.
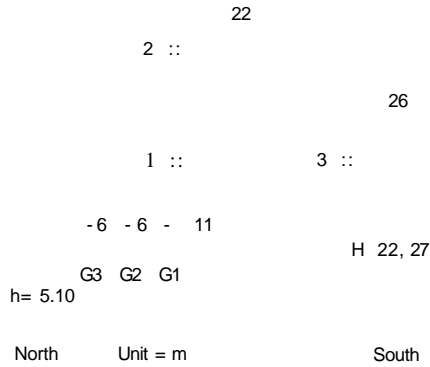
Figure 2.17: Arrangement of Shield Wires under HVDC Test Line (Gl, G2, G3) [12]

Figures 2.18 and 2.19 shows the effect of the shield wires in reducing the electric field and ion current density at ground level. There is a remarkable decrease in both the electric field and ion current density when all 3 shield wires are grounded.
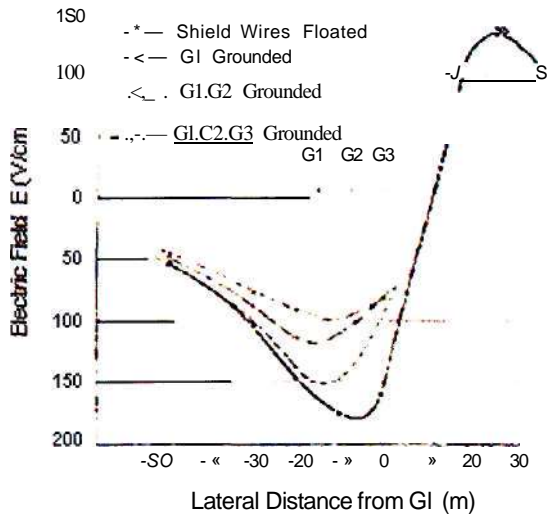
Figure 2.18: Shielding Effect of Shield Wires - Electric Field [12]
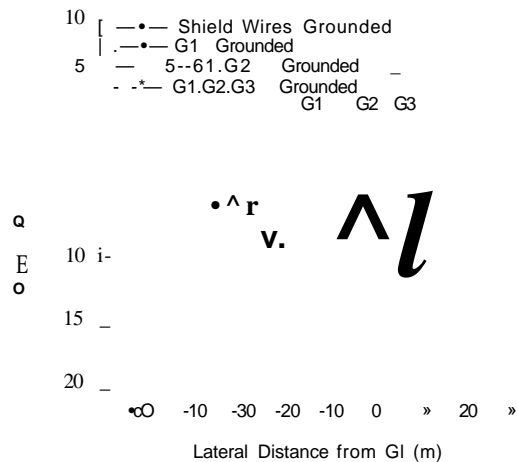
Figure 2.19: Shielding Effect of Shield Wires - Ion Current Density [12]

2.10 SPACE CHARGE MEASUREMENTS DOWNWIND FROM A MONOPOLAR 500 kV HVDC TEST LINE:

The electrical environment in the vicinity of a HVDC line is characterised by a few different electrical parameters and one such parameter is space charge. We are already aware that space charge consists of both air ions and charged aerosols.

Work was carried out at the Electric Power Research Institute (EPRI) at their High Voltage Transmission Research Centre (HVTRC) to determine the concentration of space charge [13]. Measurements were taken downwind from an HVDC test line and the influence of wind on the space charge level was also determined. The concentration of small air ions and charged aerosols are of interest and they are characterised by their electrical mobility. The electrical mobility (u) of a small air ion or a charged aerosol is defined as the ratio between the drift velocity (V) and the electric field (E). This is shown in equation 2.7.

$$V$$

The measurements have found that small air ions have mobilities greater than 0.5×10^{-4} m^2 / V.s and the small ions are easily moved by the electric field. The mobilities for charged aerosols (large ions) were found to be less than 1×10^{-6} m^2 / V.s and the large ions are moved predominantly by wind [13]. This agrees with previous suggestions that the small ion density will be the greatest in the vicinity of the conductor or directly under the conductor. When a HVDC line is operating above its corona inception voltage, positive and negative small air ions are directly produced. The main aim of the work carried out at EPRI HVTRC was to evaluate the effect of wind on the movement and density on space charge downwind of a 500 kV monopolar HVDC test line.

At the EPRI - HVTRC, there are two test lines. The short line is 150 meters in length and main test line is 500 meters in length. The short test line can be used for tests up to 500 kV and the main test line is used for tests up to 1500 kV [13]. For the space charge measurements taken, the main test line was energised. There are two methods that can be used to measure the space charge produced by a line. One method is to use an electric field meter and ion current instruments to take measurements at ground level and then calculate the small air ion density by using equation 2.3. The space charge density can then be calculated by using equation 2.2. The second method is to use specially designed space charge cages that are made from wire mesh and are about 1 meter in height and diameter.

From the results, shown in figure 2.20, it can be seen that the peak of the small air ion density shifts downwind as the wind speed increases. The small air ion densities decreases rapidly further away from the line.
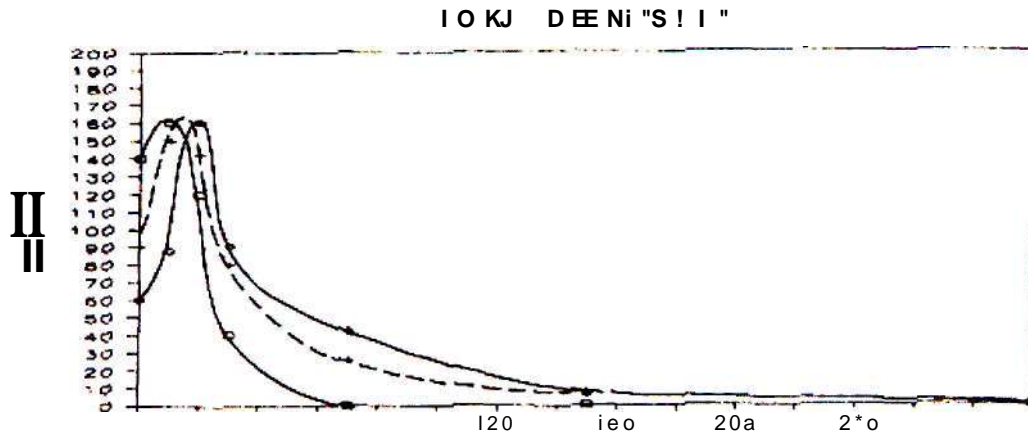
Figure 2.20: Small Air Ions versus Distance Downwind
Wind Speeds of 0 m/s, 4 m/s and 8 m/s [13]

2.11 MEASUREMENT OF ION CURRENT DENSITY AT GROUND LEVEL IN THE VICINITY OF HVDC TRANSMISSION LINES:

As mentioned in previous sections, ion current density is one of the electrical parameters that describe the electrical environment in the vicinity of HVDC transmission lines. Work done by R.H McKnight, F.R Kotter and M. Misakian of the National Bureau of Standards, Washington DC, describes the use of sensors for measuring vertical current density at ground level near HVDC lines. The sensors are subjected to error when its point of measurement is not in the ground plane. The work presented is from an IEEE working group meeting on the measured errors for guarded and unguarded sensors [14].

Measurements of the vertical current density at ground level is important for estimating the electric potential to which an insulated person or object which intercepts the current can be elevated. Current to a conducting plate lying in the ground plane, but insulated from earth, can be measured using electrometer circuits. Current density measuring devices of this type have been used for many years in atmospheric electricity research and are commonly known as "Wilson Plates". Because the levels of current density measured near HVDC lines are higher than those measured for atmospheric research, the required sensitivity of the current measuring instrument is much lower [14].

The vertical conduction current density (je) at the surface of a Wilson plate is given by equation 2.8.

$$je = p_p KE \qquad (2.8)$$

where E = electric field, K = average mobility and p_p = ion density.

The current measuring plates used in these studies were made from 0.157 cm thick copper clad fibre glass sheets. On six of the plates, a central section of the copper is isolated from the outer band (known as the guard ring) by a narrow slot of about 0.5 mm wide, which is milled through the copper. These plates are referred to as miniature Wilson plates and are commonly used in laboratories. The Wilson plates used by the National Bureau of Standards for this study are shown in figure 2.21.

Plate Designator	Harnina Dimensions cm	t
A	It	7 t
I	ID	'it
L	It	25
t	ID	10
A'	E5	75
B'	£5	5C
C	«5	7 c
I	e*	£5

Siot tc pass
ir.n.alu '• cca> cable

CD' • *He* guarii ring

Figure 2.21: Miniature Wilson Plates [14]

 The results of the measurements show that the errors are as large as 25 percent for guarded sensors and significantly larger for unguarded sensors. The errors in Wilson plate current density measurements as a function of width and elevation can be seen in figure 2.22.

a.»ic H." i,

N<.|IT allies WIwv HUv I>nr»-nMu>i * 0
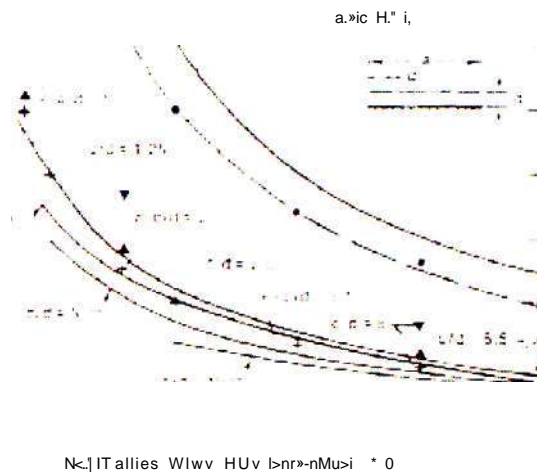
Figure 2.22: Wilson Plate Measuring Errors [14]

2.12 ELECTRIC FIELD AND ION CURRENT AT GROUND LEVEL AND THE VOLTAGE OF CHARGED OBJECTS UNDER HVDC LINES:

Studies done by Y. Sunaga, Y. Amano and T. Sugimoto found that insulated objects under HVDC transmission lines can be charged by ion currents generated by corona discharge. This ion current causes a high voltage to be produced which charges the insulated object. The extent to which insulated objects are raised to a high potential by these ion currents is an important factor in determining the conductor height for HVDC transmission lines. The quantity of ions generated depends greatly on environmental and design conditions, as well as the condition of the conductor surface. The condition of the conductor surface affects the roughness factor of the conductor, which in turn will result in a lower corona inception voltage [15].

Long term measurements were undertaken by CRIEPI on the Shiobara and the Takeyama test lines in order to predetermine the ion current and the voltage of charged objects under HVDC lines. The long term measurements taken on the BPA Celilo-Sylmar DC Intertie have also made it clear that the electric field at ground is greatly enhanced by space charge [15].

The work introduces the conductor surface gradient in the presence of space charge, i.e. the resultant conductor surface gradient. The results of the measurements taken on the Shiobara line for the corona current are shown in figure 2.23. It is clear that the corona current increases exponentially as the maximum conductor surface gradient (Gmax) increases.

j"

Figure 2.23: Corona Current versus Maximum Surface Gradient [15]

The electric field at ground level were calculated to be in the order of 21 - 29 kV/cm. It was found that the electric field under the lines increased by a factor of 1.4 to 2.3 in the presence of space charge. It was also found that for the same applied voltages, the static electric field increases but the resultant field decreases as the subconductor number increases. The following diagrams, figure 2.24 and figure 2.25, show the effect of conductor height and pole spacing on the values of electric field and ion current density at ground level.
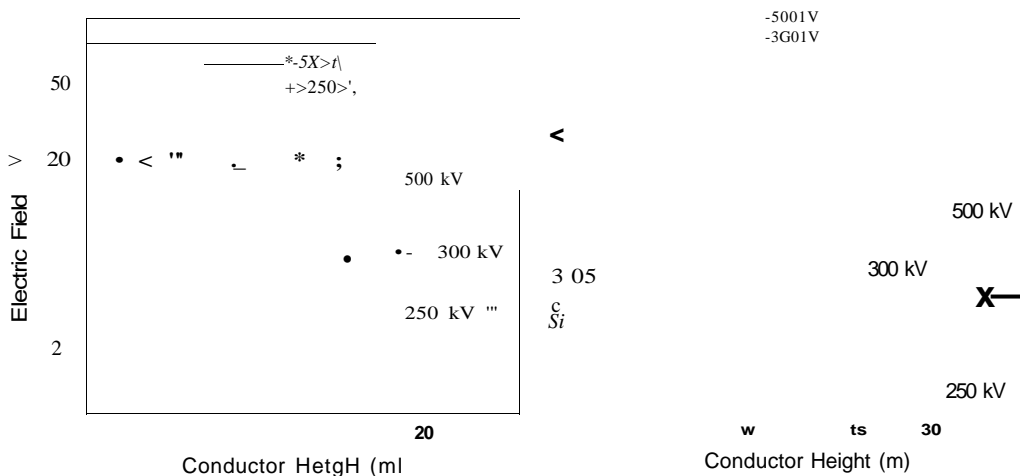
Figure 2.24: Influence of Conductor Height on a) Peak Value of Electric Field b) Ion Current Density [15]
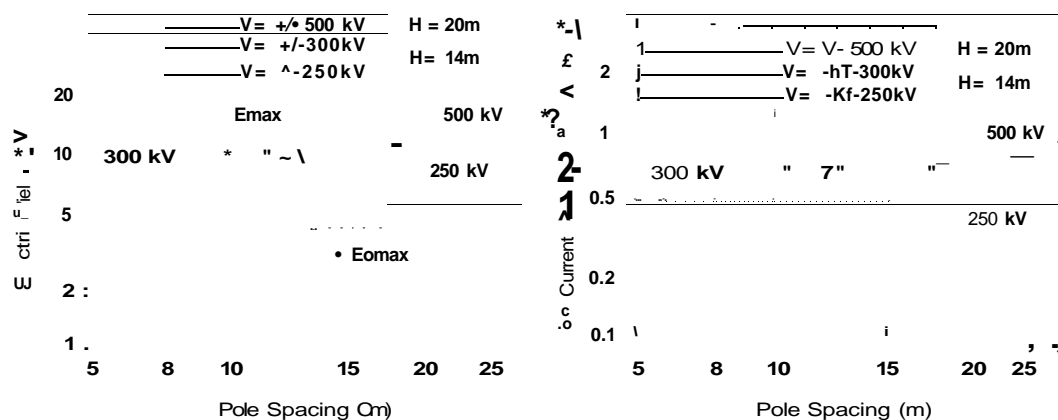
Figure 2.25: Influence of Pole Spacing on a) Peak Value of Electric Field b) Ion Current Density [15]

The results of all the measurements taken by CRIEPI on the Shiobara and Takeyama have found that the corona current decreases as the pole spacing increases [15]. It has also been found that for a constant applied voltage, the peak value of the electric field at the ground is inversely proportional to the conductor height and the ion current density at ground level is inversely proportional to about 2.3 - 2.8 the power of the conductor height.

2.13 THE RESULTS OF ELECTRIC FIELD AND ION CURRENT MEASUREMENTS - PROJECT UHV:

Work was carried out by Gary B. Johnson and Michael G. Comber to try to characterise the electrical environment in the vicinity of HVDC transmission lines. The results of the measurements of ground level electric field and ion current density that were performed at Project UHV are described in these papers [16].

In 1977, the U.S. Department of Energy (DOE) initiated a 30 month research program at Project UHV in Lenox, Massachusetts, to investigate the effects of the electric field and ion current of HVDC lines. A 150m long bipolar test line was constructed and this line could be energised up to + 750 kV. The test line geometry was a 4 conductor bundle, 3.05 cm per sub-conductor, 13.2 m pole spacing and a midspan height above ground of 13.5 m.

In 1980, concurrent research programs were initiated by EPRI and the DOE. The DC facilities at Project UHV were expanded with sponsorship from EPRI, to extend the capability of the test facility to + 1500 kV. Project UHV now had two bipolar DC test lines which they call a "short line" of 150 m in length and a "long line" which is 500 m in length. The ion current sensors used for the measurements were simple Wilson plates having an area of 1 m^2 and a 7.5 cm guard ring. The electric field sensors use Monroe type field probes [16].

The results of the measurements taken over a 3 month period between August to November 1980, are presented and described. Figures 2.26 and 2.27 show the values of ion current density and electric field respectively. It can be clearly seen from both diagrams that the highest levels of the ion current density and electric field occur at about 5 meters on either side of the test line. The tests were performed on the short line for test voltages of + 250 kV, + 350 kV and + 400 kV. There is quite a rapid change of the ion current density and electric field when + 400 kV is applied as compared to the two lower voltages. This suggests that the test line could have been producing more space charge at the higher voltage and hence the field

and ion current density at ground level is enhanced. What is also important to note is that the levels of ion current density and electric field for the + 400 kV case are higher on the negative pole than the positive pole respectively [16].
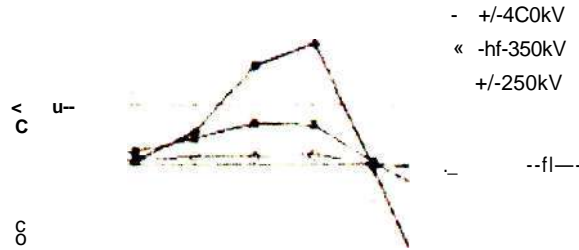
Figure 2.26: Ion Current Density versus Lateral Distance [16]
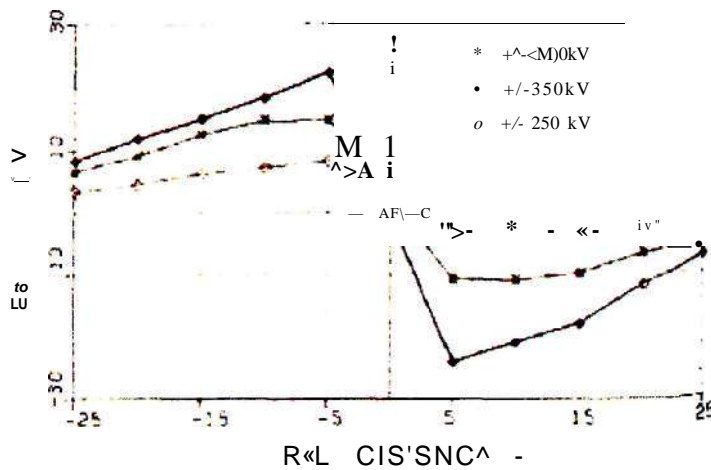
Figure 2.27: Electric Field versus Lateral Distance [16]

Relative humidity (RH) is another source that has caused variations in the level of ion current density measured below the test lines. Below 70 % RH there is not much effect but above 70 % RH there is a rapid increase in ion current density especially at higher voltages and on the negative side of the line. It is believed that at high relative humidities, potential sources of corona, like insects, become more conducting and are more likely to start coronating. The effect of RH on the ion current density can be seen in figure 2.28.
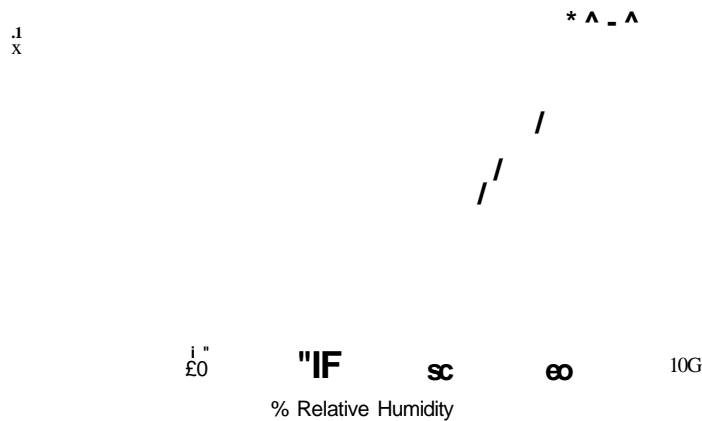
Figure 2.28: Ion Current Density versus % Relative Humidity at + 1200 kV [16]

2.14 LONG-TERM STATISTICAL STUDY OF THE CORONA ELECTRIC FIELD AND ION-CURRENT PERFORMANCE OF A +/- 900 kV BIPOLAR HVDC TRANSMISSION LINE [171:

A long term study of the electric field and ion current performance of a HVDC transmission line was carried out by P.S Maruvada, R.D Dallaire, P Heroux and N Rivest at IREQ in Canada. The electric field and ion-current performance of a 6 conductor bundle, that was chosen for use on a + 900 kV bipolar HVDC transmission line, was studied using a test line for a period of 18 months. Nine current measuring probes were placed under the test line. Each probe consisted of the main measuring plate (25.1 cm x 20 cm) and a grounded outer guard plate (1 m^2). The probe was located 6.35 cm above the ground plane. For the electric field measurements, a rotating type field mill was used [17].

The results of the study found that the electric field directly under the positive pole was calculated to be 26.5 kV/m at + 900 kV in the absence of space charge. The weather conditions had a significant influence on the lateral profiles of ion-current density. In general, higher current densities were measured under the negative pole than under the positive pole [17]. This can be seen in figure 2.29 and figure 2.30.
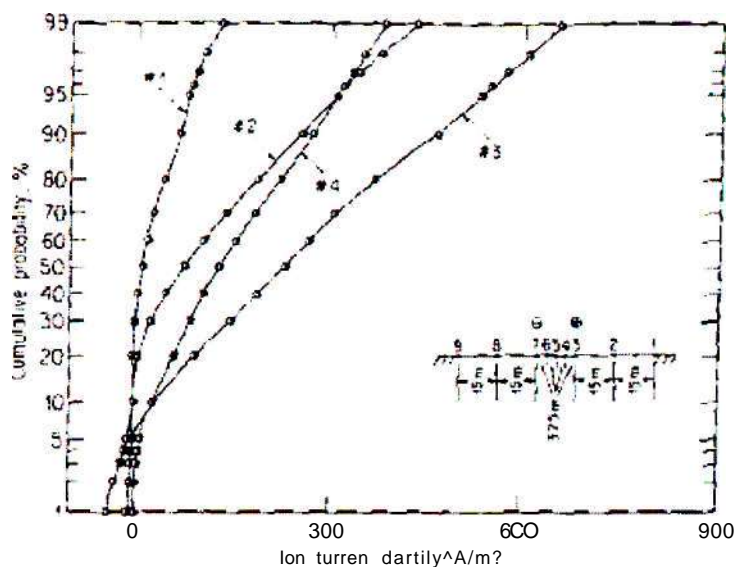
Figure 2.29: Ion Current Density under Positive Pole [17]
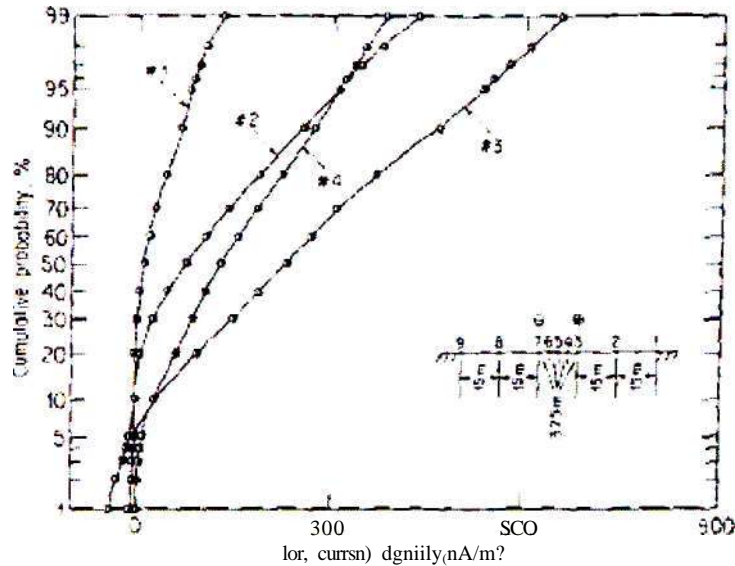
Figure 2.30: Ion Current Density under Negative Pole [17]

2.15 ENVIRONMENTAL EFFECTS OF THE NELSON RIVER HVDC TRANSMISSION LINES - RL AN, ELECTRIC FIELD, INDUCED VOLTAGE, AND ION CURRENT DISTRIBUTION TESTS F181:

This paper reports on the electrical environmental tests conducted by P.S Maruvavda, R.D Dallaire, O.C Norris-Elye, C.V Thio and J.S Goodman in 1979 on the Nelson River HVDC Transmission lines. Measurements of radio interference, audible noise, electric field, induced voltage, and ion flow were taken. The electric field causes charged particles to migrate to ground and onto objects at ground level. Voltages are induced on to such objects, and touching such objects can give an electrical shock. The space charge around a DC conductor alters the electric field strength. The presence of space charge of like polarity under a conductor can increase the electric field at ground level and that of opposite polarity, will decrease the electric field [18].

The ion current and electric field at ground level was measured using a current probe and a rotating field mill. The induced voltages and currents were measured using two electrostatic voltmeters and a multimeter. The results of the tests found that for a bipolar dc line, wind direction and magnitude affect the magnitude and asymmetry of the electric field and ion current density. The highest values of electric field and current density occur under no wind conditions [18].

For the bipolar configuration tested at + 450 kV, the influence of space charge increased the maximum ground level gradient by about 14 kV/m above the theoretical static field level. The maximum electric field measured was about 20 kV/m and the maximum current density was below$70nA/m^2$[18].

2.16 INVESTIGATION INTO THE CAUSE OF "UNKNOWN" LINE FAULTS ON A + / - 533 KV DC LINE IN SOUTH AFRICA:

The publication discusses the findings made by F.F Bologna, A.C Britten, R.E Kohlmeyer and H.F Vosloo on the cause of "unknown" line faults on the Cahora Bassa HVDC line. The Cahora Bassa + 533 kV DC lines run from Apollo substation, near Pretoria to Songo in Mozambique, a distance of 1414 km. The lines consist of two monopolar lines with isolated earth conductors. The South African section of the line runs from Apollo to Pafuri over a distance of 518 km. Existing line performance data (for South African section only) established from faults recorded since 2001 suggest that a high number of faults (62 %) are attributable to unknown causes [1].

Line faults are generally categorised as the following: Lightning, Fire, Pollution, Bird Streamers, Mechanical or Anomalous. There were a total of 57 "unknown" faults over the period June 2001 to September 2005. The line fault breakdown categories are shown in figure 2.31. Each fault was analysed by using a combination of time-of-day analysis, weather information, engineering tools (Lightning Positioning Tracking System and Advanced Fire Information System) and field investigations [1].

2.16.1 Veld Fires:

Veld fires occur mainly in savannah and grass fields during winter (June - September), usually after first frost. The time of the day also plays and important part in veld fire faults, as they usually occur during the hottest part of the day. Eskom Transmission makes use of a satellite monitoring system known as the "AFIS - Web Fire Mapper". This system monitors and records fires in the country on a daily basis. Each of the 57 "unknown" faults were analysed using this system and the number of faults due to fire was found to be approximately 21 % [1].

2.16.2 Lightning:

Lightning predominantly occurs during the summer rainfall period (September - March). Lightning faults occur when lightning strikes the tower or earth wire of the line. The Lightning Positioning and Tracking System (LPATS) data was correlated with each line fault. This showed that most lightning activity occurs between the hours of 14h00 to 22h00 and based on this, 18 % of the "unknown faults" can be attributed to lightning [1].

2.16.3 Insulator Pollution:

When a polluted insulator is subjected to light wetting i.e. dew, light rain etc, the pollutant and water combine to form an electrolyte which allows surface currents to flow. If the surface leakage currents become large enough, the insulator or insulator string will flashover.

Both monopolar lines are insulated with a combination of glass cap and pin and silicon polymer insulators. The polymer insulators have a specific creepage length of 31 mm/kV whilst the glass insulator's creepage varies between 25 and 26.3 mm/kV It has also been shown that the relative humidity (RH) values exceeding 80 % is sufficient to "wet" the insulator surface causing leakage current to flow. The relative humidity data obtained from the South African Weather Bureau was correlated with the line fault data [1],

The influence of polarity was also found to be significant. The analysis found that the negative polarity is more susceptible to pollution flashovers. Based on operational experience, faults due to insulator pollution account for approximately 50 % of the "unknown" faults.

- P> utbn
- Ved Fires
- j Lightning
- D Unhnow n
- Tree
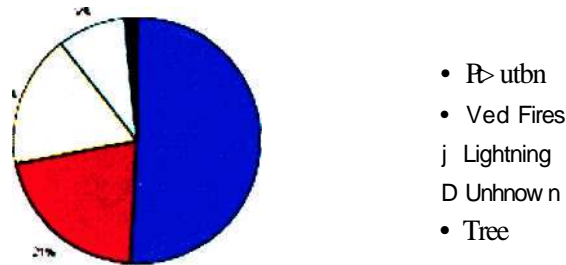
Figure 2.31: Cahora Bassa Line Fault Breakdown - 57 Faults (2001 - 2005) [1]

2.17 ELECTRIC FIELD CALCULATIONS:

Formulas for predicting the electric field at ground level under a monopolar line was developed by previous studies. The electric field strength under a monopolar FTVDC line, with the absence of space charge, is given by equation 2.9 [3]

$$E = \frac{2V}{//\ln \frac{2//}{R}} \frac{H^2}{H^2 + x^2} \quad kV/m \qquad [2.9]$$

Where: E = electric field at ground level in kV/m, V = applied voltage in kV. H = height of conductor in m, R = radius of conductor or equivalent radius of bundle in m and x = horizontal displacement from centre of conductor.

The formula for the electric field at ground level, in the presence of space charge, is more complicated and it is given by equation 2.10 [19]

$$E = *^{\wedge}\_ \qquad \frac{/2 \quad r^{1/2}}{H} \qquad [2.10]$$

Where: E is the electric field, E_0 is the corona inception gradient of the conductor, r_0 is the radius of the conductor or conductor bundle used in m, 1 is the distance away from the conductor towards the ground in meters, H is the height of the conductor in meters and *C,* is a normalizing function, taking the line geometry into account. For a monopolar line *C,* is given by equation 2.11:

$$c = \frac{PI}{2ft\pounds_0/U} < \frac{H*}{V^{\wedge}o^ro J} \qquad [2.11]$$

Where: P is an empirical constant, I is the total corona current per unit length, (j. is the ionic mobility and e_0 is the permittivity of free space. I is given by equation 2.12:

$$I = 2nrJ_e \qquad\qquad [2.12]$$

Where: je = corona current density at conductor surface, je is defined as follows:

$$Je = MP_e E_0 \qquad\qquad [2.13]$$

Where: p_e = charge density at conductor surface.

The EPRI green book gives another formula for calculating the electric field in the presence of space charge:

$$E(L) = S^\wedge dL\text{-}^\wedge_{E\backslash L)\text{-}c} + V?\; ^{1/2} \quad \frac{E'(L)}{V} \qquad [2.14]$$

Where: E' (L) is the electric field at a distance L below the line, in the absence of space charge, Vc is the corona inception gradient of the conductor, V is the applied voltage in kV and $S = V\text{-} \dfrac{2j(0)}{ekE'(0)}$ where, V is the applied voltage in kV, j (0) is the corona current density at the conductor surface

CHAPTER 3

TEST EQUIPMENT: DESIGN AND OPERATION

This chapter describes the equipment used to carry out the different tests for the project and also looks at the designing of some of the test equipment.

3.1 WILSON PLATE DESIGN: LARGE AND MINIATURE PLATE

3.1.1 Operation of Wilson Plate:

The vertical component of ion current density *(J)* in the vicinity of HVDC transmission lines can be measured by using a flat collecting plate, commonly known as a Wilson plate, and an electrometer. The Wilson plate should be mounted flush with the ground plane and the current density *(J)* is averaged over the area of the plate. The current density is given by equation 3.1 [2].

$$J = \qquad\qquad\qquad (3.1)$$

where I = measured current & A = area of the plate

Figure 3.1 shows a Wilson plate that is mounted flush with the ground plane. The Wilson plate is isolated from ground but it is grounded via the ammeter that is being used to measure the ion current. There are guard bands on either side of the sensing plate which are at ground potential and are used to reduce fringing field effects.
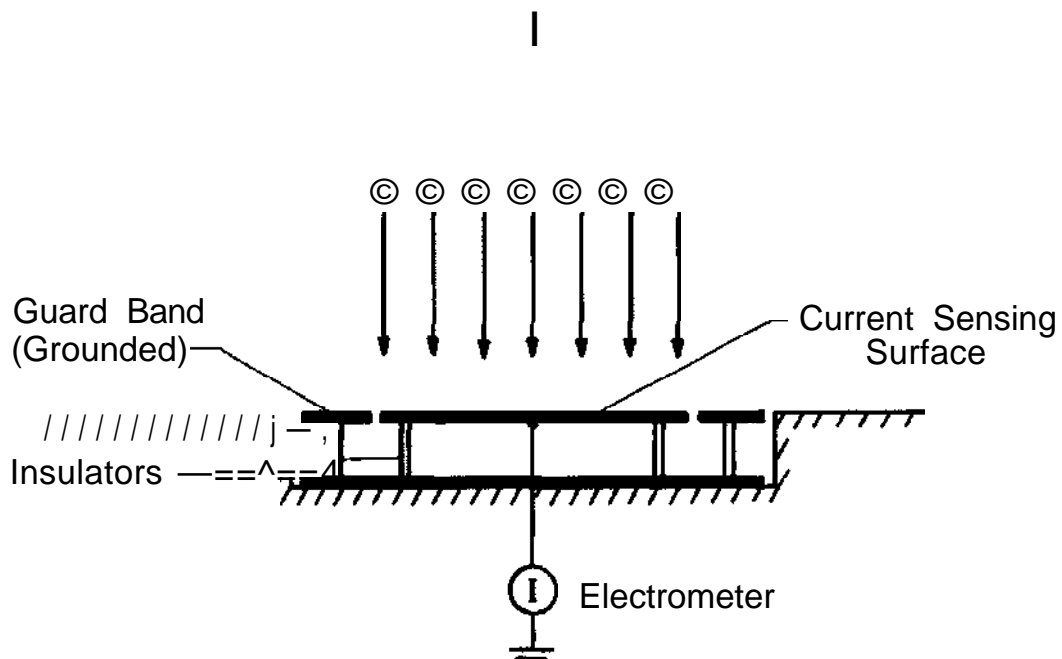
Figure 3.1: Wilson Plate Mounted Flush with Ground Plane [2]

3.1.2 Design of Wilson Plate:

Two Wilson plates were designed for this project, a large plate and a miniature plate. The large plate is 2 meters in length and *Vi* meter wide giving a total area of 1 m^2. The guard bands on either side of the plate are 25 centimetres long and !4 meter wide. Both the sensing plate and the guard bands were made from copper plate that was accurately cut to the correct dimensions required.

Miniature Wilson plates are commonly used for measurements taken in laboratories. The size of the miniature Wilson plate that was fabricated for this project was 10 cm x 10 cm. The miniature plate is made from copper clad printed circuit board and is about 2 millimetres thick. A central section of the plate was isolated from the outer band in order to create a guard band. This was done by removing a narrow slit (1 mm) of copper from the surface of the sensing plate. The central section of the miniature plate measures 7.5 cm x 7.5 cm and the guard band width is 2.4 cm around the entire plate. This is shown in figure 3.2.

Figure 3.2: Miniature Wilson Plate [14]

Two sets of insulators were made for the measurements to be taken with the Wilson plates. The first set was milled from PVC with a height of 2 cm. These insulators were accurately cut on a lathe to ensure that the Wilson plate was at a consistent height above the ground. The second set of insulators is commonly used in LV switchgear and these are 2.5 cm in height. The Wilson plate will be placed on these insulators to isolate it from ground.

3.1.3 Calibration of Wilson Plate and Electrometer:

There are possible uncertainties when making measurements with a Wilson plate. The area (A) of the plate may not be very accurate and the measured current (I) may also be incorrect. In order to reduce the uncertainty value of the area, the gap spacing between the guard band and the sensing plate can be reduced. It is then assumed that the effective ion collecting of the plate extends up to the midpoint of the gap [2].

Calibration of the electrometer can be done by using a current injection circuit which consists of a high-standard resistor, a dc power supply and an accurate voltmeter. The current is calculated by using Ohm's Law (I = V/R) and this is then compared to the measured value of current.

3.1.4 Accuracy of Wilson Plate Measurements:

When Wilson plates are operated above the ground plane, there is an enhancement of the electric field strength and ion current at the surface of the Wilson plate. Measurements are taken above the ground plane for practical reasons, such as to eliminate the effects of vegetation and in situations where the measurement cannot be made flush with the ground plane. Errors that result when measurements are taken above the ground plane can be significant, and needs to be minimised. Figure 3.3 shows the flux lines terminating on the surface of the sensing plate located above the ground plane. The enhancement of the electric field will result in excessive ion current reaching the current sensing surface, and this will negatively impact the measurements taken.

Sensor

$J_{zz}\underline{r/r/m}$ Li. / 7~1x/_'7 /1ll j

Insulating Support

/ // // 7 //Y/v 7777777777V777
Ground Plane
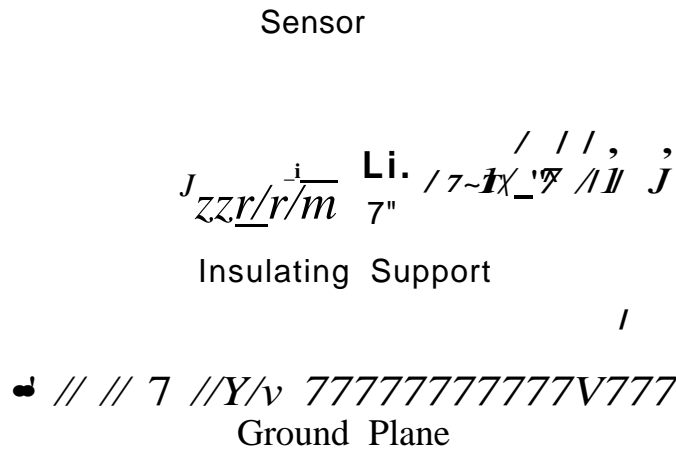
Figure 3.3: Flux Lines Terminating on Wilson Plate above the Ground Plane [14]

Studies have been conducted to determine the errors in measurements of vertical current density above ground [2]. The study has found that the errors can be as large as 35 %. These errors can be made minimal for measurements above the ground plane by varying the dimensions when designing a Wilson plate. For the large Wilson plate that was designed for this project, the dimensions were calculated such that the maximum error for measurements of this nature would be limited to 5 %. The study shows that the ratio of the total length (a) of the plate, including guard bands, to the height of the insulator (d) needed to be between 40 - 50 and the ratio of the guard band (c) to the height of the insulator (d) needed to be between 5 - 10 in order to achieve an accuracy of within 5 %. The results of the study for the errors of above ground measurements of vertical current density is shown in figure 3.4.
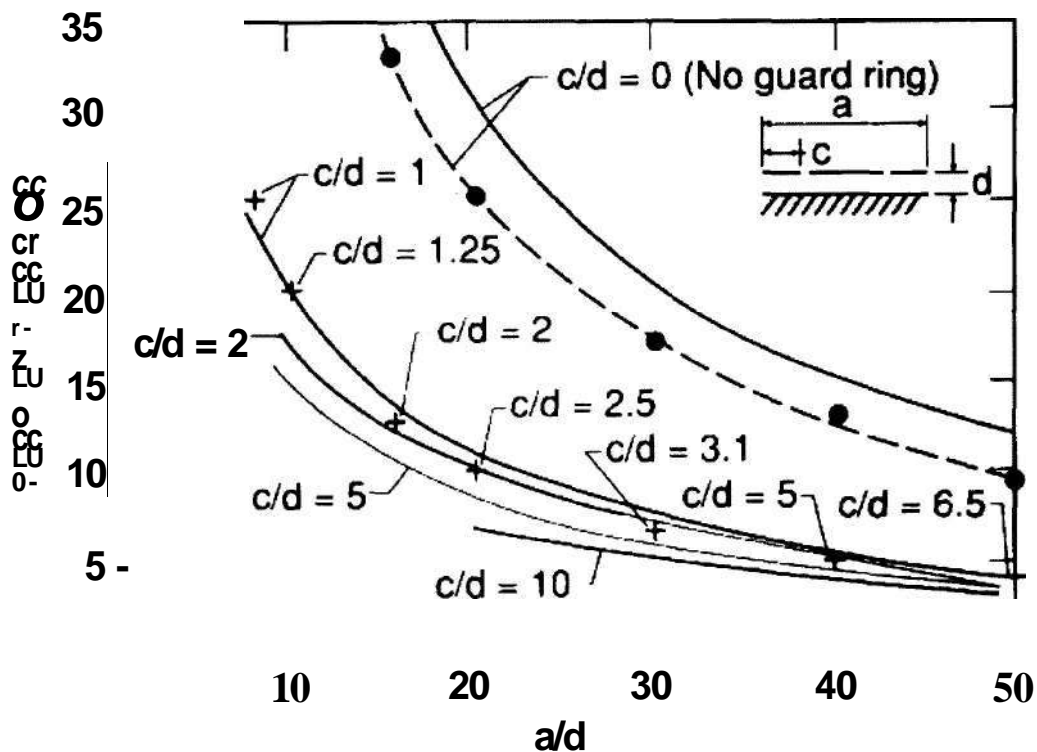
Figure 3.4: Errors for Wilson Plates Located above the Ground Plane [2]

3.2. FIELD MILL DESIGN: ROTATING SHUTTER TYPE

3.2.1 Operation of Field Mill:

There are two types of commonly used dc electric-field strength meters, the field mill (generating voltmeter) and the vibrating plate electric-field meter. Both meters determine the field strength by measuring modulated, capacitively induced charges or currents sensed by metal electrodes.

The vibrating plate sensor is placed below the aperture facing the dc electric field. Charges that are induced on the plate by the electric field are modulated by the vibrational action of the mechanical driver. The amplitude of the current induced on the plate is proportional to the magnitude of the electric field. A current amplifier is used to keep the sensing plate at ground potential and is also used to monitor the resultant current [2]. The vibrating type field meter is used for measurements at ground level under HVDC lines, but taking measurements with it in bad weather conditions have been found difficult. The vibrating plate electric field meter is shown in figure 3.5.
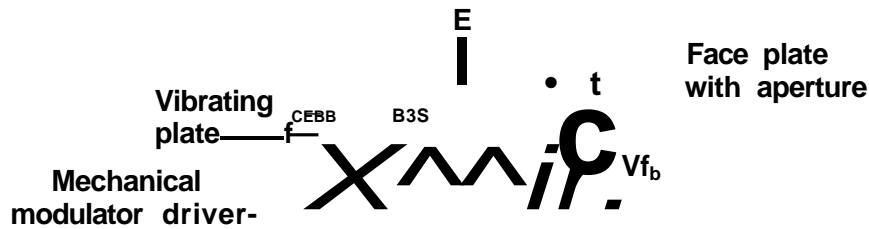
Figure 3.5: Vibrating Plate Electric Field Meter [2]

The shutter type field mill (figure 3.6) has a sensing electrode that is periodically exposed and shielded from the electric field by a grounded rotating shutter. These field mills are operated in the ground plane with the shutter flush with the ground plane itself. The charge induced at any instant, q_s, and the induced current (i_s) are both proportional to the strength of the electric-field (£). The induced charge is given by equation 3.2.

$$?,(0 = {}^*o^£«(0 \tag{3.2}$$

where, $s_0 =$ permittivity of free space

and $a(t) =$ exposed area of sensing electrode at time t

The induced current is found by taking the derivative of equation 3.2 [5].

$$'',(') = \frac{dq_s(t)}{d\{t)} \qquad \frac{s_0Eda(t)}{d(t)} \tag{3.3}$$

The electric-field strength can be determined by the measurement of the induced charge, induced current or the voltage across an impedance that is located between the sensing electrode and ground.
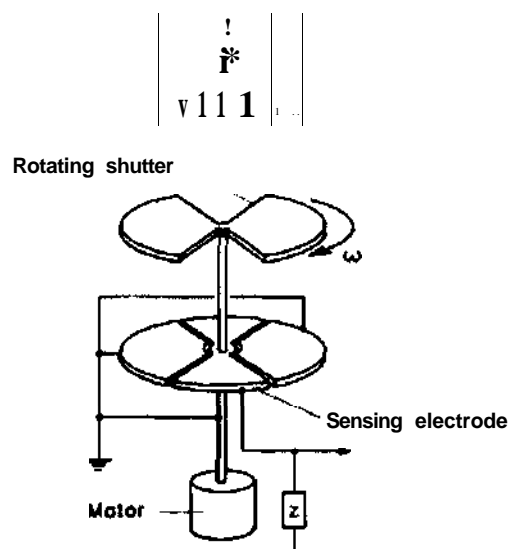
Figure 3.6: Shutter Type Electric Field Mill [2]

3.2.2 Design of Shutter Type Field Mill:

A shutter type electric field mill was built specifically for this project by the University of Witwatersrand, School of Electrical Engineering. The maximum surface area of an electrode must be half the cross sectional area of the shield can in order to modulate the field by the rotary shutter. The rate of modulation is proportional to the angular velocity of the rotary shutter. If the number of pairs of arms of the rotary shutter is increased, then the rate of modulation of the electric field is given by equation 3.4. The number of sensor electrodes needs to be increased as the number of arm pairs is increased. The minimum number of sensor electrodes will be twice the number of arm pairs [20].

$$w_e = nw_r \qquad\qquad (3.4)$$

where,

w_e = effective angular velocity (rads/s)

w_r = actual angular velocity (rads/s)

n = number of arm pairs

A special measurement circuit was incorporated with the field mill. The charge accumulated on the sensor electrode is seen as a voltage measured across a resistor. A high input impedance stage of 200 kΩ is required to minimise the loss of sensitivity due to driving the signal into the input stage. The signal is then sampled by a microcontroller and then transmitted serially to a recording device.

L'idcl Mill

Filler*

Mici'ocutiti; I'IUT

Serial
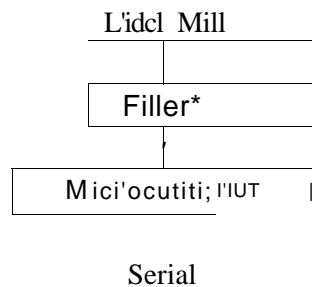
Figure 3.7: Schematic Diagram of Field Mill Measurement System [20]

This signal needs to be buffered, amplified and filtered before it can be sampled by the microcontroller. This is achieved by the circuit shown in figure 3.8. The signal is buffered by the high impedance FET amplifier, then amplified by the common small signal inverting op-amp and finally it is rectified into a peak detect network.
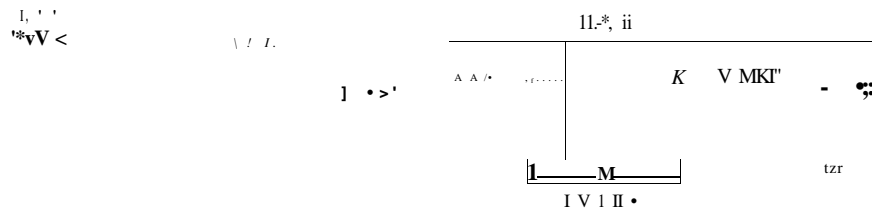
Figure 3.8: Active Filter and Rectification Circuit for Sensor Signal [20]

3.2.3 Calibration of Shutter Type Field Mill:

The electric field mill is calibrated with an electric field generated by an HVDC generator. The generator uses a single stage Cockroft-Walton circuit that generates a DC voltage that is twice the AC input voltage. A maximum voltage of 20 kV DC is used to calibrate the field mill. Calibration is performed by using two large parallel plates as explained in the IEEE standard 1227-1990. This set up is shown in figure 3.9. The electric field between the two parallel plates is given by equation 3.5 [2].

$$\frac{}{d} \tag{3.5}$$

where,

E = Electric field (V/m)
V = Voltage between the plates (V)
d = Distance between the plates (m)

The magnitude of the electric field used for calibration can be varied by adjusting the applied voltage or the distance between the two plates.
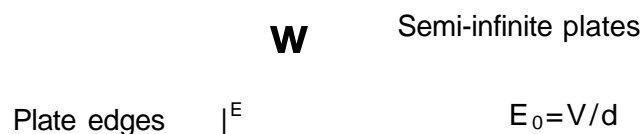
Figure 3.9: Calibration by Parallel Plates [2]

3.2.4 The JCI 140 Static Monitor Field Meter:

The field mill used for the initial tests was a JCI 140 Static Monitor type. The field mill and its specifications are shown in figure 3.10 and table 3.1 respectively.

Figure 3.10: JCI 140 Static Monitor

Table 3.1: JCI Static Monitor Specifications [46]

Sensitivity:	• 2,000 and 20,000 volts fult scale at 100mm separation between surface and sensing aperture. • Sensitivity selected via on/off switch or by external control signal
Zero stability:	• Noise within 1V p-p surface potential. Zero stable +10 volts.
Accuracy and linearity:	• Within +2%FSD
Response:	• -3dB at 35Hz. (-3dB at 400Hz for JC1140 F)
Display:	• 3V* digit liquid crystal display of surface voltage directly in kilovolts at 100mm with polarity and LO BATT indication
Audio alarm:	• Pulsing audio signal when above user set level
Controls:	• On/off slide switch: off - range 1 - range 2 • Screwdriver set alarm threshold • Screwdriver zero setting adjustment
Power supply:	• Replaceable PP3 battery • via 8w mini DIN from external floating 12V supply • 2.1mm d.c. power connector for 12V external floating power supply input
External connections:	• via 8w mini DIN connector: - analogue output signal (±2V FSD) - sensitivity range indication and external control of sensitivity -earth - external power supply inputs
Earth bonding:	• Combination 10mm Durable and 4mm bayonet socket earth bonding point. Supplied with Durable Dot earth bonding cord
Dimensions:	142x66x34mm.Weiaht: 320arams

3.3. PICOSCOPE PS3204 - OSCILLOSCOPE:

The oscilloscope that was used for the measurements was a Picoscope PS3204. This scope connects to your computer and then functions as an oscilloscope. Special Picoscope software is provided with the scope and this software needs to be loaded onto a computer for test purposes. The Picoscope PS3204 is shown in figure3.11.

Figure 3.11: Picoscope PS3204

The picoscope has two input terminals for the two measuring channels. The input terminals are of the coaxial BNC terminals. The scope has one USB output terminal. The internal resistance of the picoscope is 1 MΩ. The sampling rate of the picoscope is 50 MHz which is shown in table 3.1.

3.3.1 Calibration of Measurement Scope:

The oscilloscope used for measurements was calibrated using a DC source and a resistor of known resistance. The measuring scope has an internal input resistance of 1 MΩ and the known resistor that was connected in series with the scope was also 1 MΩ. A DC voltage was applied to the calibration circuit and the voltage across the known resistor was measured. The voltage that was measured by the oscilloscope was half of the applied voltage and this correlated to calculated values. This test was repeated for several different applied voltages and hence it was concluded that the scope was making correct measurements. The circuit is shown 3.12:
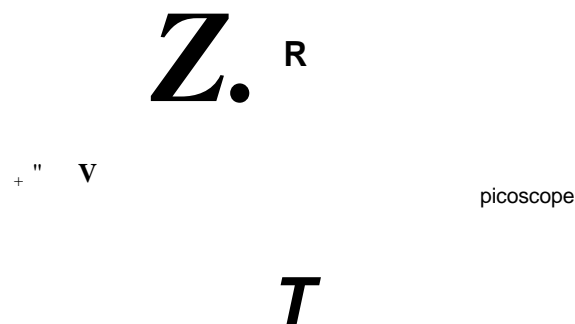
Figure 3.12: Calibration Circuit

3.3.2 Specifications of the Picoscope PS3204:

The picoscope model that was used for the measurements was the PS3204. The specifications for this model are given in the table 3.1:

Table 3.2: Picoscope Specifications [21]

Variant	3204	3205	3206	3224	3424
Vertical resolution	8 bits			12 bits	
Analog bandwidth	50 MHz	100 MHz	200 MHz	10 MHz	
Max. sampling rate One channel in use Two channels in use 3 or 4 channels in use Repetitive signals	50 MS/s 50 MS/s 2.5 GS/s	100 MS/s 100 MS/s 5 GS/s	200 MS/s 100 MS/s 10 GS/s	20 MS/s 10 MS/s	20 MS/s 10 MS/s 5 MS/s
Trigger bandwidth	50 MHz	100 MHz	150 MHz	10 MHz	
Buffer size (samples per channel) One channel in use Two channels in use 3 or 4 channels in use	256 K 128 K	512 K 255 K	1 M 512 K	512 K 256 K	512K 256 K 128 K
Inputs	2 BNC channels				4 BNC channels
	I MO impedance AC/DC coupling 20 pF capacitance				
Outputs Signal generator	Fixed (Note 1)	Variable (Note 2)		None	
External trigger	1 BNC input shared with signal generator Variable trigger threshold ± 20 V Rising/falling 12.2 mV resolution 1 MQ impedance			None	
Voltage ranges	± 100 mV to ± 20 V in 8 ranges			± 20 mV to ± 20 V in 10 ranges	
Accuracy	3% voltage 100 ppm time			1 % voltage 100 ppm time	
Operating environment Temperature range Humidity	0'C to 70^{C}C (25^{C}C for quoted accuracy) 25% to 75% RH			D^{o}C to 70°C (2D'C to 30^{5}C for quoted accuracy) 25% to 75% RH	
Overload protection Channels External trigger	±100V ±30V			±100V	
PC connection	USB 2.0 Compatible with USB 1.1				
Power supply	From USB port: 4.6 to 5.25 V 500 mA External power supply is not required			From USB port	
Dimensions	140 mm x 200 mm x 45 mm				
Compliance	CE standardl sh: FCC Part 1 5 1 ^				

(1) 1 BNC shared with external trigger. Fixed frequency 1 kHz. 5 V square wave. 600 O output impedance.
(2) 1 BNC shared with external tngger. Variable frequency 100 Hz to 1 MHz. 5 V square wave, 1 V sine wave and triangle functions. Repeat sweep function. Dual slope function. 600 *Cl* output impedance.

3.4. FERRITE CHOKES:

Due to coupling effects that we were picking up in the measurements, a set of ferrite chokes were purchased. These chokes clip over the co-axial measuring cable and help to eliminate coupling effects and earth loop currents. Ion current and electric field measurements were conducted with and without these chokes in the measuring circuit. The results showed that these chokes had very little or no effect on reducing the coupling from the AC transformer into our measuring circuit. The reason for this could be that these ferrite chokes are not able to reduce coupling within the frequencies that were picked up. These chokes are used in the MHz range while we are picking up predominantly a 50 Hz frequency. The ferrite chokes that were ustilised can be seen in figure 3.13 [22].
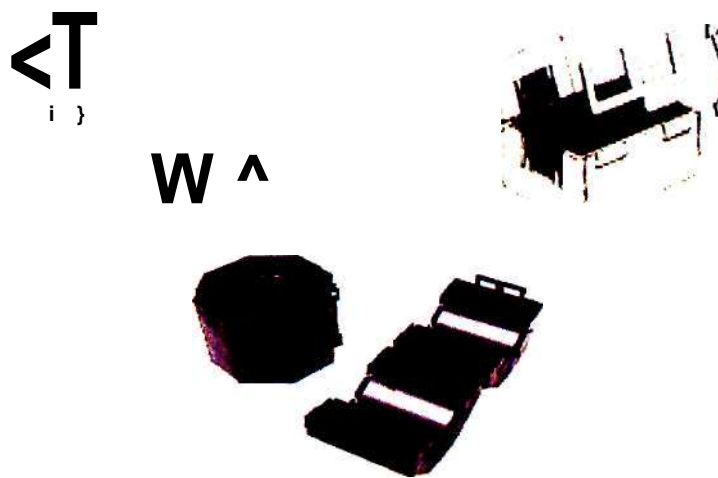
Figure 3.13: Ferrite Chokes [22]

3.5. MONROE ELECTROSTATIC FIELDMETER (257D):

A Monroe Fieldmeter (25 7D) was purchased in order to measure the electric field under the test line and to take measurements on an operating HVDC line. The portable electrostatic fieldmeter measures the electric field in kV/cm. It can also be used to measure surface voltage. The fieldmeter can be operated from an internal re-chargeable battery source or from an AC mains supply. An analogue output for monitoring is provided via a BNC connector. The Monroe Electrostatic Fieldmeter can be seen in figure 3.14 [23].

Figure 3.14: Monroe Electrostatic Fieldmeter - 257 D [23]

3.5.1 Applications:

The Model 257D is used for monitoring electrostatic charge accumulation. It can also be used for monitoring the effectiveness of static elimination equipment, atmospheric electricity measurements, FTVDC transmission terminal measurements and monitoring of coating, capping or filling processes [23]. The probe that is used with the field meter is shown in figure 3.15 [23].

Figure 3.15: Monroe 1036F-5 Probe [23]

3.5.2 Specifications - Monroe Fieldmeter 257D:

The specifications of the Monroe Fieldmeter Model 257D is shown in table 3.2:

Table 3.3: Monroe Fieldmeter 257D - Specifications [23]

Ranges:	+2 kV/cm and ±20 kV/cm
Sensitivity:	1 Wcm and 10 v/crn, respectively
Static accuracy:	Better than 5% of reading
Drift:	<30 V.'cmyhour, non-cumulative after 30 minute stabilization, referred to input
Noise:	<10 V'/cm rms, C - 200Hz. referred to input
Response speed	250 ms 10% to 9G% (typical)
Analog output:	$1/10.000^n$ of input, <10Q impedance
Battery:	Built-in, re-chargeable, gel-type, 12 v, 1.2 AH, >8 hours with backlight on - charging system on-board, <6 hours re-charging time
AC power:	Power adapter supplied for 105 to 130 VAC, 47 to 63 Hz-optional adapter for 90 to 242 VAC. 47 to 63 Hz
Dimensions:	$1Qy_s"Dx6VWx2VH$ (26.7 x 16.2x6.7 cm)
Weight:	2 lbs., 6oz. (1.1kg)
Instrument operating environment:	25^CC, ±1C°C. 0-85% RH non-condensing
Probe:	1036F-5, 1 %"Dx 1 Vi"H (4.4 x 3.2 cm), 8 oz. :0.2kg) with 10 ft. (3m) cable - optional extension cable up to 1000 ft (300m) permitted
Probe operating environment:	-3CC to +100°C, 0-85% RH non-condensing
Industry approvals:	Probe approved by Factory Mutual Research Corporation as intrinsically safe for use in Class I. Division 1, Groups C and D hazardous locations when used with approved IS barriers CE approvals pending

3.5.3 Calibration of Probe - 1036F-5:

The probes are standardised using a "perfect parallel field". The set up for calibrating the probes is shown in figure 3.16 [23]. The plates are separated by a distance 'd' and a calibrating voltage is applied to the gradient plate in order to establish a reference field between the plates.
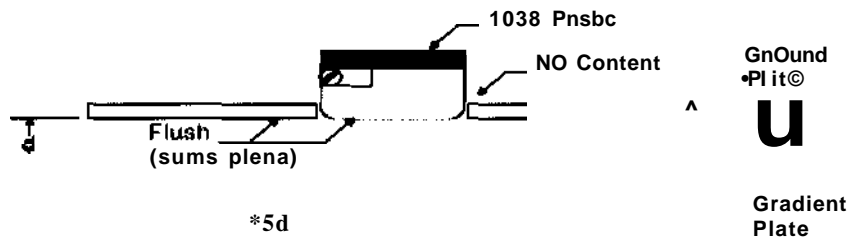
Figure 3.16: Probe Calibration Circuit [23]

CHAPTER 4

TEST PROCEDURES

This chapter describes the procedures used to carry out the different tests in the laboratory.

4.1 CORONA CURRENT MEASUREMENT:

The corona current that is induced on a floating object was measured at the HVDC laboratory at UKZN using the test line (refer to Appendix B). These tests were carried out over two separate periods in order to do both negative and positive polarity tests. The voltage that was induced onto the floating object was also measured. For these tests, the shield wire was used as the floating object while voltage was applied to the pole conductor.

For each polarity, four sets of tests were conducted to determine the variation in corona currents. The pole conductor was energised (negative and positive polarity) and the corona currents to ground, were measured using a HV probe and an ammeter. The measurements were taken for both polarities and for the four test set ups described below (4.1.1 - 4.1.4).

The sharp objects that were used as the corona sources were obtained from another damaged pole conductor. The individual strands were cut into several pieces about 7 cm in length. These cut up pieces were then tightly attached to the pole conductor and shield wire (depending on which test set up was being used) by using electrically insulated tape. About 10 of these sharp objects were attached to each sub conductor within the bundle. They were spaced equally apart at approximately 40 cm from each other.

4.1.1 Smooth Shield Wire and Smooth Pole Conductor:

For the first test, the pole conductor and the floating object were both totally smooth. Neither the pole conductor nor the shield wire had any damage to it.

4.1.2 Damaged Shield Wire and Smooth Pole Conductor:

For the second test, a shield wire with damaged strands was simulated. This meant that the floating object had several sharp points on it while the pole conductor had a smooth surface.

4.1.3 Smooth Shield Wire and Damaged Pole Conductor:

For the third test, a damaged pole conductor was simulated. The pole conductor had several damaged strands which created sharp points along the length of the line. The floating object was now a smooth conductor.

4.1.4 Damaged Shield Wire and Damaged Pole Conductor:

For the fourth test, a damaged pole conductor and a damaged shield wire were created. This meant that both the conductor and the floating object had several sharp points on them.

4.1.5 Test Set Up - Corona Current and Induced Voltage Measurement:

The test set up for the corona current and induced voltage measurement is shown in figure 4.1. The pole conductor is energised via the DC supply (Vi) and the leakage current to ground is measured using a HV probe that has an input resistance of 1000 MΩ. The leakage current is obtained by connecting the HV probe through an ammeter to ground. The Fluke HV probe that was used can measure up to 40 kV AC/DC (model Fluke 80K-40). The voltage induced on to the floating object is measured using a Fluke multimeter (model Fluke 189) via the Fluke HV probe. The corona current can be measured directly by using the HV probe via the multimeter to ground or by connecting the HV probe outputs to the Picoscope (oscilloscope).
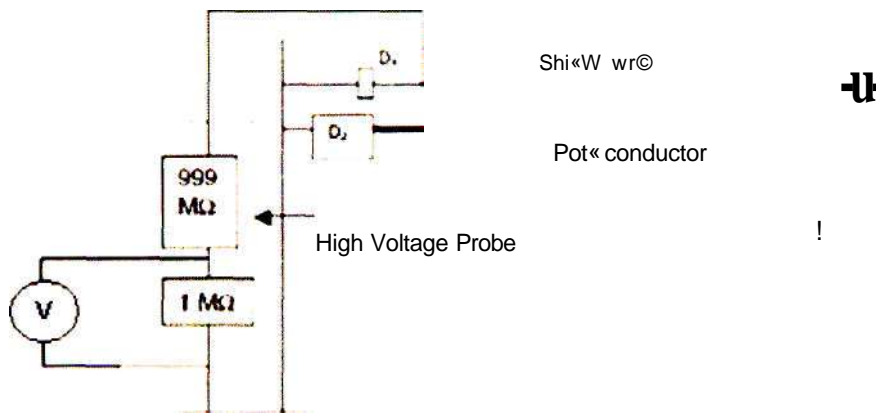
Figure 4.1: Induced Voltage - Measurement Circuit [24]

4.2 ION CURRENT DENSITY MEASUREMENT:

The current density measurements were conducted under the test line in the HVDC laboratory. The large Wilson plate was used for the measurements. The results of the small Wilson plate were not stable (the measurement continuously fluctuated) and hence only the large plate was used. The first set of tests conducted with the large plate and the guard rings had huge fluctuations and was very unstable. The measurement (current) would stabilise and then sudden fluctuations would occur. We assumed that these fluctuations were caused by the space charge and atmospheric conditions. The results were recorded and plotted. The Wilson plate arrangement for the initial tests is shown in figure 4.2. The test parameters for the Wilson plate was as follows: Wilson plate (2 meters x 0.5 meters), guard rings (0.25 meters x 0.5 meters), insulators (height = 2 cm), distance between guard ring and plate = 10 cm.

Pole Conductor

HIr   *U\-*

Guard Band
(Grounded)-   Current Sensing
                                                        Surface

insulators   J-II   T   'II T

                        (T) Electrometer

Figure 4.2: Wilson Plate Arrangement

4.2.1 Calibration of Pico Ammeter and Pico Scope:

In order to verify the accuracy of our equipment and measurements, a quick calibration test was conducted. Both the pico ammeter (Keithly) and the Pico scope were tested. The circuit that was used for the calibration is shown in figure 4.3. Three resistors of known resistance were connected in series to make up R. Rf is the internal resistance of the measuring instruments (picoscope and pico ammeter). A DC voltage was applied by using a small variable DC supply. The output of the DC supply (V) was also verified by using a calibrated multimeter. The output voltage (V_0) of the calibration circuit was measured by using a second calibrated multimeter. V_0 was also calculated by using the voltage divider rule and this result was compared to the measured output. The test results found that the pico ammeter was inaccurate (measured values could not even be compared to the calculated values) or even damaged. The results showed that the Pico scope measurements were very accurate (99.7 % accuracy - refer to page 45 for calculation of accuracy).
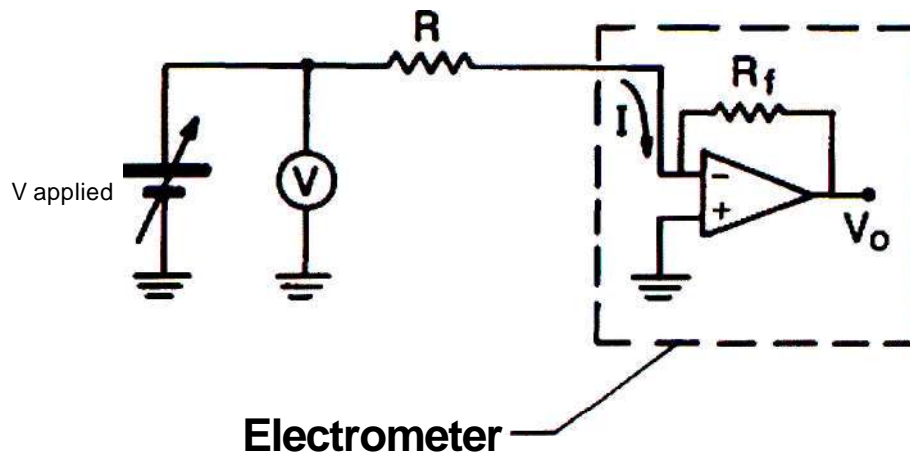
Figure 4.3: Pico Scope Calibration Circuit [2]

R = 328,8 k£2 x 3 (three known resistors in series) = 986,4 kQ

R_f (internal resistance) = 1 MQ

1) **Testl**

Vapplied = 1.0975 V, Vo (measured) = 544 mV, Vo (calculated) = 544.9 mV (99.83%)

2) **Test 2**

Vapplied = 1.578 V, Vo (measured) = 784.8 mV, Vo (calculated) = 783.6 mV (99.84 %)

3) **Test** 3

Vapplied = 0.4925 V, Vo (measured) = 245.6 mV, Vo (calculated) = 244.1 mV (99.4 %)

Average Accuracy = (99.8 % + 99.8 % + 99.4 %) / 3 = 99.7 %

4.2.2 Ion Current Density Measurements - Elevated Earth Plane:

Due to the fluctuations in the initial tests of current density, it was decided that the earth plane be elevated flush with the Wilson plate. The height of the JCI electrostatic field meter is 18 cm and hence it was decided to elevate the earth plane to 18 cm above ground. The new test set up helped improve the stability (the readings on the measurement equipment had stopped fluctuating) of the measurements. The improvement was immediately seen as the measured values for all test ranges were stable. The original Wilson plate arrangement is shown in figure 4.4 while the Wilson plate with the elevated earth plane is shown in figure 4.5.
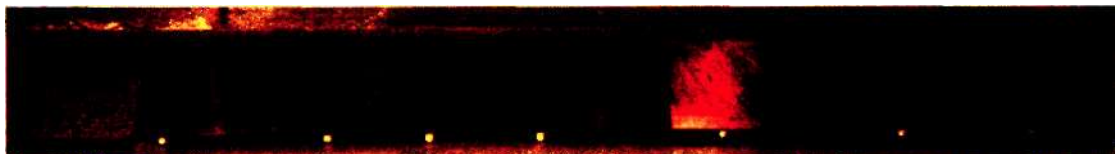
Figure 4.4: Original Wilson Plate Arrangement - Flush with Ground Plane

Figure 4.5: Wilson Plate Flush with Elevated Ground Plane

4.3 VOLTAGE MEASUREMENT – JCI ELECTROSTATIC FIELD METER:

A JCI Electrostatic Voltmeter was used to measure the voltage at ground level. The meter measures the voltage 10cm above the sensing aperture of the meter. According to the information supplied by JCI, a 0.001 (ImV) reading on the voltmeter equates to 23 V/m in terms of field strength, 10cm above the sensing aperture. The test set up is shown in figure 4.6.

Pole Conductor

/^A

18 cm

Electrostatic Field Meter

/   /   /   /   /   /   /   /   /   /   /   /   /

Figure 4.6: Electrostatic Voltmeter - **Measurement Set Up**

With the elevated earth plane, a portion of the plane was cut out for the aperture of the voltmeter. This was done so that the electrostatic voltmeter was flush with the earth plane and Wilson plate. The elevated earth plane can be seen in figure 4.7.

Figure 4.7: Field Mill Aperture - Elevated Earth Plane

4.4 ION CURRENT AND VOLTAGE MEASUREMENT - WITH METAL GRID SCREEN INSTALLED:

The measurements of ion current density and electric field, with an elevated earth plane, showed much more stable results. The waveforms of these measurements showed that there was a 50 Hz component in the measured results. A discussion regarding this 50 Hz component led us to believe that there was some coupling from the AC transformer (in the generator circuit) into our measuring circuit. We looked at two different types of coupling circuits (inductive and capacitive) to try to explain what was causing this coupling. It was then decided that we needed to shield our measuring circuit from the AC transformer. This was done by using ferrite chokes, double screened co-axial cable and a metal grid screen. The metal screen grid that was added into the circuit is shown in figure 4.8.

The measuring circuit and procedures remained the same except that the shielding equipment was added into the circuit one at a time to verify their effect. A ferrite choke was connected onto both input signals into the Pico scope. We then made up a metal wire grid that was two meters wide and three meters high. This metal screen was mounted in front of the AC transformer and it was strung from the roof of the laboratory. The metal screen was high enough and wide enough to block the coupling from the AC transformer. Measurements with a grounded and an ungrounded metal screen were carried out. The metal screen was used to try to reduce the capacitive coupling effects. In order to reduce the inductive coupling effects, we decided to use double screened co-axial cable (RG 223).

The metal screen was found to be very effective in reducing the AC component that was found in the ion current measurement. The results of the effect of the metal screen are shown in figure 5.16. The AC current measured by the Wilson plate is almost zero at 55 kV AC applied voltage (220 kV DC on test set output). At 65 kV AC (260 kV DC), the AC component that is measured with the screen grounded is reduced by 73 %. It should also be noted that the AC component that is in the ion current measurement is very small (negligible) as compared to the DC component.
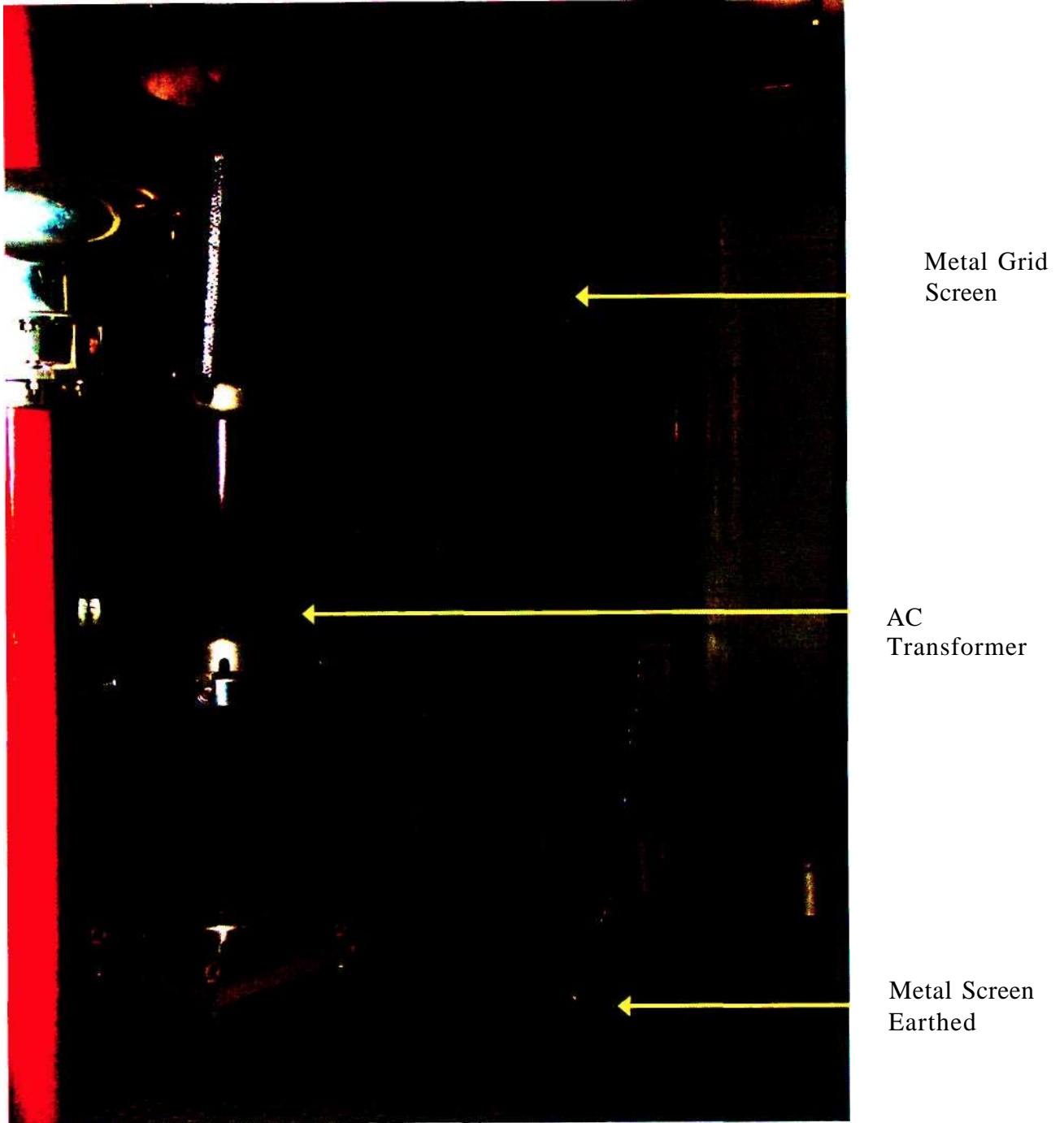
Figure 4.8: AC Transformer with Metal Grid Screen

4.5 ELECTRIC FIELD MEASUREMENTS:

The electric field below the laboratory test line was measured using a Monroe Portable Electrostatic Fieldmeter (257D). The technical data and specifications of the field meter were discussed in chapter 3. The Monroe field meter is made up of the main measuring instrument and a field probe. The probe is placed directly below the test line for measurements.

4.5.1 Calibration of the Monroe Electric Fieldmeter:

The fieldmeter was first tested for calibration before it was utilised in the laboratory. This was done by using the calibration circuit that was discussed in chapter 3. The probe is placed in a known electric field and this is compared to calculated values. Initially the measurements were not comparable; this was due to a poor ground plane. An earth plane was then made up and the results looked more stable (there were no sudden fluctuations in the readings). The set up for calibration of the fieldmeter can be seen in figure 4.9.
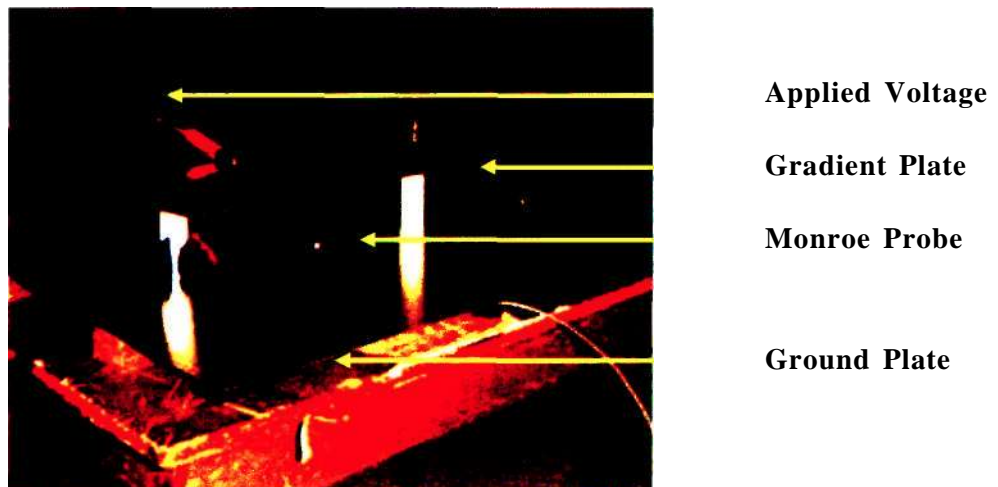
Figure 4.9: Fieldmeter Calibration - Test Set Up

4.5.2 Measuring the Electric Field - Monroe Electric Fieldmeter:

The electric field below the laboratory test line is measured with the Monroe Electric Fieldmeter. The probe was placed directly under the test line. The probe was in the same earth plane as the JCI voltmeter and the Wilson plate. This can be seen in figure 4.10. The Monroe measuring instrument was found to be unstable (the readings would fluctuate from an expected value to a much lower value) under high electric fields and hence, it was placed into a grounded metal cage which significantly improved the stability of the instrument. The high electric fields within the laboratory seemed to be affecting the measuring capabilities of the Monroe Fieldmeter.

The Monroe Fieldmeter has two ranges and we utilised the 20kV7cm range. With the applied voltage at zero, the Monroe fieldmeter was zeroed. Voltage was then applied to the pole conductor in lOkV increments up to +280 kV (positive polarity tests were conducted first). The reading on the Monroe instrument was then recorded. This test was conducted for a plain pole conductor and a damaged pole conductor (nails on the pole conductor). This was done to verify the effect of corona and space charge on the electric field at ground level. The output of the

Monroe fieldmeter and the JCI voltmeter were also monitored using the Pico scope. The relationship between the Monroe measurement and the JCI measurement was found to be fairly linear. The results of the calibration tests are shown in chapter 5 (figure 5.18).
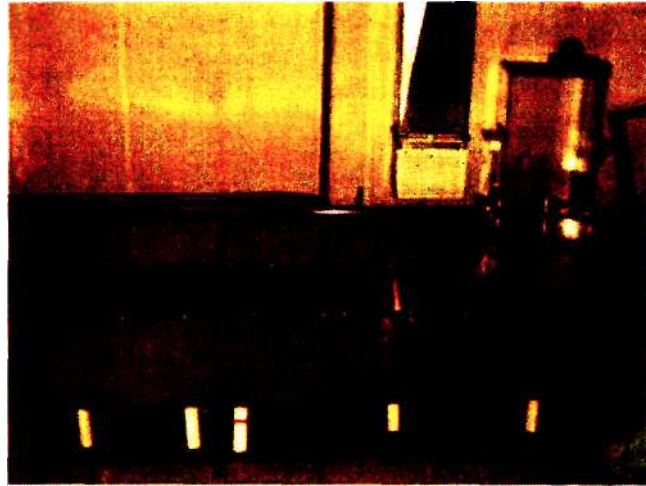
Figure 4.10: Electric Field Measurement - Test Set Up

CHAPTER 5

RESULTS

In this chapter, the results of all the tests that were conducted are presented. The first laboratory tests started in February / March 2006. The tests were conducted at the HVDC Centre at the University of Kwazulu Natal. The main focus of the initial tests was to compare the coupling to a floating shield wire between the negative and positive polarity. This was done by measuring the voltage that was induced onto the shield wire as well as the leakage current to ground from the shield wire. More tests were conducted in 2007 using a Wilson plate to measure the current density. The voltage at ground level under the line was measured using an electrostatic field meter and the electric field is also measured using a field mill. Field measurements were also conducted under the Cahora Bassa line.

5.1 RESULTS OF INDUCED VOLTAGE AND LEAKAGE CURRENT MEASUREMENTS:

Abbreviations and Definitions:

PP - Plain pole conductor (no corona sources applied)
PS - Plain shield wire (no corona sources applied)
NP - Nails on pole conductor (corona sources applied)
NS - Nails on shield wire (corona sources applied)
ABSOLUTE - Absolute value of negative measured and applied voltages (figure 5.5 - 5.8)

5.1.1 Positive Polarity:

•Induced Voltage pp and ps -'—Induced Voltage, pp and ns

'Induced Voltage, np and ns -"-Induced Voltage, np ps
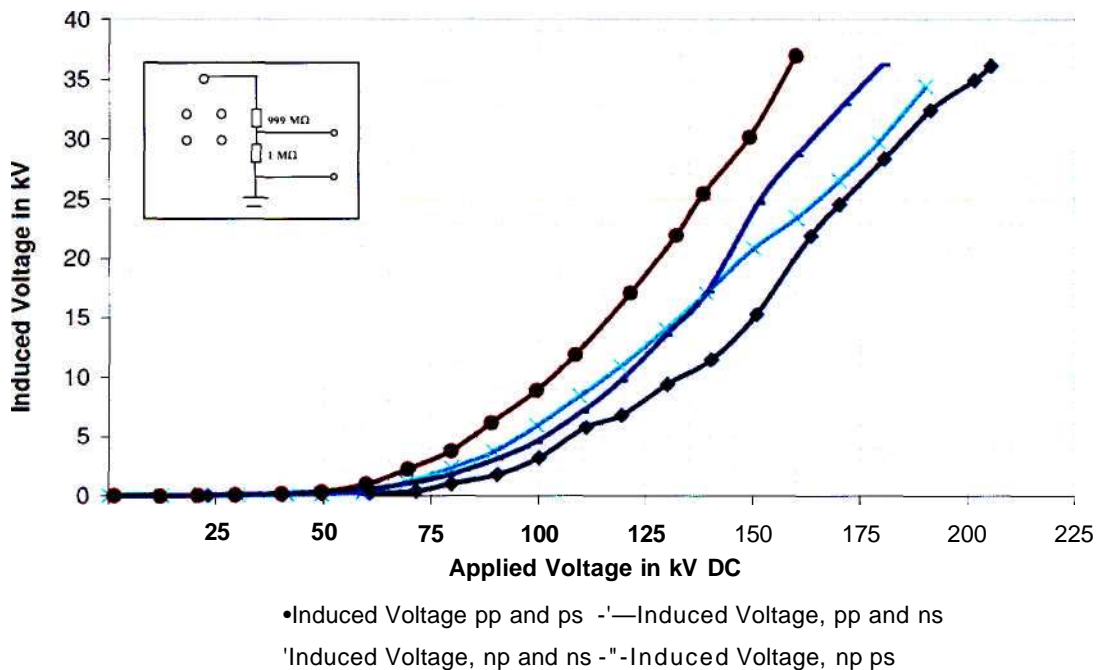
Figure 5.1: Induced Voltage versus Applied Voltage (+ ve)
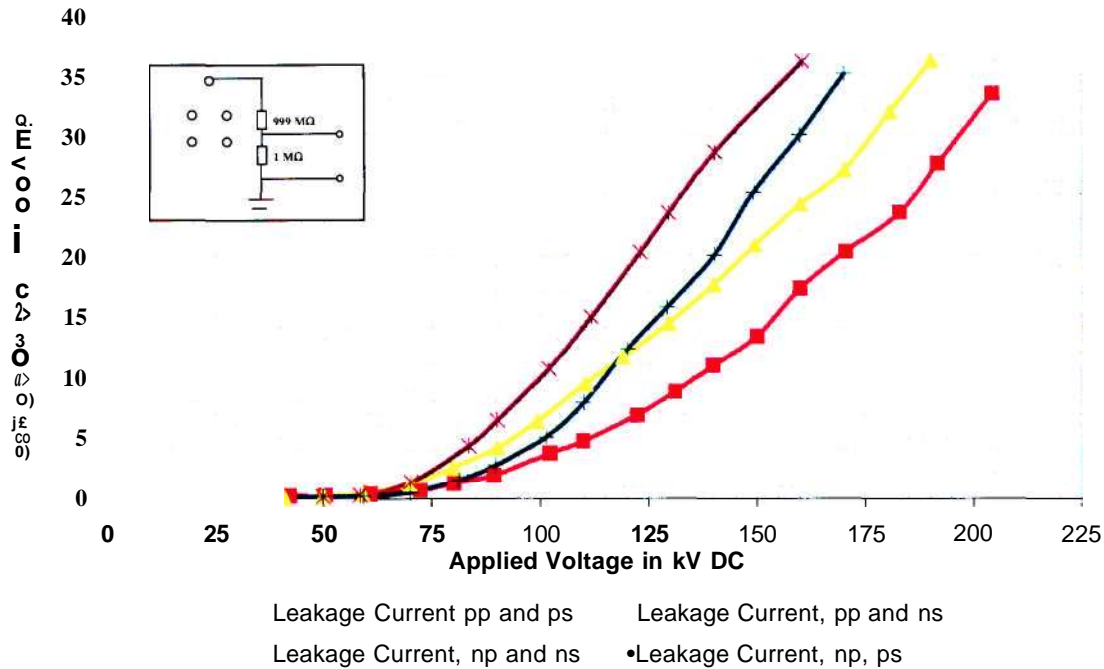
Figure 5.2: Leakage Current versus Applied Voltage (+ ve)

Leakage Current pp and ps   Leakage Current, pp and ns

Leakage Current, np and ns   •Leakage Current, np, ps

5.1.2 Discussion of Results - Positive Polarity:

From figures 5.1 and 5.2, it is clear that the inception voltages for each of the four test set ups differ from one another. When there are no corona sources applied to the pole conductor, the inception voltage is about 75 kV. When corona sources are applied to the pole conductor, the inception voltage is much lower at 55 kV. This is due to the pole conductor going into corona at a much lower voltage because of the sharp corona sources that were attached to it. This causes more corona and hence more space charge.

The highest induced voltages and leakage currents are measured when corona sources are applied to both the pole conductor and the shield wire. This implies that when the pole conductor is in corona, more space charge is created and this causes higher induced voltages and leakage currents. One should also take notice that the maximum induced voltage (37.5 kV) is reached at 170 kV applied voltage when there are corona sources on both the pole conductor and shield wire. The induced voltage measurement is limited to 40 kV as this is the maximum voltage that the HV probe can withstand. When there are no corona sources, the maximum voltage that can be applied is 210 kV (36 kV induced voltage). This clearly shows how the applied voltage is limited by the effect of the corona sources.

For voltages below 140 kV, it is noticed that the induced voltage is lower when only corona sources are applied to the pole conductor as compared to having only corona sources on the floating object. Above 140 kV, the induced voltage with only corona sources on the pole tends to dominate.

The lowest levels of induced voltages and leakage currents are measured when there are no corona sources present.

Negative <u>Polarity:</u>

- •Induced Voltage, pp, ps   Induced Voltage, pp, ns
- •Induced Voltage, np. ns   •Induced Voltage, np, ps
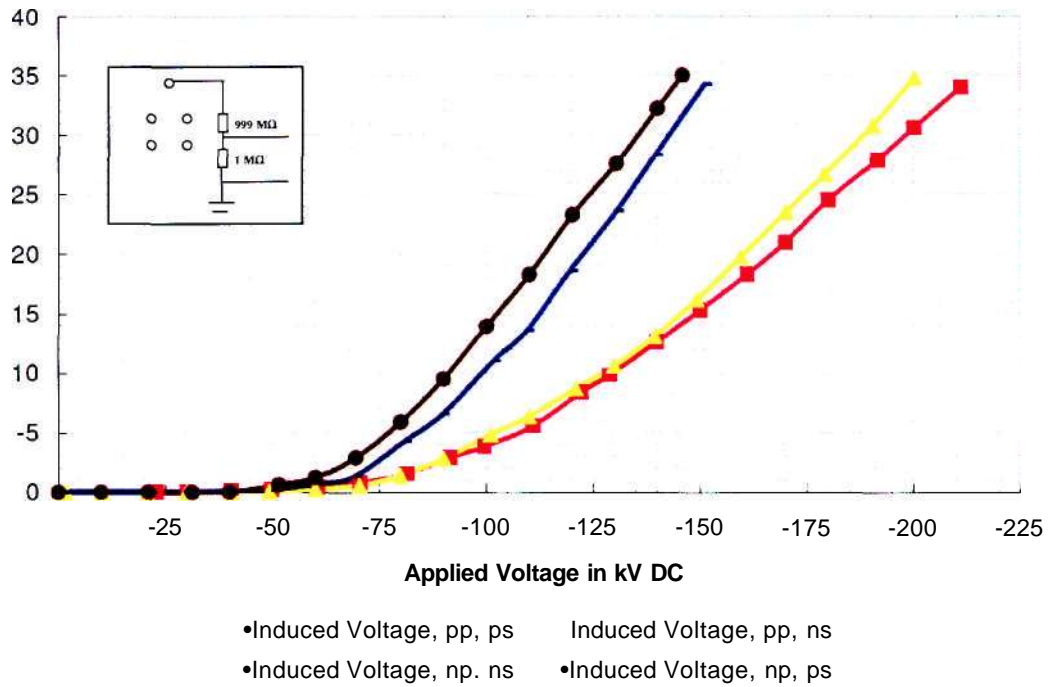
Figure 5.3: Induced Voltage versus Applied Voltage (- ve)

Leakage Current, pp, ps   •Leakage Current, pp, ns
Leakage Current.np, ns   •Leakage Current, np, ps
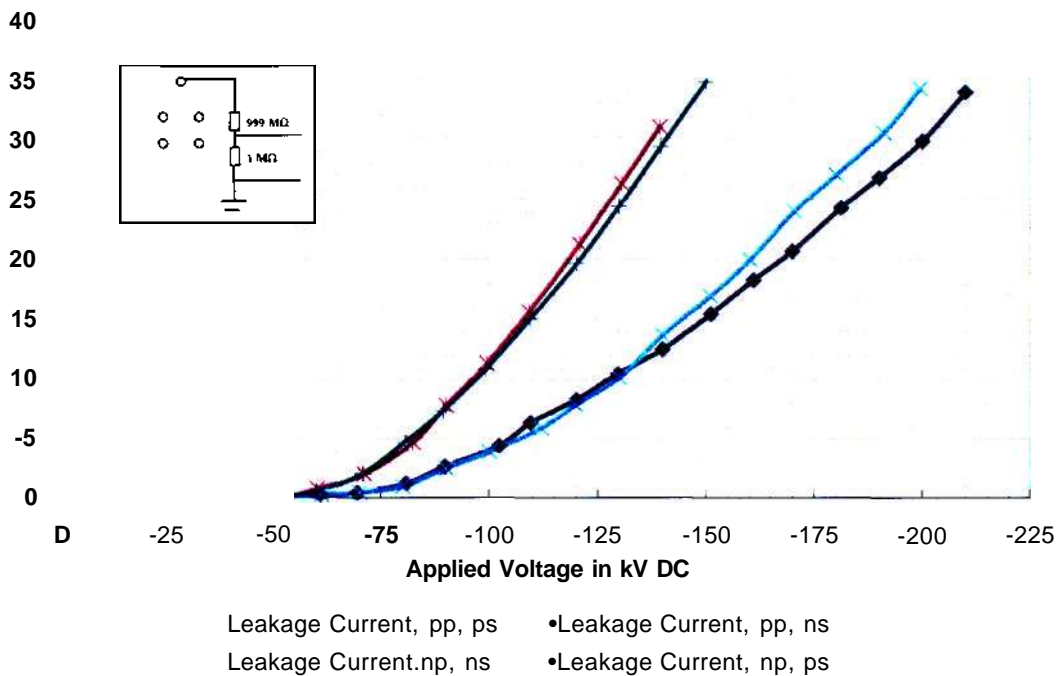
Figure 5.4: Leakage Current versus Applied Voltage (- ve)

5.1.4 Discussion of Results - Negative Polarity:

From figures 5.3 and 5.4, it is clear that the inception voltages for each of the four test set ups differ from one another. When there are no corona sources applied to the pole conductor, the inception voltage is about 70 kV. When corona sources are applied to the pole conductor, the inception voltage is much lower at 50 kV. There is a distinct difference for the negative results when corona sources were applied to the pole conductor as compared to when no corona sources were applied.

The induced voltages and leakage currents measured are only marginally higher when corona sources are applied to both the pole conductor and shield wire as compared to when corona sources are only applied to the pole conductor. This shows us that when a pole conductor is in corona, the induced voltages and leakages currents to ground are much higher. In terms of ionic coupling to the floating object, it is very clear that having corona sources / corona on the pole conductor creates the highest levels of coupling. The curves are a lot more linear when they are compared to the results for positive polarity. The applied voltage is limited to 145 kV (corona sources applied) as compared to 220 kV (no corona sources applied).

5.1.5 Comparison of Results - No Corona Sources:

Negative • Positive Pole Comparison

-*-Voltage, PP, PS, Pos -•-Voltage, PP, PS, Neg
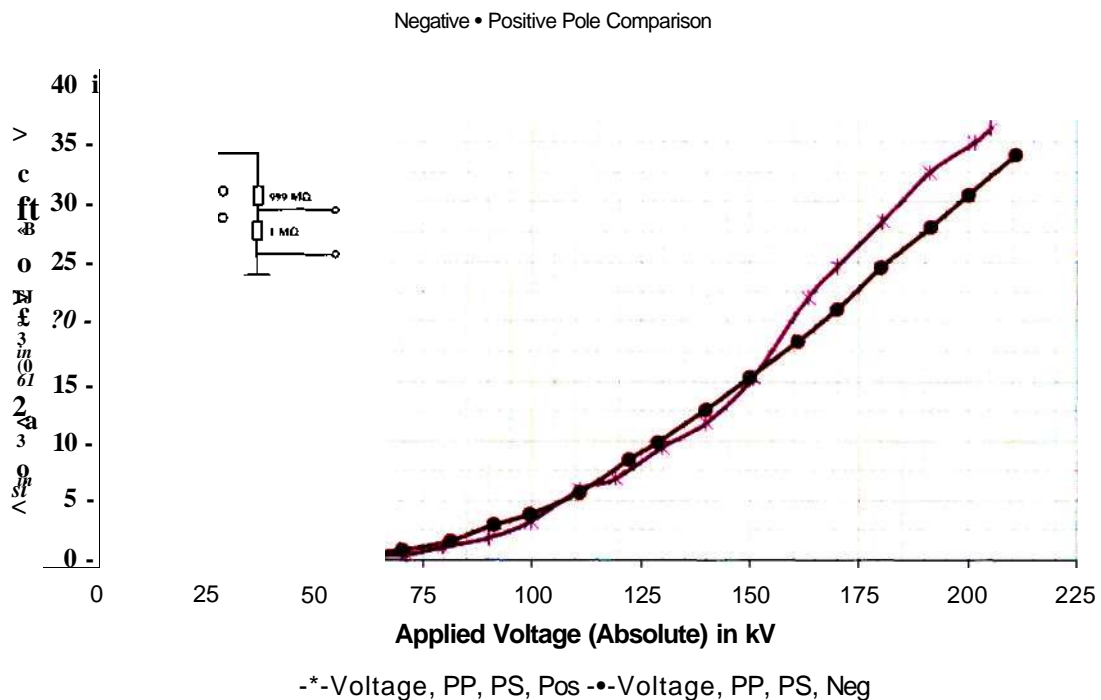
Figure 5.5: Induced Voltage - Positive versus Negative (PP PS)

5.1.6 Discussion of Results - Positive versus Negative (PP PS):

The results in figure 5.5 show that there is not much difference in the levels of induced voltage between positive and negative applied voltage. The positive induced voltage is marginally higher than the negative induced voltage above 150 kV. The positive polarity shows a sharp rate of increase above 150 kV applied voltage while the negative is fairly linear. It seems that the shield wire itself is going into corona above 150 kV (-ve) and this is causing space charge to be generated between the pole conductor and the shield wire.

5.1.7 Comparison of Results - Corona Sources Applied to Shield Wire:

Negative - Positive Pole comparison
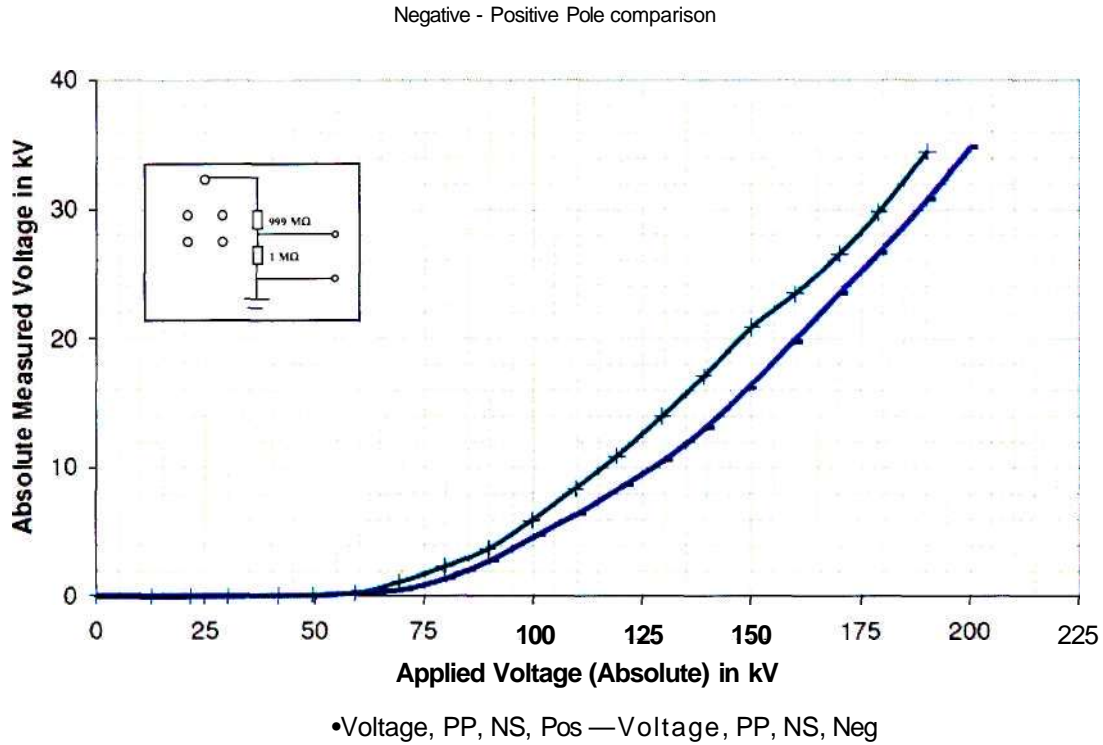
Figure 5.6: Induced Voltage - Positive versus Negative (PP NS)

5.1.8 Discussion of Results - Positive versus Negative (PP NS):

The results in figure 5.6 show that the inception voltage is about the same for both the positive and the negative. The induced voltage for the positive is marginally higher (about 2kV) than the negative across the applied voltage range. Here it is seen that the negative induced voltage is more linear than the positive induced voltage. What is also strange is that this is the only case where the positive induced voltage dominates over the negative induced voltage. This could suggest that when considering coupling at ground level, one can expect higher induced voltages on sharp objects below the positive pole. This result was also very repeatable as well because this test was repeated to verify this finding.

5.1.9 Comparison of Results - Corona Sources Applied to Pole Conductor:

Negative - Positive Pole comparison
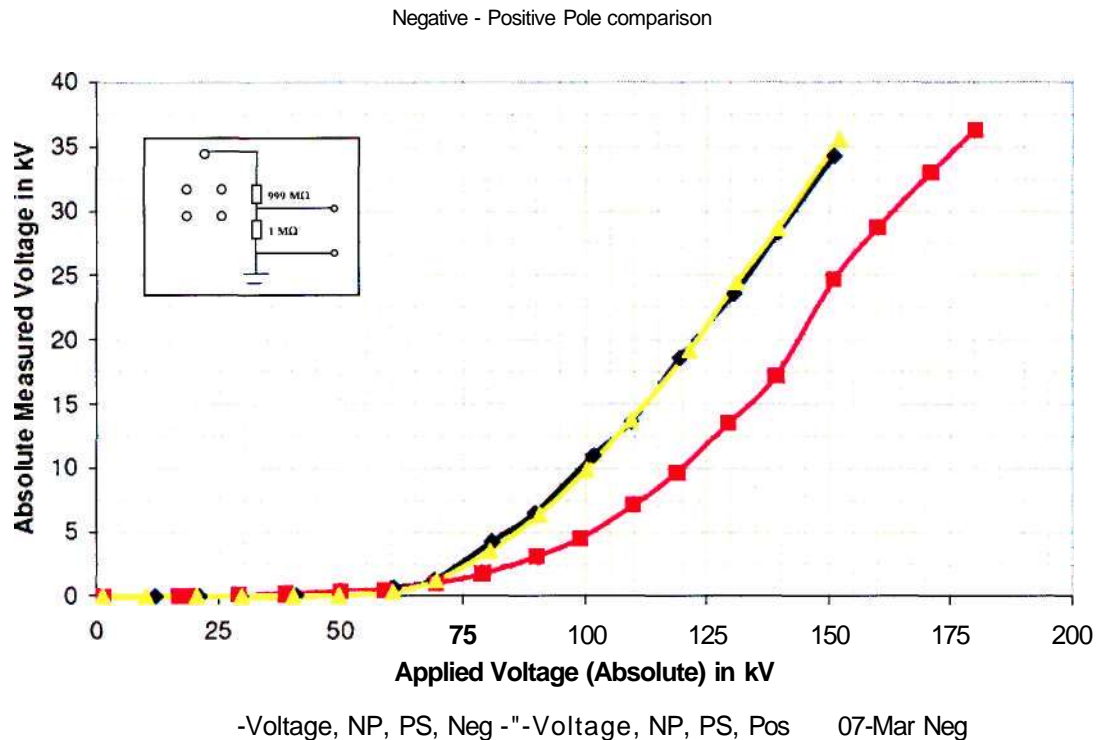
Figure 5.7: Induced Voltage - Positive versus Negative (NP PS)

5.1.10 Discussion of Results - Positive versus Negative (NP PS):

The results in figure 5.7 show that there is a large difference (greater than 5 kV) between the measured induced negative and positive voltages. The negative induced voltage is about 10 kV higher than the positive induced voltage for applied voltages greater than 125 kV. Their inception voltages are almost the same (70 kV) but the measured negative induced voltage tends to rise a lot faster than the measured positive induced voltage. A second set of tests were undertaken for the negative induced voltages and these results are almost identical.

The results also show that the ionic coupling for the negative case is much higher than the positive. It tends to imply that the positive pole can be operated at a much higher (25 kV higher than the negative pole for 35 kV induced voltage) voltage than the negative pole for the same levels of coupling.

5.1.11 Comparison of Results - Corona Sources Applied to Pole Conductor and Shield Wire:

Negative - Positive Pole comparison

Voltage, NP, NS, Neg •"——Voltage, NP, NS, **Pos**
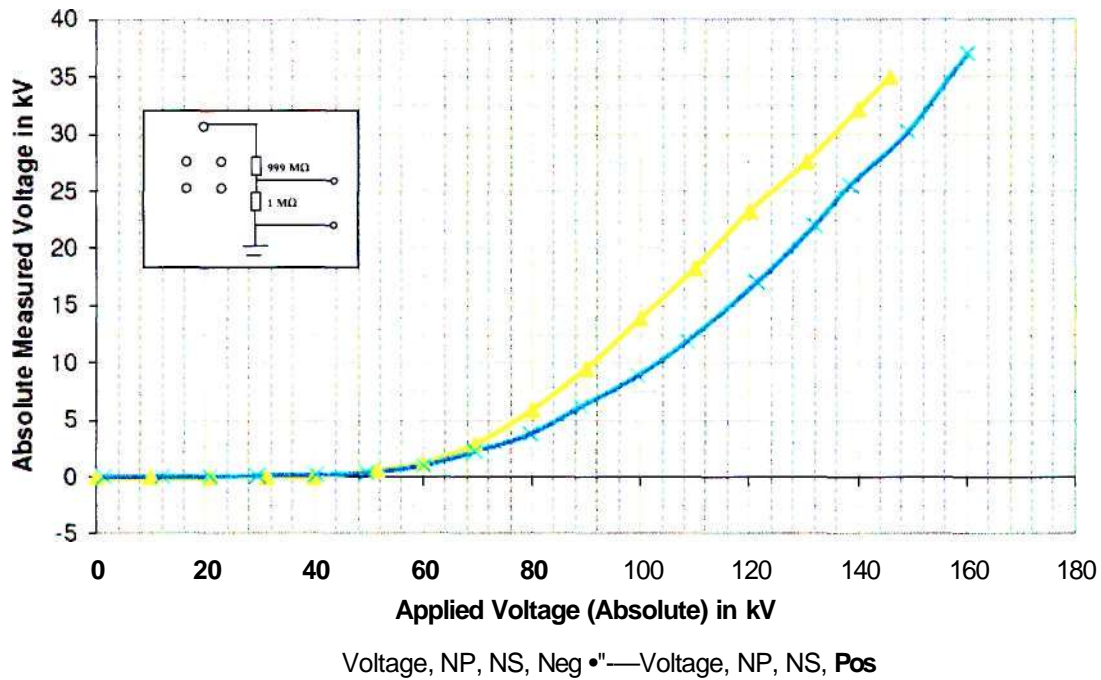
Figure 5.8: Induced Voltage - Positive versus Negative (NP NS)

5.1.12 Discussion of Results - Positive versus Negative (NP NS):

The results in figure 5.8 show that the induced voltage for the negative applied voltage is higher than that of the positive. It also shows that their inception voltages are about the same. When corona sources are applied to the pole conductor, the ionic coupling for the negative case is always higher.

From figure 5.6, the positive induced voltage was higher than the negative when corona sources were only applied to the shield wire. Here it can be seen that even though the negative induced voltage is higher than the positive induced voltage, the voltage difference has been reduced when comparing it to figure 5.7. This shows that the positive induced voltage has indeed increased when coupling to sharp objects at ground level. The difference between the negative and positive induced voltage above 100 kV is about 5 kV, as compared to 10 kV previously.

5.2 RESULTS OF ION CURRENT MEASUREMENTS - NEGATIVE POLARITY:

The results of tests conducted in January 2007 are discussed in this section. These tests were conducted above the earth plane and under negative polarity. The test that was conducted was the measurement of ion current density using the Wilson plate.

Figure 5.9: Ion Current Measurement - Negative Polarity

From figure 5.9, it can be seen that there is a huge difference (220 % higher at 260 kV) in the ion current measured when there are corona sources on the pole conductor as compared to when there are no corona sources present. The results also show that there is very little difference in the ion current measured when the guard plates are grounded or ungrounded. The measured current is slightly higher when the guard plates are grounded and this is due to the elimination of fringing effects. The inception voltage is also a lot lower (100 kV) when there are corona sources on the pole conductor as compared to when no corona sources are applied (175 kV).

The results tend to indicate that the ionic coupling to ground is a lot higher (5.5 micro amps as compared to 2.5 micro amps at 260 kV applied voltage) when the pole conductor is in corona. This could also mean that the current path between the conductor and ground has now become more conductive. This could be due to the corona generated space charge and higher ion densities beneath the pole conductor.

Figure 5.10: Ion Current Measurement - Raised Wilson Plate

Figure 5.10 shows the results of the ion current measurement with the Wilson plate raised up from ground plane with an elevated earth plane. This result is compared to the ion current measurement when the Wilson plate was at ground level but without a full earth guard ring. The results show that the ion current is slightly higher when the Wilson plate is in the ground plane. The lowered Wilson plate was slightly (3 cm) above ground and it also did not have an elevated earth plane. This resulted in an average measuring error of 10 %. This does not necessarily mean that the ion currents are higher at ground level as this could be due to measurement errors (fringing effects) with the Wilson plate when taking measurements above the ground plane. From figure 3.3 we understand why the current is slightly higher and we also verify that we can expect errors up to 10 % when we refer to figure 3.4.

For the ion current measurement with the low Wilson plate, one must remember that the Wilson plate was still about 3cm above the ground plane (this was due to insulator height). For the raised Wilson plate (20 cm above ground); the current is lower as we are reading the actual current because the fringing effects were eliminated by using an elevated earth plane.

5.3 RESULTS OF ION CURRENT AND ELECTRIC FIELD MEASUREMENTS - RAISED EARTH PLAP

The results of tests conducted in February 2007 are discussed in this section. These tests were conducted using a raised earth plane. The earth had to be raised because the JCI field mill stands 18 cm from the ground. In order to obtain accurate measurements, the ground plane was raised to this height. The results of the ion current and electric field measurements are shown in figure 5.11 and 5.12. The tests were conducted under negative polarity.
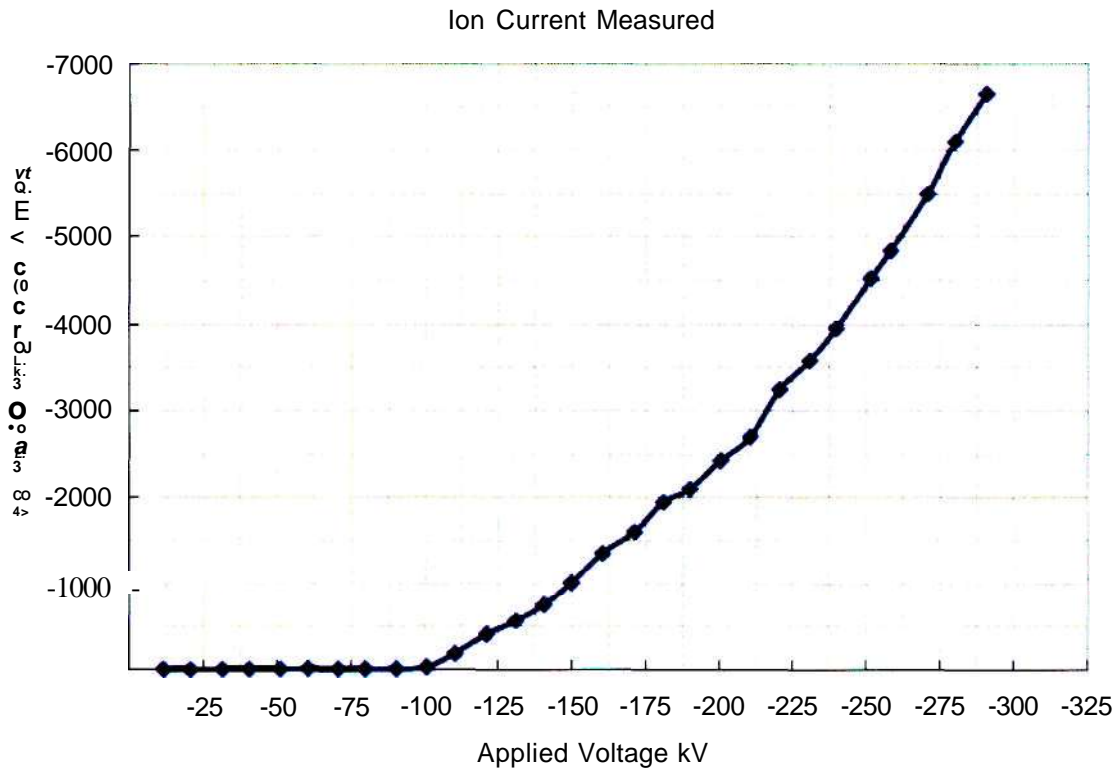
Figure 5.11: Ion Current Measurement - Raised Earth Plane

Figure 5.11 shows the results of the measurement of ion current with the earth plane raised to 18 cm. The results show that the current measured is the same as in figure 5.10 for the raised Wilson plate. This shows us that our results are repeatable and that the new earth plane is very effective. It can also be seen how this result compares to the Wilson plate measurement (figure 5.10 - yellow curve) without a raised earth plane. This clearly indicates that the difference in the current measured in figure 5.10 is due to a measurement error when taking Wilson plate measurements above ground.

One should take note that the inception voltages (figure 5.10 and 5.11) are the same (100 kV). When comparing figures 5.10 & 5.11 to figure 5.12, it is noticed that the voltage that is measured at ground level using the JCI field mill is proportional to the current measured from the Wilson plate (above 100 kV). This shows that there is good correlation between the measured voltage and measured ionic current at ground level.
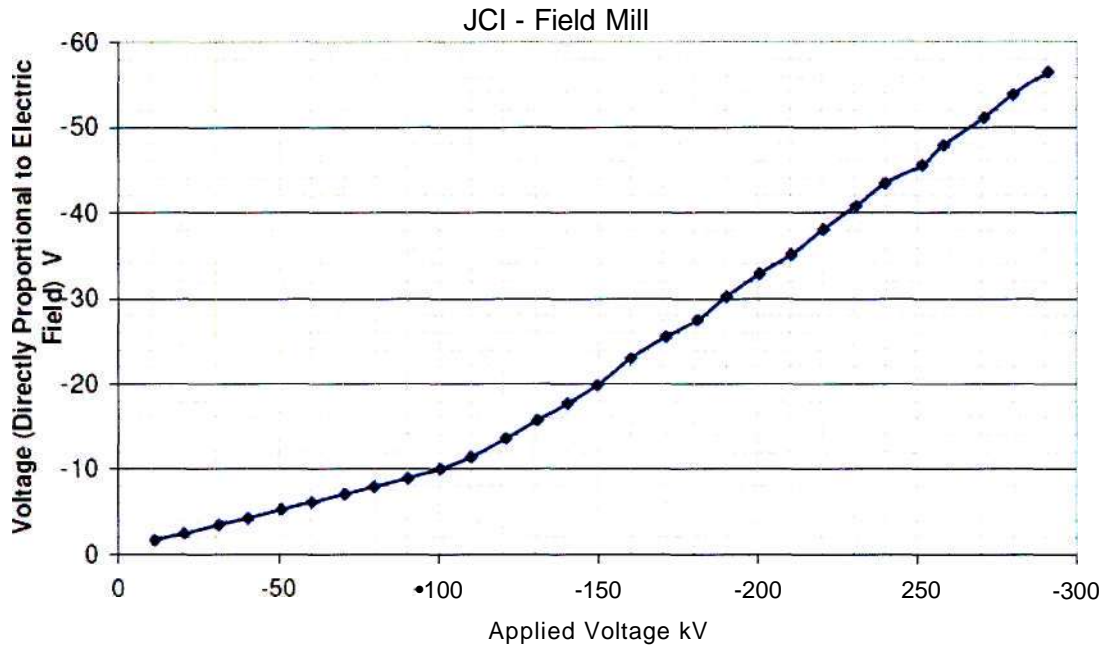
Figure 5.12: Voltage Measurement - Raised Earth Plane

The voltage at ground level directly below the pole conductor was measured using the JCI static monitor. The results of the measurements are shown in figure 5.12.These measurements were taken with the raised earth plane and a small cut out was made in the earth plane for the JCI aperture. The results show a linear relationship between the applied voltage and the measured voltage. It is further observed that the gradient of the linear relationship becomes a lot steeper above 100 kV. Comparing this to previous results, it is noted that the inception voltage for these measurements was about 100 kV, hence the sudden change in slope. The electric field at ground level is proportional to the voltage measured using the JCI static monitor. Comparing this result to figures 5.9 and 5.11, it is noticed that the ion current started to increase rapidly from approximately 100 kV. This could possibly be due to corona inception which was causing more space charge to be produced and hence the ionic currents and electric field at ground level are enhanced as well.

The JCI static monitor measures the surface voltage 100 mm above its field aperture. The output is given in voltage (V) and this needs to be converted into electric field (kV/cm). If we compare the results in figures 5.12 and 5.23, we are able to see the relationship between the JCI static monitor and Monroe fieldmeter measurements. The error between the measured values (Monroe) and the calculated values (JCI) increased as the voltage increased. The JCI gives the voltage 10 cm above its aperture (approximately 30 cm above ground if the height of the JCI static monitor is included) and this can be used to calculate the electric field at ground level. The electric field is calculated using figure 5.12 as follows:

E (-100 kV) = V/d = -10 kV / 0.3 m =   33.33 kV/m (Monroe = - 32 kV/m)
E (-150 kV) = V/d = -20 kV / 0.3 m =   66.66 kV/m (Monroe = - 60 kV/m)
E (-200 kV) = V/d = -32 kV / 0.3 m =   106.0 kV/m (Monroe = - 84 kV/m)
E (-250 kV) = V/d = -46 kV / 0.3 m = • 153.3 kV/m (Monroe = -110 kV/m)

Based on the error between the measured and calculated values of the electric field, and the fact that the JCI static monitor does not give the electric field (directly) as an output, no further tests were done using the JCI static monitor.

5.4 RESULTS OF ION CURRENT AND ELECTRIC FIELD MEASUREMENTS - POSITIVE POLARITY:

Measurements of ion current density and electric field were conducted in June 2007. The tests were conducted using the raised earth plane and under positive applied voltage. During these tests, several methods were used to try to eliminate the AC 50 Hz frequency component that was in the measured ion current. There seemed to be some electrostatic coupling between the AC transformer and the Wilson plate. The first method used was the application of ferrite chokes into the measuring circuit. Double screened co-axial cable was then used for the measurements and lastly a metal screen grid was installed in front of the AC transformer. The results of the tests for mitigation of the AC component in the ion current are shown in figure 5.13.

5.4.1 Mitigation of AC Component from Ion Current Measurements:
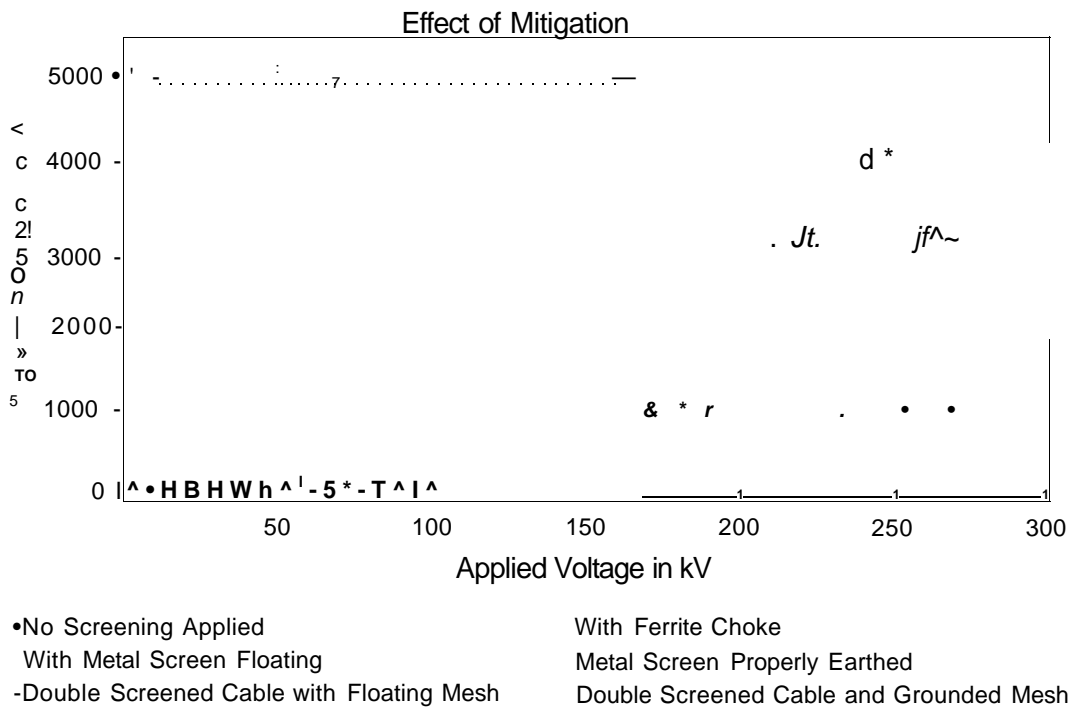
Figure 5.13: Effect of Mitigation of AC Current Component

Figure 5.13 shows the following results:

The ferrite chokes have no influence on the measurement.
The use of double screened cable for measurements has no effect.
The use of the floating metal screen grid in front of the AC transformer reduces the ionic current as it removes the AC coupling from the transformer to the Wilson plate.
The use of a grounded metal screen shows the best effect of mitigation. The AC component is reduced from the measurement but there was still some harmonic interference present. This can be seen in figure 5.14.

10

»
a
E
<
a
c
m
C
3

4«y»H --

• ^ X A $S**r*y$ $\textit{\underline{tffafr}}$ ***&Sr-Y+W)W-~¹-*^

Time (16ms diw)
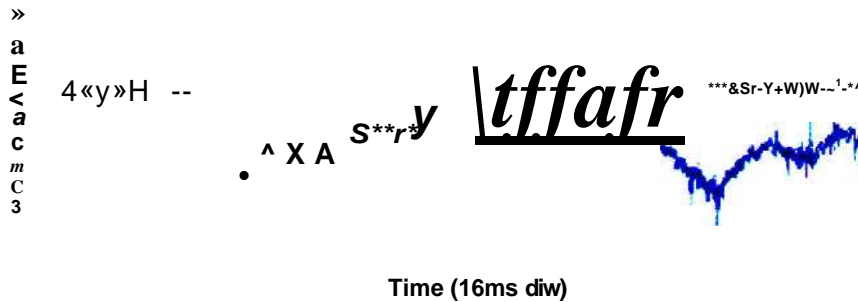
Figure 5.14: Current Waveform (blue trace) - Metal Screen Grid Grounded

5.4.2 Voltage Induced on Metal Screen Grid:

The AC voltage (with respect to earth) that was induced onto the floating metal screen grid was measured. Two measurements were taken. The first measurement was with the DC connection from the generator to the pole conductor and the second was without the DC connection. The results of the voltage measured on the screen are shown in figure 5.15.

Coupling between Mesh Screen and AC transformer

6 -

£

5 -

o

4 - ············ *jS* . -

O >
&

3 -

O

V O   **2 -**
0)
3 (A
CO
0)   **1 -**

0 - ^^—

10   **20**   **30**   **40**   **50**   **60**   **70**   **80**

Applied AC Voltage

With DC connected to line - " - N o DC connection
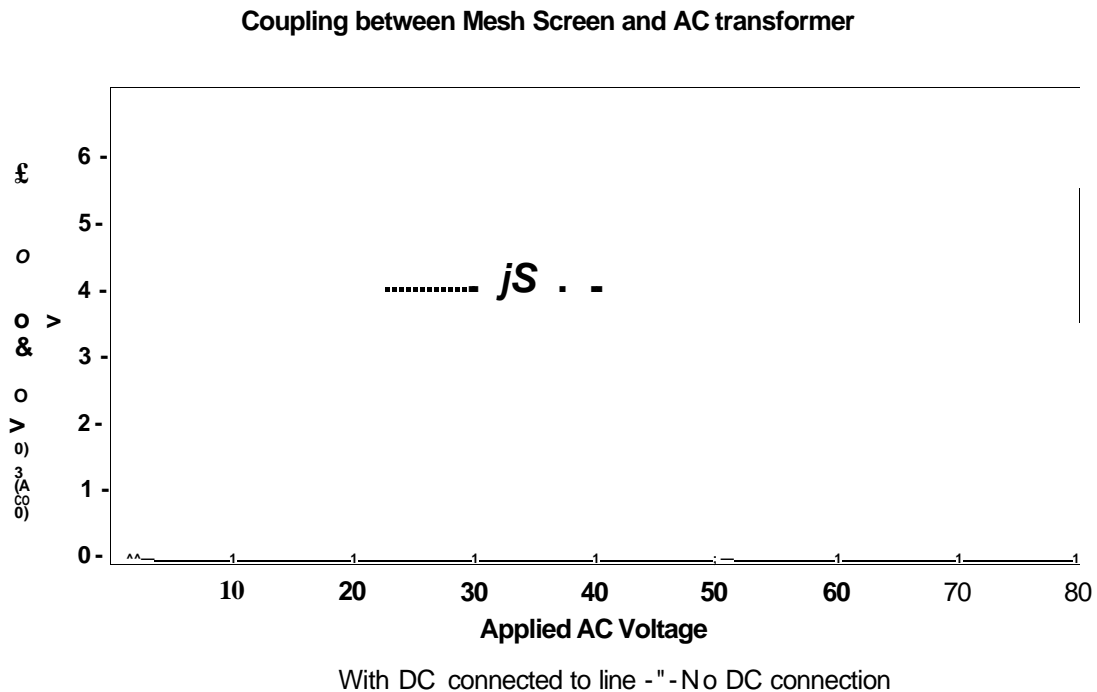
Figure 5.15: Voltage Induced on Metal Screen Grid

When the DC supply from the generator is connected to the pole conductor, the voltage on the screen is high. Without the DC supply connected, the induced voltage on the screen is lower as there is only coupling from AC transformer to the mesh. The reduction in voltage above 60kV applied voltage was due to the screen flashing to ground. The DC applied voltage is approximately 4 times the AC input voltage to the Cockroft Walton generator.

5.4.3 Wilson Plate Current - Only AC Transformer Energised:

The ion current induced on the Wilson plate was measured with only the AC transformer energised. This test was used to verify the effect of the AC component on the total current that was measured.
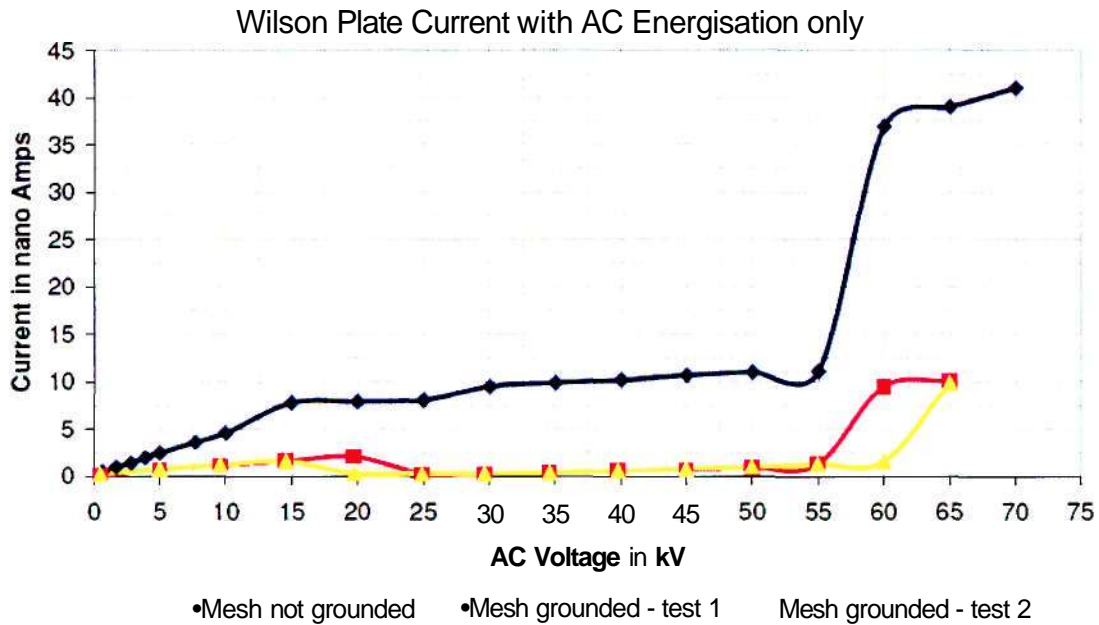
Figure 5.16: Wilson Plate Current - AC Transformer Energised

From figure 5.16 it can be seen that the AC current on the Wilson plate is about 45 nano Amps when the mesh screen is ungrounded. This explains the AC component that was found in the Wilson plate current measurements. With the mesh grounded, the AC component is reduced to almost zero (at 55 kV AC the Cockcroft Walton generator output is 220 kV DC). At 65 kV AC the current measured is 10 nano amps which is very small compared to the total current measured. The current waveform with the screen ungrounded is shown in figure 5.17.

Figure 5.17: Wilson Plate Current Waveform (blue trace) - Mesh Ungrounded

5.5 RESULTS OF ION CURRENT AND ELECTRIC FIELD MEASUREMENTS - MONROE FIELDMETER:

Measurements of ion current density and electric field were conducted in July 2007. These tests were conducted under positive polarity. The ion current measurements were repeated and the electric field measurements were now taken using a Monroe Electrostatic Fieldmeter (257D).

5.5.1 Calibration of Monroe Field Meter - Results:

Monroe Calibration

—^-Ftrst test 30 July 2007   ^ S e c o n d run

   Second run expected values   -»«. proper earth plane

•*-Proper earth plane expected values   -••First test expected values

Figure 5.18: Monroe Fieldmeter Calibration Tests

The results of the calibration tests for the Monroe Fieldmeter are shown in figure 5.18. The first test conducted shows that there is a large discrepancy (about 60 % error) between the measured values and the expected values. The expected values were calculated ($E = V/d$) using the IEEE 1227 standard for calibration. For the second test, there is an improvement in the percentage error as a make shift earth plane was used. For the third calibration test, a proper earth plate was made up. A flat piece of sheet metal was used for the earth plane and a circular cut out was made for the probe. This reduced the error between the measured and predicted values. The percentage error was reduced to approximately 10 %.

The errors between the measured values and calculated values are shown in figure 5.19. The error is calculated by looking at the percentage difference between the measured values and the expected (calculated) values. With a proper earth plane, the error between values has been reduced and is found to be between 10 - 14 %. This shows good improvement when compared to the first calibration test which had an average error of approximately 60 %.

The plates that were used for the calibration test were not according to the recommended IEEE 1227 dimensions. The calibration tests were unplanned and hence the plates that were used

were not cut correctly. It is believed that the error can be reduced to within 5 % if proper plates (dimensions according to IEEE 1227) are used for calibration of the Monroe Field Meter.

Percentage Error

Second run   Proper earth plane   •First test

Figure 5.19: Monroe Fieldmeter - Percentage Error

5.5.2 Results of Ion Current Measurements - Positive Polarity:

Positive Ion Currents

•^»No Nails -•-Nails on Pole

Figure 5.20: Ion Currents - Positive Polarity

Figure 5.20 shows the results of the ion currents that were measured under positive polarity. It shows that there is a large difference (420 % difference at 260 kV applied voltage) in the ion currents (beyond 100 kV applied voltage) measured when there are corona sources applied to the pole conductor as compared to when no corona sources are applied. This implies that a damaged or dirty conductor will go into corona at a much lower voltage as compared to a clean conductor as well as produce higher ionic currents for the same applied voltage. The ion current measured with corona sources applied is about 2.75 uA at 250 kV DC applied voltage.

5.5.3 Results of Electric Field Measurements - Positive Polarity:

Effect of Corona on Electric Field

-•-Nails on Pole -"-No Nails on Pole   Predicted —Linear (No Nails on Pole)
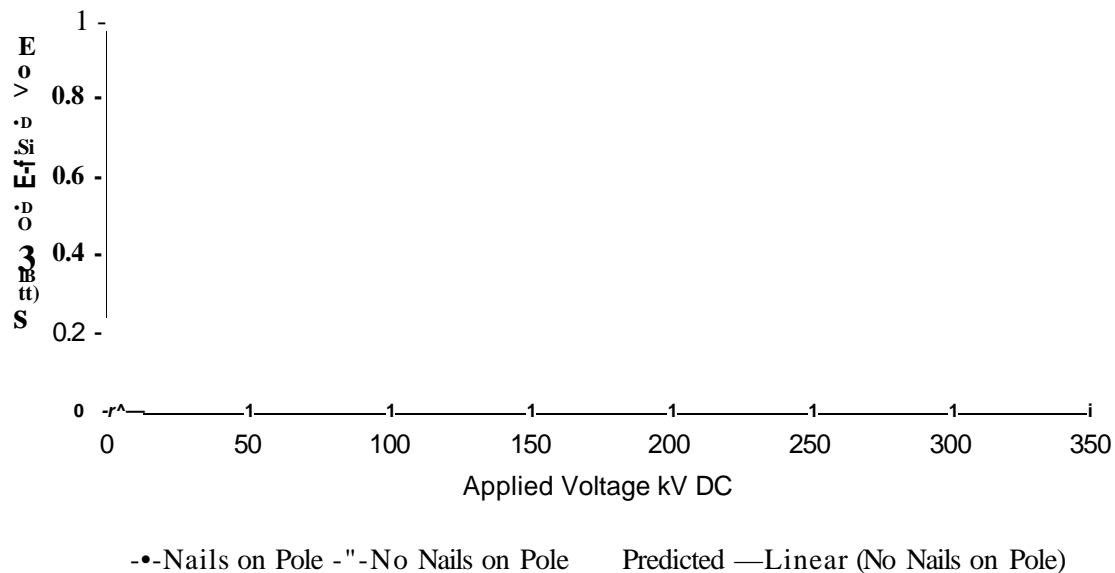
Figure 5.21: Electric Field - Positive Polarity

Figure 5.21 shows the results of the electric field measurements which were recorded simultaneously with the ion current measurements. From the results for the positive polarity, the following conclusions are made:

- The electric field is higher when corona sources are applied to the pole.
- At voltages below 150 kV, the measured values are very similar to the predicted values (electrostatic field).
- At voltages above 150 kV (above corona inception), the measured values are much higher than the predicted values.
- When linear curve fitting is applied to the corona free field, the measured values are virtually the same as the predicted values.
- It is also seen that the electric field is higher than the linear curve when corona sources are applied. This is due to the corona generated space charge which tends to enhance the electric field strength at ground level.
- From figures 5.20 and 5.21, one can see that applying corona sources has a more prominent effect on the ionic current than on the electric field.

5.6 RESULTS OF ION CURRENT AND ELECTRIC FIELD MEASUREMENTS - NEGATIVE POLARITY:

The measurements of ion current density and electric field at ground level below the laboratory test line were repeated in September 2007. These tests were conducted under negative polarity. The measurements were conducted using the same Wilson plate and Monroe Fieldmeter as used for the positive polarity.

5.6.1 Results of Ion Current Measurements - Negative Polarity:

Negative Ion Currents
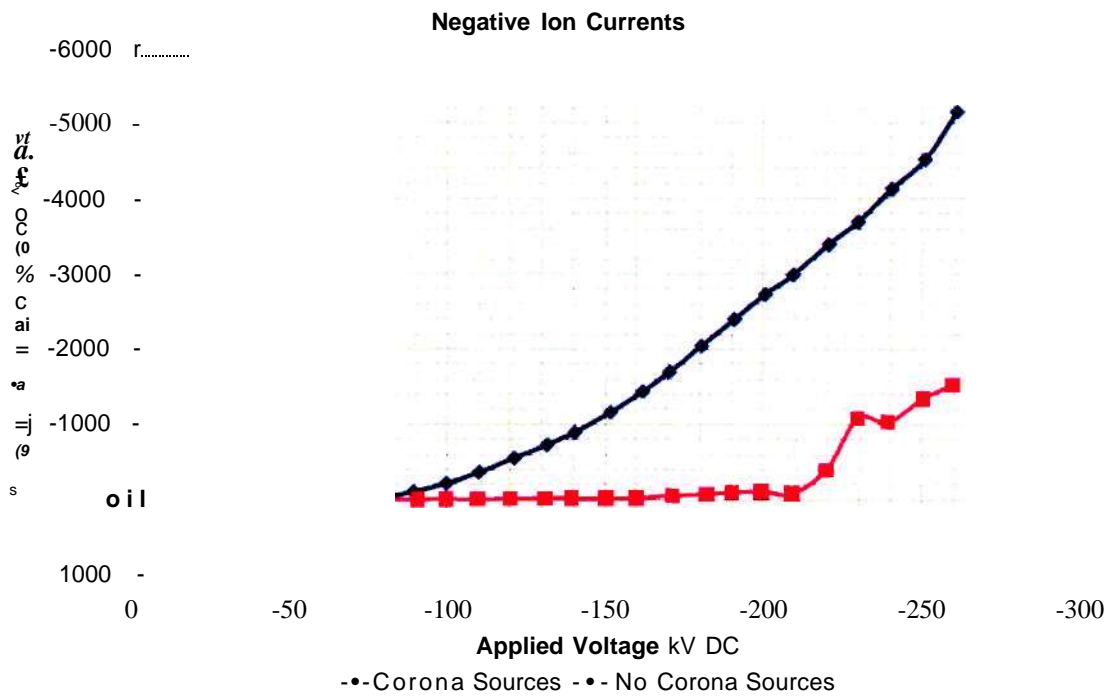
Figure 5.22: Ion Currents - Negative Polarity

Figure 5.22 shows the results of the ion current measurements that were taken under negative polarity. From the graph, the following can be seen:

- The inception voltage is about 80 kV when corona sources are applied to the pole conductor.
- The inception voltage is about 210 kV when no corona sources are applied.
- The ion current measured is a lot higher when corona sources are applied to the pole conductor as compared to when no sources are applied.
- When corona sources are applied, the ion current at maximum voltage is about 3 ½ times more than when no corona sources are applied.

5.6.2 Results of Electric Field Measurements - Negative Polarity:

Effect of Corona on E-field
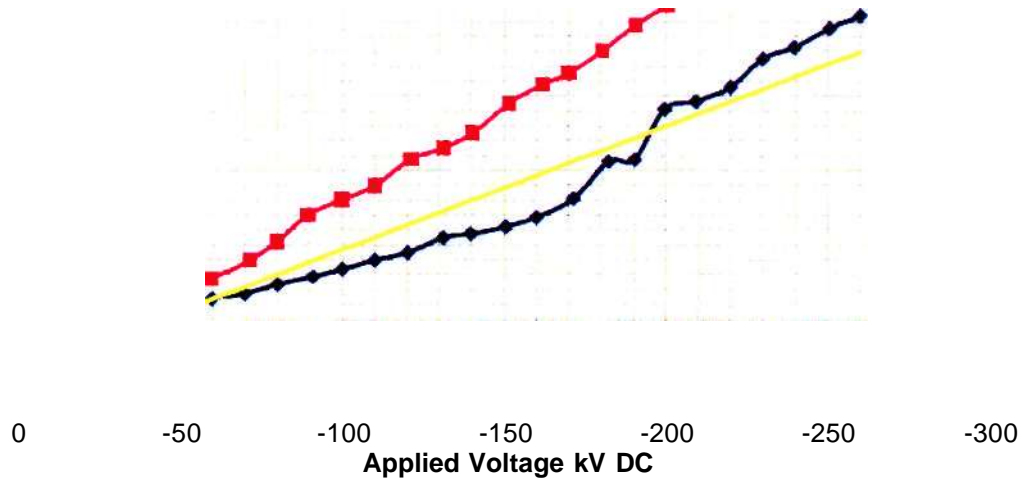
^^No Corona Sources on Pole **^HCorona** Sources on Pole

Figure 5.23: Electric Field - Negative Polarity

The results of the electric field measurements under negative polarity are shown in figure 5.23. From figure 5.23 the following conclusions are made:

- The electric field is much higher when corona sources are applied (average of 32 % higher).
- The rate of change (slope) of the electric field above 80 kV (corona sources on pole) is higher than when the applied voltage is below 80 kV.
- With a trend line applied (yellow curve), the effect of corona on the electric field is quite clear. The electric field is enhanced and has a steeper gradient than the trend line as the applied voltage is increased.
- The electric field is enhanced even more when the pole conductor goes in corona at a lower voltage (corona sources applied) as compared to when the inception voltage is higher (no corona sources). This is done by comparing the positive and negative measurements to the trend line above 80 kV.
- The difference in slope between the trend line and the graph of when corona sources were applied to the pole conductor are also noted.

5.7 COMPARISON OF RESULTS - ION CURRENT MEASUREMENTS:

The measurements that were taken for ion currents in July 2007 and September 2007 are compared below.

Comparison • Ion Currents

-^ Positive   ^N-Negative
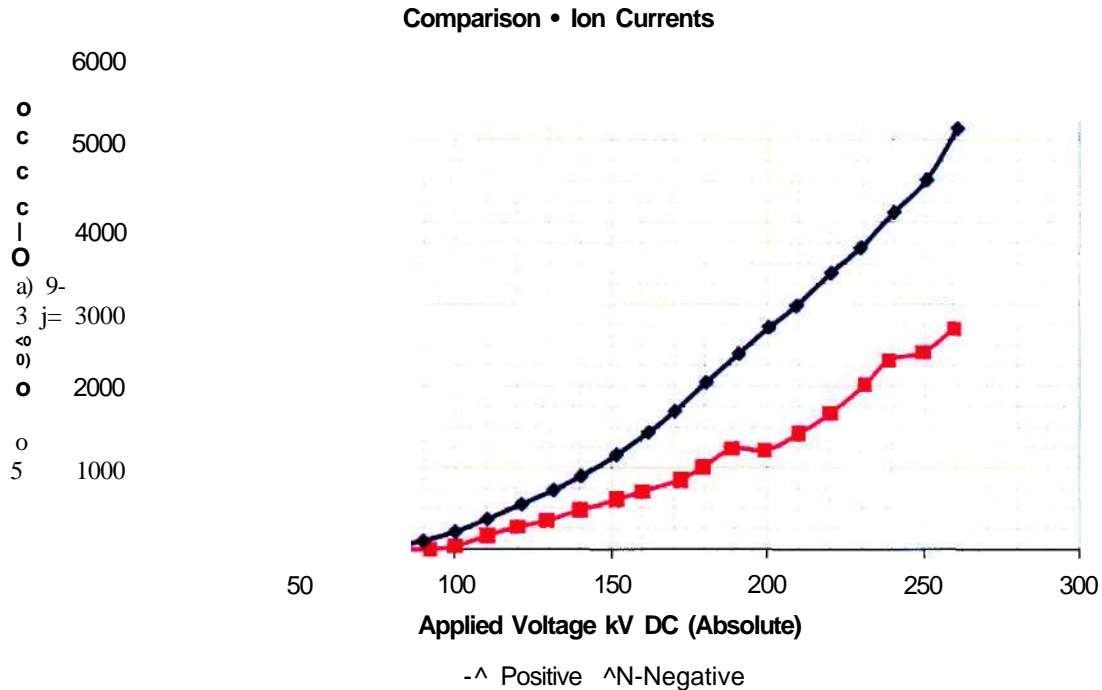
Figure 5.24: Comparison of Ion Currents - Negative versus Positive

Figure 5.24 shows the comparison of results for the ion current measurements taken for both polarities. The results that are compared are for the case when corona sources are applied to the pole conductor. From the graph it is evident that the negative ion currents are much higher than the positive ion currents that were measured. The maximum negative ion current is - 5.1 uA and the maximum positive ion current is 2.7 uA. This means that the negative ion current is about twice the positive ion current at maximum applied voltage (260 kV). The inception levels are also lower under negative polarity and this agrees with previous studies on corona currents.

From this it is concluded that when the pole conductor is in corona, the ion currents flowing to ground are higher under negative applied voltage. This means that the ion density will also be higher and that the path to ground is also more conductive for negative polarity. From the results, it seems that the path to ground is twice as conductive under negative polarity.

When comparing the ion current measurements taken in the laboratory to the EPRI simulations (table 6.5), we make the following findings. The EPRI simulation gives an ion current of 10361 nA for the positive polarity (+250kV) and - 13541 nA for the negative polarity (-250kV). The measured values at + 250 kV were 2416 nA and - 4519 nA for positive and negative polarity respectively. The simulated values for the positive polarity is 330 % higher than the measured values while the simulated values for the negative polarity is 200 % higher than the measured values.

From this it is concluded that the relationship between the EPRI simulations and the actual laboratory measurements do not correlate. The simulations are much higher than the actual measured values in the laboratory.

5.8 COMPARISON OF RESULTS - ELECTRIC FIELD MEASUREMENTS:

The measurements that were taken for the electric field at ground level in July 2007 and September 2007 are compared below.

Comparison - Electric Field

'Corona Sources +ve
No Corona Sources -ve

^ * N o Corona Sources +ve
""Corona Sources -ve
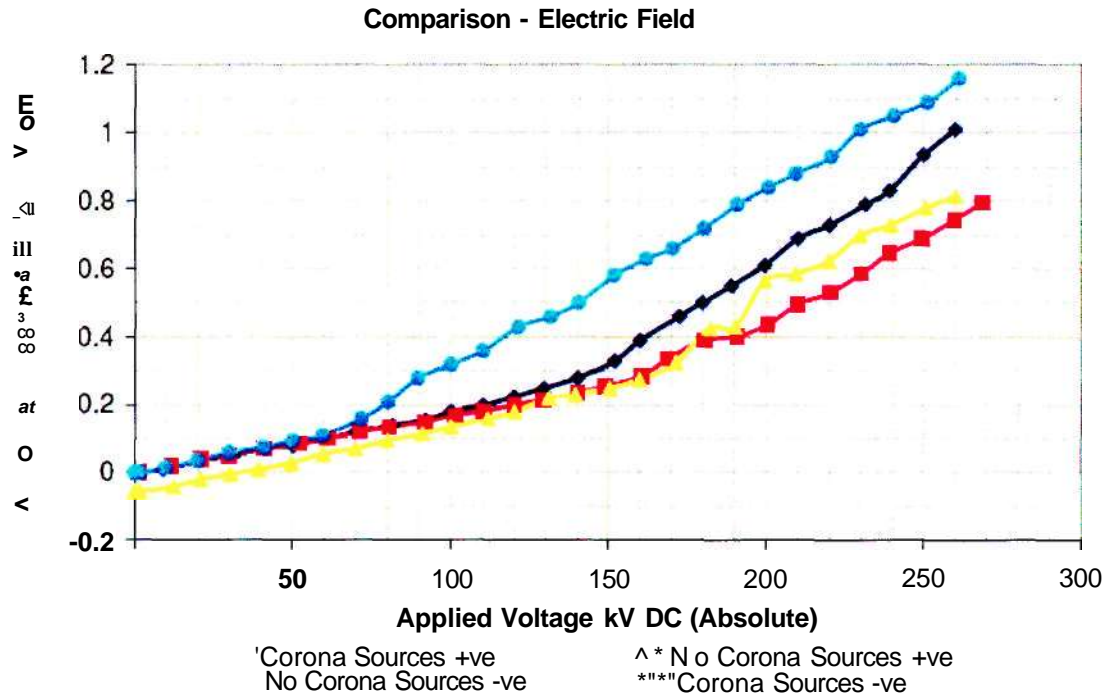
Figure 5.25: Comparison of Electric Field - Negative versus Positive

Figure 5.25 shows a comparison of the results for the electric field measurements that were taken under both positive and negative polarity. The results show that when there are no corona sources applied, the electric fields at ground level for both polarities are very similar. The graph also indicates that the inception voltage for the negative polarity (with corona sources applied) is about - 70 kV which is much lower than the positive case. This indicates that the conductor goes into corona at a much lower voltage under negative polarity.

The results also show that the electric field at ground level can be much higher for negative applied voltage as compared to positive applied voltage. This agrees with literature [16] that was reviewed. Under negative polarity, the conductor goes into corona at a lower voltage, thus creating more space charge which tends to enhance the electric field at ground level.

It is also noticed that the results of the negative (no corona sources) and the positive (corona sources applied) are very similar. This immediately indicates to us that even though corona sources are applied to the positive pole, the negative electric field is just as high as the positive. This suggests that we can expect higher electric fields under the negative pole. It also indicates that the corona activity under negative applied voltage is more significant.

The results of the Microsoft Excel and EPRJ simulations find the electric field (electrostatic) below the laboratory test line to be + 64.34 kV/m and + 60.01 kV/m respectively (at + 250 kV). The actual measured electric fields were 93.5 kV/m and - 109 kV/m for positive and negative polarity respectively. The measured electric fields are higher than the EPRI simulations by 56 % and 82 % for positive and negative polarity respectively.

If the space charge density is calculated (using equation 2.2) by using the EPRI simulations and the actual measurements, one will be able to make a better comparison because currently we see no correlation between the actual values and simulated values.

Measured Values (Negative):

$$P = \frac{}{KE}$$

$= 4519 \times 10^{-9}/(1.5 \times 10^{-4})*(109000 V/m)$

$= \mathbf{2.76 \times 10^{-7} (C/cm^3)}$

Measured Values (Positive):

$$P = \frac{J}{KE}$$

$= 2416 \times 10^{-9}/(1.15 \times 10^{-4})*(93500 V/m)$

$= \mathbf{2.247 \times 10^{-7} (C/cm^3)}$

EPRI Simulated Values (Negative):

$$\frac{}{KE}$$

$13541 \times 10^{-9}/(1.5 \times 10^{-4})*(60000 V/m)$

$15 \times 10^{-7} (C/cm^3)$

EPRI Simulated Values (Positive):

$$P = \frac{J}{KE}$$

$10361 \times 10^{-7} (1.15 \times 10^{-4})*(60000 V/m)$

$= 15 \times 10^{-7} (C/cm^3)$

From the measured results and calculations above it is seen that the negative ion current and electric field is higher than the positive case. This agrees well with previous work carried out on measurements of ion currents and electric fields.

From the EPRI simulated results we see that the negative ion current is higher than the positive ion current, which was expected when looking at previous studies carried out. It is also seen that the electric field levels for positive and negative are the same. This does not agree with the actual measurements in the laboratory and previous studies. The space charge density is also the same which further indicates that the EPRI simulations are based on calculated values by using different equations. It does not take into account the effect of space charge on induced voltages, leakage currents, ion currents and electric fields.

From the laboratory measurements, one can clearly see the effect of corona generated space charge on induced voltages, leakage currents, ion currents and electric fields. The effects of the corona generated space charge was more prominent under negative polarity and the EPRI simulations find the space charge density (p) to be identical for both polarities.

5.9 COMPARISON OF RESULTS - SPACE CHARGE DENSITY:

Figure 5.26 shows the comparison of the calculated space charge density for positive and negative applied voltages. The space charge density was calculated using the simultaneous measurement of ion current density (J) and electric field (E). Equation 2.2 was used for the calculations.

The space charge density at 260 kV (negative and positive) was calculated as follows:

Negative: Positive:

$$KE$$

$$P = \frac{}{KE}$$

$= 5147 \times 10^{-9}/(1.5 \times 10^{-4})*(116000 \text{ V/m})$

$= \mathbf{2.96 \times 10^{-7} \ (C/cm^3)}$

$= 2710 \times 10^{-9}/ (1.15 \times 10^{-4})*(101000 \text{ V/m})$

$= 2.33 \times 10^{-7} \ (C/cm^3)$
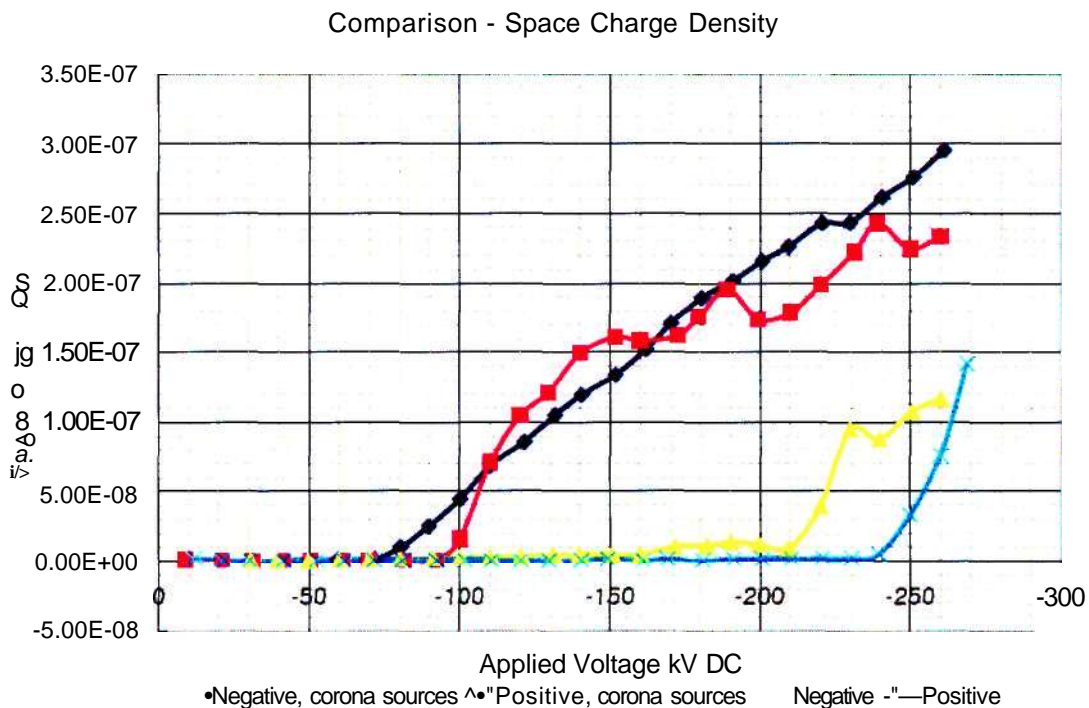
Figure 5.26: Comparison of Space Charge Density - **Negative versus Positive**

Figure 5.26 shows the comparison of the space charge density under positive and negative applied voltages, with and without corona sources. The space charge density is slightly higher when negative voltage is applied (without corona sources) than when positive voltage is applied. It is also evident that the inception voltage is also lower for the negative (-210 kV) as compared to the positive (+240 kV). The space charge density for the positive applied voltage (above 240 kV) also shows a very linear increase as compared to the negative.

When there is corona sources applied to the pole conductor it is evident that under negative applied voltage, the space charge density is very stable and linear. The positive space charge density is not as stable and linear. At the higher voltages (above 160 kV), the space charge density for negative applied voltage is higher. It is also evident the inception voltage for the negative is about -70 kV as compared to the positive which is about +90 kV.

5.10 COMPARISON OF RESULTS - WILSON PLATE CURRENT AS A FUNCTION OF ELECTRIC FIELD:

Figure 5.27 shows the comparison of Wilson plate current as a function of electric field under positive and negative applied voltages.
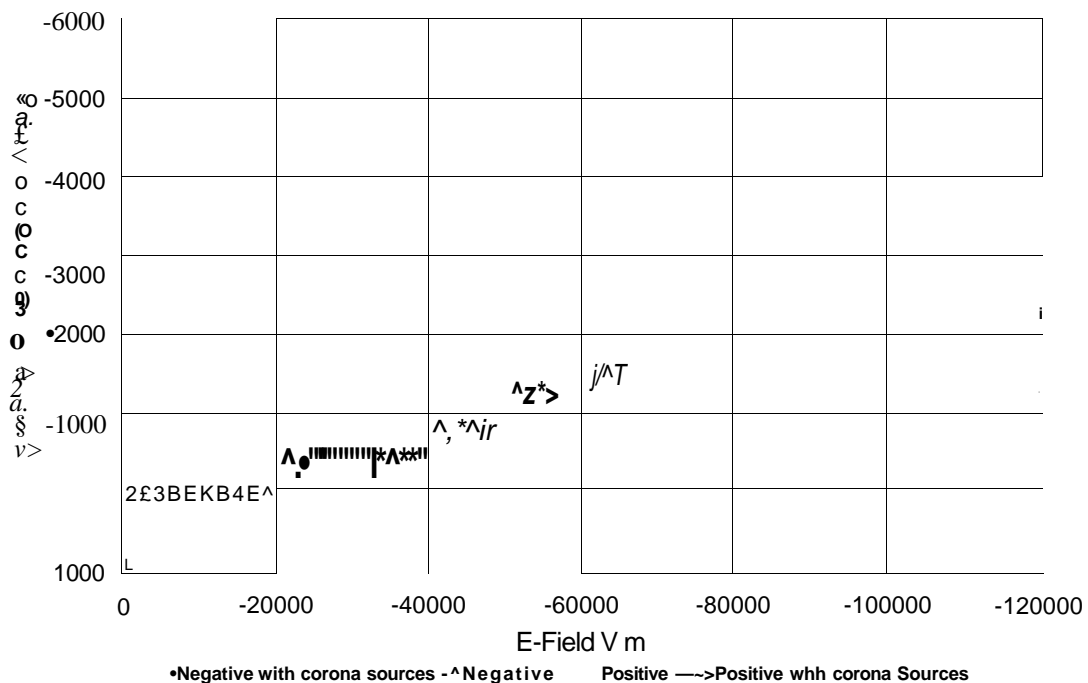
Figure 5.27: Comparison of Wilson Plate Current - Negative versus Positive

When there are no corona sources applied to the pole conductor, the Wilson plate current for both the negative and positive are very similar. The negative ionic current is slightly higher than the positive for the same levels of electric field.

For the case where corona sources are applied to the pole conductor, the behaviour of the ionic current is very different. The inception for the positive is lower than the negative. The positive pole produces higher ionic currents for electric fields between 20 to 60 kV/m. For electric fields above 60 kV/m, the ionic currents are higher for the negative pole. The graph also shows that the negative pole produces higher ionic currents and higher electric fields. This could mean that the higher electric field is attributed to the higher space charge density which enhances the electric field at ground. With a higher ion density, the ionic currents also seem to be higher and hence it would seem that the path to ground is more conductive.

5.11 MEASUREMENTS OF ELECTRIC FIELD AND ION CURRENT DENSITY UNDER THE CAHORA BASSA HVDC TRANSMISSION LINE:

Electric field and ion current density measurements were conducted under the Cahora Bassa HVDC line on 24th October 2007. The measurements were conducted near the Cahora Bassa earth electrode site just outside Zwavelspoort, South Africa.

When these measurements were taken, the voltage on the positive pole was 370 kV and the voltage on the negative pole was - 503 kV. These voltages remained constant for the duration of the tests. The conductor surface gradient for the positive pole was calculated to be 14.63 kV/cm while the conductor surface gradient of the negative pole was calculated to be 19.89 kV/cm (using equations B.l and B.2).

5.11.1 Results of Ion Current Density Measurements:

The ion current density was measured using the same Wilson plate that was used for the laboratory measurements. The plate measures 2 m by 0.5 m, thus giving a 1 m^2 surface collecting area. The plate was placed directly under the line at midspan. The area where the measurements were taken is fairly flat. The Wilson plate test set up is seen in figure 5.28:

Figure 5.28: Ion Current Density Measurement

The midspan height of the positive pole during the measurements was 11.99 m above ground while the midspan height of the negative pole was 11.96 m. The pole height was measured from ground using a Suparule, ultrasonic measurement device. The ambient temperature was recorded at 35 ° C at midday and the wind speeds were less than 2 m/s. Later on in the afternoon, the wind speeds did increase slightly but this was less than 5 m/s and it was not a consistent breeze. The current was 1800 A on the positive pole and 1743 A on the negative pole.

The results of the positive and negative pole ion current density measurements are shown in figures 5.29, 5.30 and 5.31.

S3
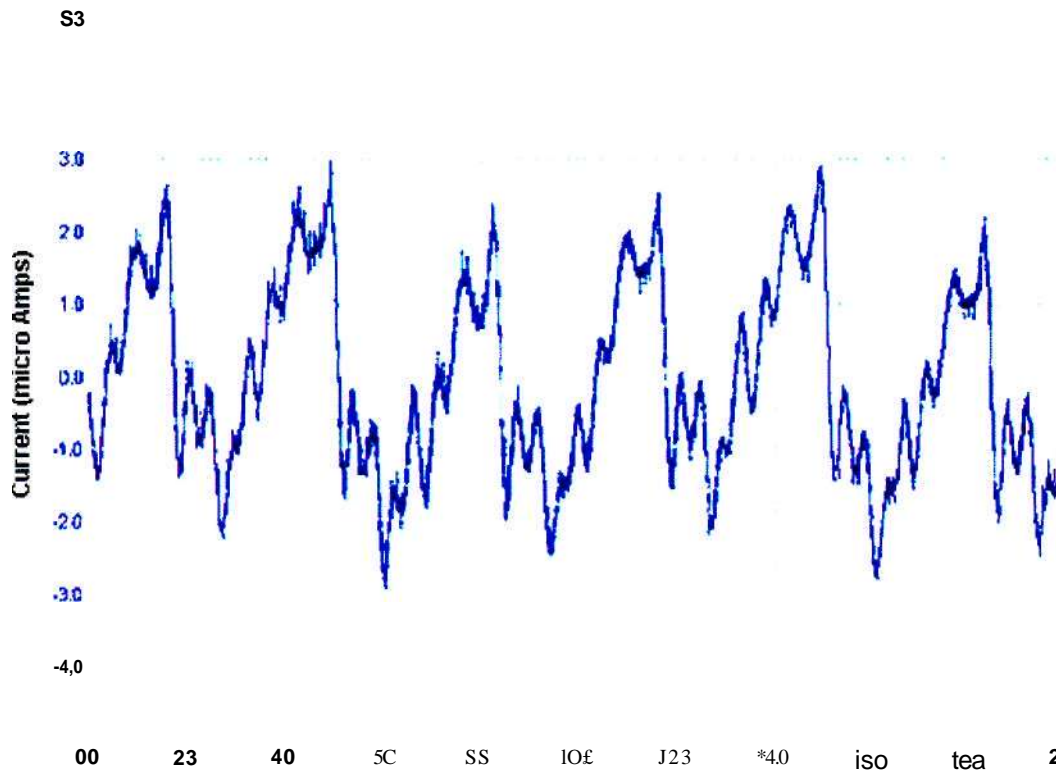
Figure 5.29: Ion Current - Positive Pole (370 kV)

From figure 5.29 the DC average value of the ion current density was 5.11 nA/m^2 (5.11 mV across a 1MQ resistor). The time measured between successive peaks was measured to be 3.33 ms. This translates into a frequency of 300 Hz, which is the 6th harmonic on the DC line. Using EPRI TL Workstation software, the ion current density was predicted to be 131.6 nA/m^2 at +370 kV. The DC average value is calculated by adding the value of the current at each point and then dividing this by the total number of points. Comparing the measured values to the EPRI simulated values, we find that the measured values are lower than the predicted values. The ripple seen in the waveform (figure 5.29) could be due to interference picked up as a result of the proximity of the measurement point to AC distribution lines which run very close to the positive pole of the Cahora Bassa line.

Figure 5.30 shows the ion current that was measured under the negative pole. Figure 5.31 shows a zoomed in picture of the ion current under the negative pole. The DC average value of the ion current below the negative pole was measured to be 150 nA/m^2. The measurements were oscillating and the maximum ion current density that was measured was 250 nA/m^2. The EPRI TL Workstation prediction for ion current density for the existing conditions is 317.2 nA/m^2 (refer to Appendix C for the results of the simulations).

For the negative case, one can see that the EPRI simulation for the actual line conditions during the measurements was 317.2 nA compared to the actual measured current below the negative pole which was 250 nA. The measured values are lower than the EPRI TL predicted values for the negative polarity but it shows good correlation between the two.

76
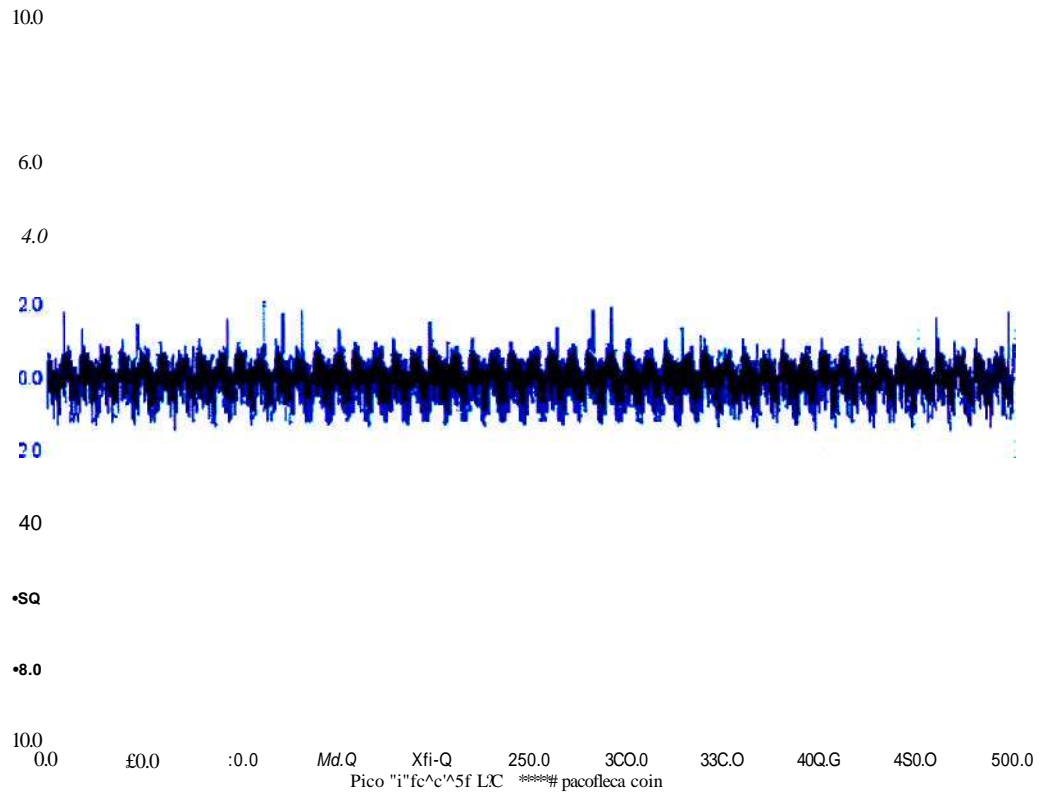
Figure 5.30: Ion Current - Negative Pole (503 kV)
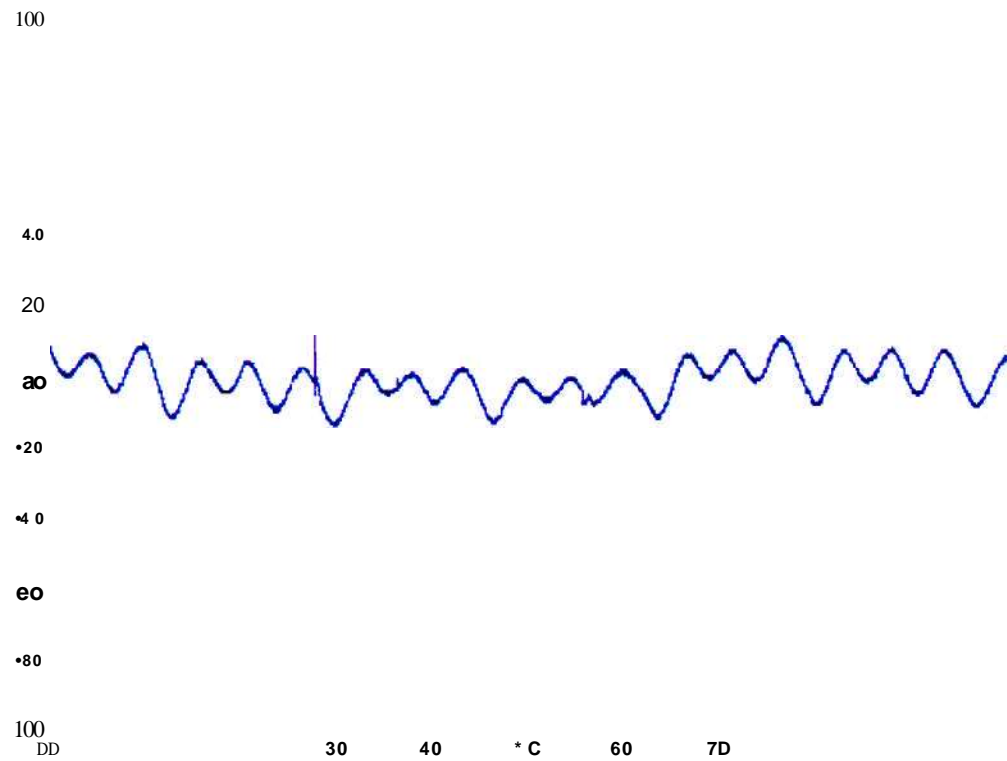
Figure 5.31: Ion Current - Negative Pole (zoomed in)

5.11.2 Results of Electric Field Measurements:

Electric field measurements were conducted under the Cahora Bassa HVDC transmission line using the same Monroe Electric Fieldmeter that was used for the laboratory tests. The probe was placed directly under the line at midspan height. The tests were conducted under both the positive and negative pole. The electric field measurements were taken simultaneously with the ion current measurements. The test set up and results are shown in figure 5.32 and 5.33.

Figure 5.32: Monroe Field Probe

Figure 5.33: Electric Field - Positive Pole

The results of the electric field measurements under the positive pole show that the electric field at ground level was fairly low. The DC average value of the electric field under the positive pole was calculated to be 4 - 5 kV/m. Measurements that were taken later showed that the electric field fluctuated to values as low as 1.5 kV/m. This could be due to the marginal increase in wind speed at the time. The EPRI TL Workstation prediction for the electric field under the positive pole at 370 kV is 12.54 kV/m for the unsaturated field and 40.92 kV/m for the saturated field. The DC average value is calculated by adding the value of the electric field at each point and then dividing this by the total number of points. Here one can see poor correlation between the EPRI simulated results for the unsaturated electric field when compared to the actual measured values. The simulated value for the unsaturated field was compared as the line was not in corona and hence very little space charge would have been present.
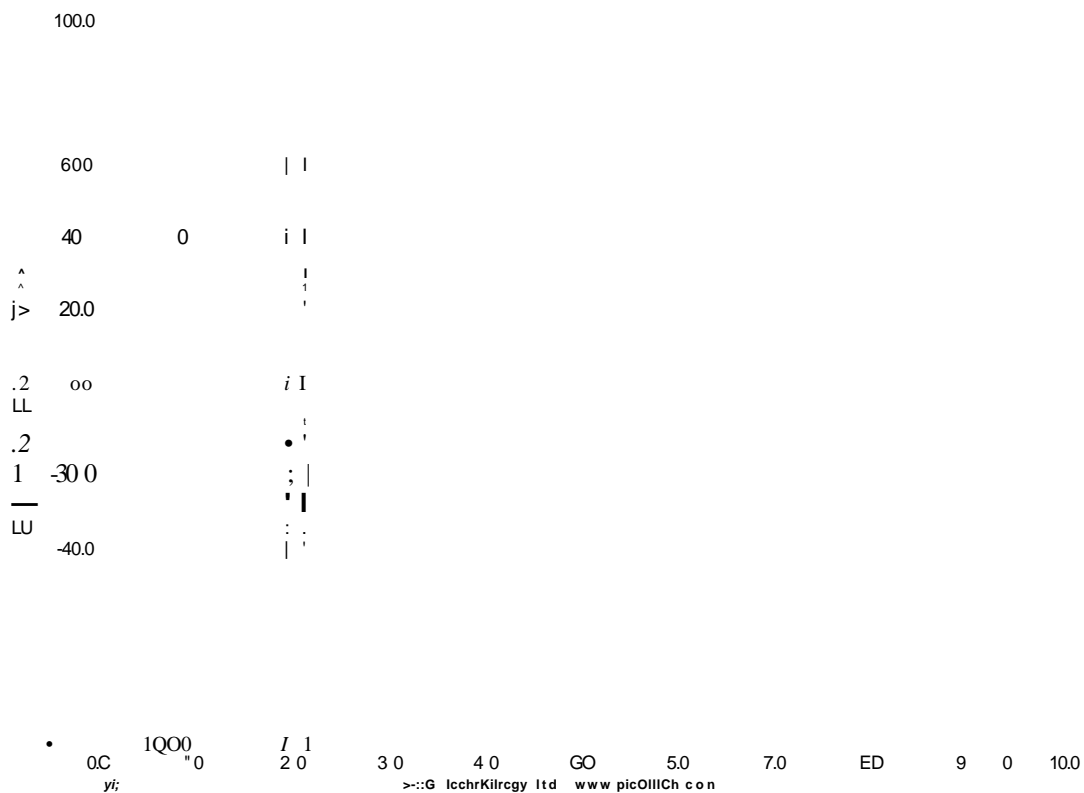
Figure 5.34: Electric Field - Negative Pole

The electric field measured under the negative pole was fairly high. This can be seen by the DC offset in figure 5.34. The calculated DC average electric field was -67 kV/m. The EPRI TL Workstation prediction for the Cahora Bassa line using the parameters at the time of the measurements was -17.05 kV/m for the unsaturated electric field and -55.62 kV/m for the saturated field (refer to Appendix C for the results of the simulations).

If one compares the measured values of electric field (negative polarity) to the EPRI simulations that were done for the line parameters during the measurements, you will find that the measured values are higher. The measured electric field is -67 kV/m compared to the simulated value of -55.62 kV/m for the saturated electric field. The negative pole was moderately in corona and the electric field at ground level was highly charged. The measured value shows good correlation with the simulated value for the saturated electric field; however the effect of space charge enhancement is shown by the higher measured electric field value.

79

5.11.3 Results of Corona Probe Measurements:

Corona currents were measured using a brass probe which was placed directly beneath the transmission line and insulated from earth. The test set up is shown in figure 5.35. The aim of this measurement was to determine the magnitude of current that could be induced due to corona on an object below the line. The height of the probe above ground was 15 m. The measurements were conducted under both positive and negative poles.

Rod

lira

15K.
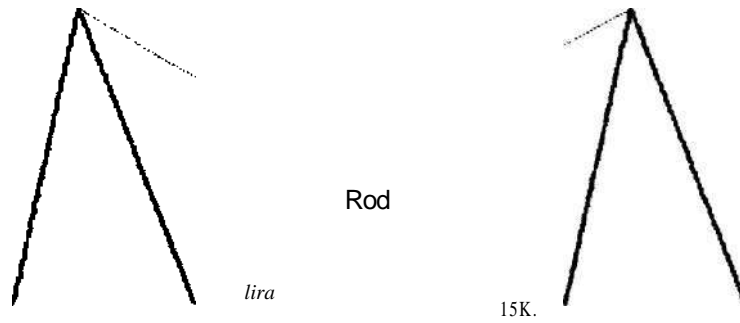
Figure 5.35: Corona Current Measurement - Test Set Up
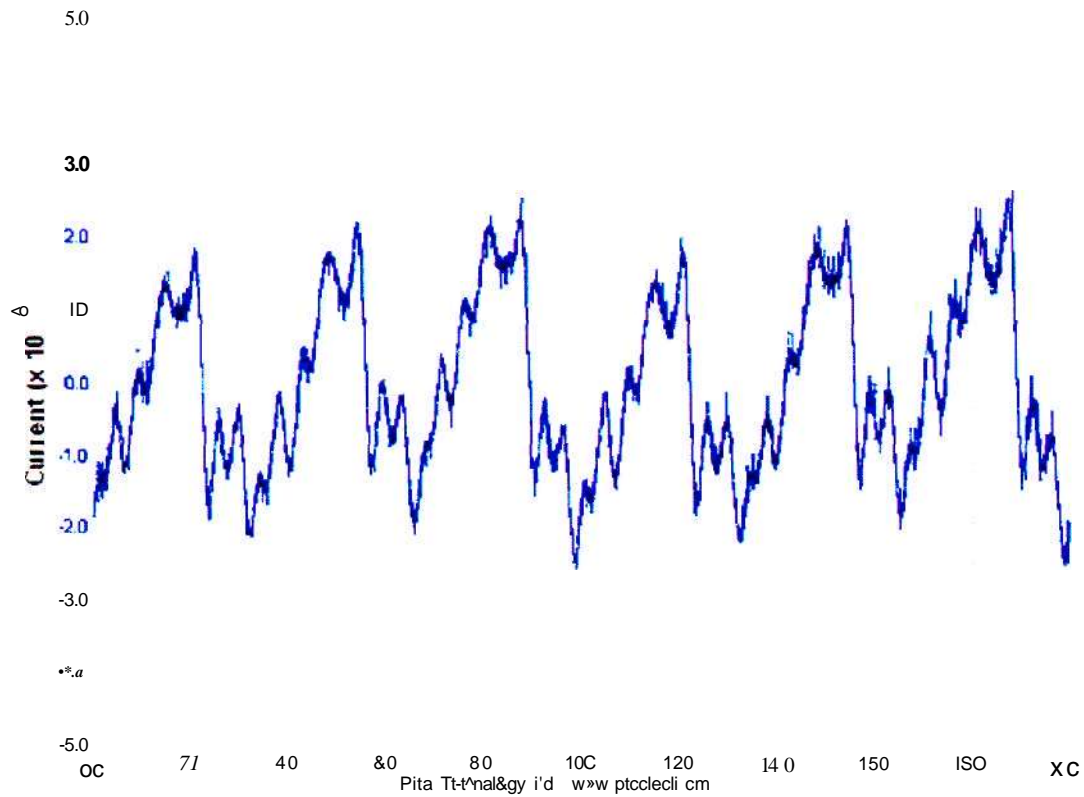
Figure 5.36: Corona Current Measurement - Positive Pole

The results of the corona current measurement under the positive pole are shown in figure 5.35. The DC average value of the corona current was 25 nA. The corona current levels that were measured were fairly stable. From figure 5.36 one can see how stable the corona current was and it is also noticed that there are no spikes in the current waveform.
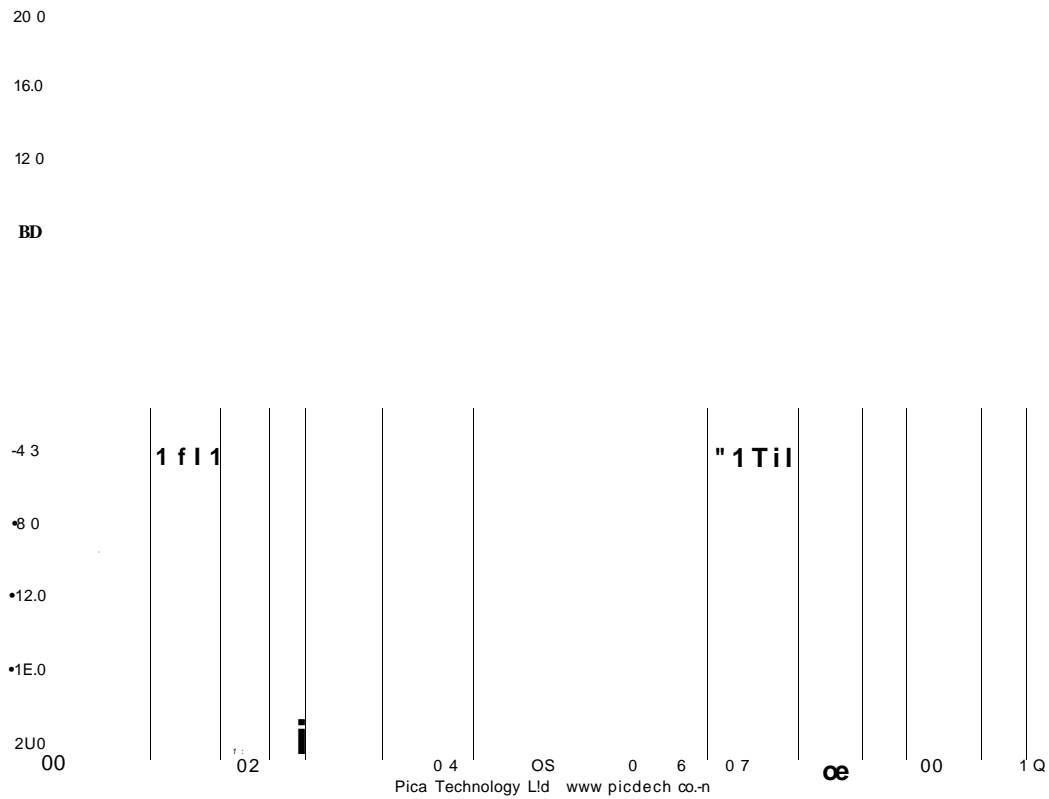
Figure 5.37: Corona Current Measurement - Negative Pole

The corona current that was measured under the negative pole is shown in figure 5.37. The results show a large difference in the corona current measured when compared to the positive pole. The probe went intermittently into corona and significant (greater than 20 uA) levels of current were measured. The scale could only read up to 20 uA but it is clearly seen that the current levels were very much higher.

From figure 5.37, one is also able to see when the probe went into corona and the frequency at which it occurred. It would seem that the space charge enhanced electric field at ground level is playing some role on the corona current spikes. The electric field at ground level is enhanced so much that the brass probe is going into corona. The probe itself did not have a smooth tip and this could be further enhancing the electric field at the tip of the brass rod. From the frequency of the corona spikes, one can see that the probe goes in and out of corona intermittently.

5.11.4 Discussion of Results - Cahora Bassa Line Measurements:

Values of ion current density and electric field strength under the positive pole were not very high. The environment under the positive pole was quiet and no real disturbances were noticed. The voltage level was fairly low and the measurement surface was fairly flat.

Values of ion currents and electric fields under the negative pole were significantly higher. The Wilson plate measurements were below predicted values, while the electric field measurement was slightly above the predicted values. The electrical environment below the negative line seemed to be highly charged as all of the staff members involved with the tests complained of getting static shocks from the vehicle used to transport the equipment as well as from the measurement equipment (computer and scope) under the line. Corona activity was audible for most of the duration of the measurements under the negative pole.

Measurements need to be repeated once the line is operating at full rated voltage, under both poles. The measurements that were taken were once off and this does not give the best indication of the electrical environment below the Cahora Bassa line. Long term measurements need to be undertaken and the actual operating parameters can be used for the EPRI simulations. This will give a better understanding of the electrical environment below the line as well as give a better understanding of the correlation between measured and simulated values.

It should also be noted that these lines are going to be upgraded to operate at 600 kV. Further investigations need to be conducted to understand the electrical environment under these lines. Depending on the results of measurements taken at full rated voltage (+ 533 kV), there could be implications to upgrade this line to 600 kV. The line conductoring (number of conductors in the bundle, diameter of conductors and GMR) and conductor height above ground may very well be affected. With the electric field under the negative pole at 67 kV/m, increasing the operating voltage to 600 kV will further increase the electric field at ground level.

There are no prescribed statutory limits for the electric field at ground level below HVDC transmission lines in South Africa. The prescribed limits for the electric field below HVAC transmission lines are l0kV/m within the servitude and 5kV/m at the servitude boundary [31]. Investigations conducted into the upgrade of HVAC transmission lines to HVDC in South Africa has shown that they expect an electric field in the order of 24.1 - 27.3 kV/m when operating at + 500 kV DC [31]. When comparing these expected values against the measured electric field below the negative pole of the Cahora Bassa line, one can see the effect of space charge enhancement on the ground level electric field. An enhancement factor for the electric field should be considered for future design of HVDC transmission lines as well as for the conversion from HVAC to HVDC.

CHAPTER 6

SOFTWARE SIMULATIONS

This chapter describes the simulations that were carried out using Microsoft Excel and the EPRI TL Workstation software [25].

6.1 LABORATORY TEST LINE SIMULATIONS:

The dimensions of the test line are used for simulations in Microsoft Excel and EPRI TL Workstation. This was done so that the simulated value of Electric Field Strength at ground level could be compared to the calculated and measured values.

6.1.1 Test Line Dimensions:

Height of pole conductors above ground, $H = 2.15$ m
Height of shield wire above ground, $H_s = 3.06$ m
Vertical distance between shield wire and pole conductor, $h = 0.91$ m
Diameter of pole conductors, $d = 3.18$ cm
Conductor type - Zambezi
Diameter of shield wire conductor, $d_s = 1.76$ cm
Shield wire type - Oden
Spacing between sub-conductors, $S = 0.2$ m
Number of sub-conductors = 4

$$GMR = \backslash.Q9^n 4r¥ \qquad (6.1)$$

Where: r = conductor radius (1.59cm), d = sub-conductor spacing (20cm), n = number of sub-conductors (4)

Therefore, $GMR = 1.09\text{^}1.59 \times 20^3 = 11.58$ cm

And the Electric field strength at ground level;

$$E\text{-} \qquad '' \qquad «\text{-}f^{\wedge} \qquad (6.2)$$
$$_{Hln(}2H_{)} \qquad H>_+x>$$
$$r$$

Where: x = lateral distance away from the line $(x = 0$ directly under the line)

Therefore, $E = \dfrac{2V}{\ln(\frac{}{r})} \times \dfrac{1}{} \qquad (6.3)$

Using the geometric mean radius (GMR) obtained and equation 6.2, the electric field strength below the test line was calculated using Microsoft Excel. The results are shown in table 6.1.

Table 6.1: Calculated Electric Field Strength - Test Line

Horizontal Distance Away From Line (m)	Voltage kV	Ground level E-Field +ve (kV, m>	Voltage kV	Ground level E-Field-ve(kV.m)
-2.5	250	27.35	-255	-27.55
-2.4	256	25.55	-255	-Z8.65
-2.9	250	30.50	-555	-Sfl.M
-2.2	25o	31.43	-250	-31.43
-2.1	250	32.03	-250	-32.8S
-2	256	34.49	-255	-34.45
-1.9	25o	36.13	-255	-36.15
-1.8	250	37.83	-250	-37.83
-1.7	250	39.58	-255	-39.53
-1.5	250	41.41	-255	-4).4i
-1.5	256	43.28	-JSO	-43.28
-1.4	256	45.15	-255	-45.15
-1.3	250	47.11	-255	-47.11
-1.2	250	49.06	-255	-4905
-1.1	256	50.99	-250	-50.99
-1	250	52.50	-258	-52.M
-fl.5	256	54.75	-555	-54.75
-0.8	250	55.52	-255	-56.52
-fl.7	250	5B.17	-550	-58.17
-fl.5	250	SflSB	-250	-59.59
-0.5	25fl	61.04	-550	-61.04
-0.4	250	62.19	-250	-55.19
-0.5	250	S5.11	-250	-59.11
-0.2	250	S5.79	-255	-63.79
-0.1	250	64.20	-255	-64.20
0	250	64.34	-255	-64.34
0.1	255	64.35	-250	-64.20
5.2	250	63.79	-255	-63.79
0.3	256	63.11	-258	-63.11
0.4	256	82.19	-255	-62.19
0.5	250	81.54	-555	-el.54
0.6	250	59.39	-255	-59.88
57	25o	56.17	-255	-58.17
!T5	sar	55T2	-555	3e''52
0.9	256	54.75	-255	-54.75
1	250	52.80	-550	-52.90
11	250	50.85	-250	-50.88
12	256	49.58	-550	-49.06
15	250	47.11	-255	-47.11
14	250	45. IS	-250	-45.18
1.5	256	43.2S	-255	-43.28
15	256	41.41	-255	-41.41
17	250	39.59	-555	
IS	250	37.83	-555	-3783
19	250	36.13	-255	-36.13
2	250	34.49	-555	-34.49
21	250	32.53	-250	-32. CB
2.2	250	31.43	-250	-31.43
25	255	30.50	-255	-30.00
24	25o	9_8		
2.5	255	27.35	-255	-27.35

E-field Strength of a Monopolar HVDC Line

-250 kV Monopolar HVDC line, 2.15 m above ground, four conductor bundle 3.18 cm in diameter.

E-field strength

Distance from centre of line in m

Figure 6.1: Calculated Electric Field Strength - Test Line (- ve)

E-field Strength of a Monopolar HVDC Line

•E-field strength

+250 kV Monopolar HVDC line. 2.15 m above ground, four conductor bundle 3.18 cm in diameter.

Distance from centre of line in m
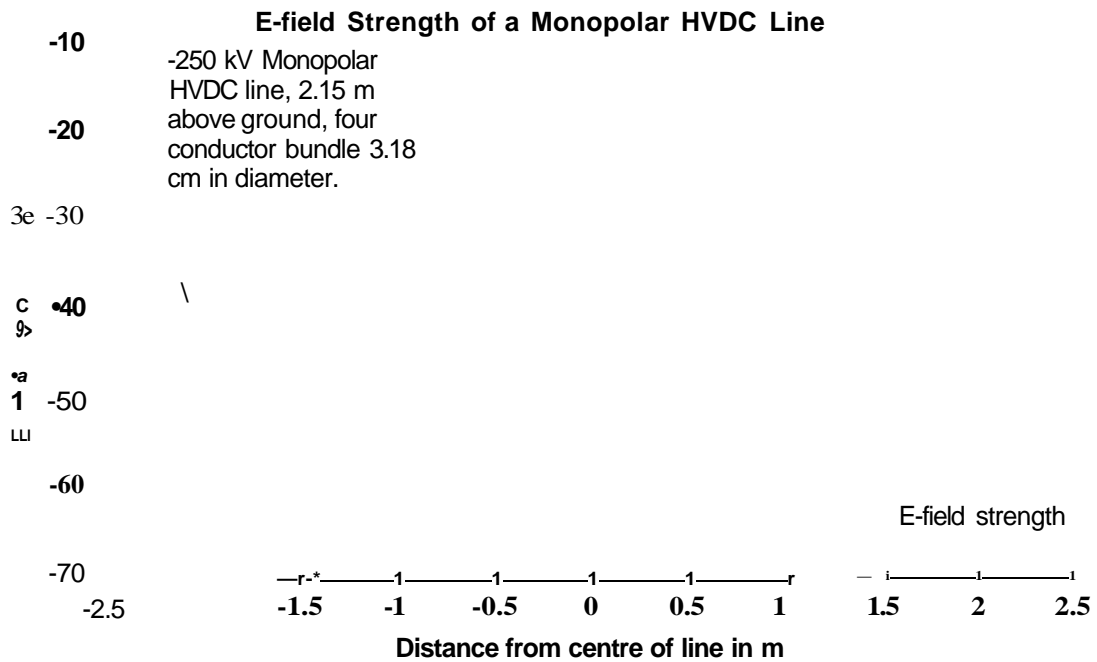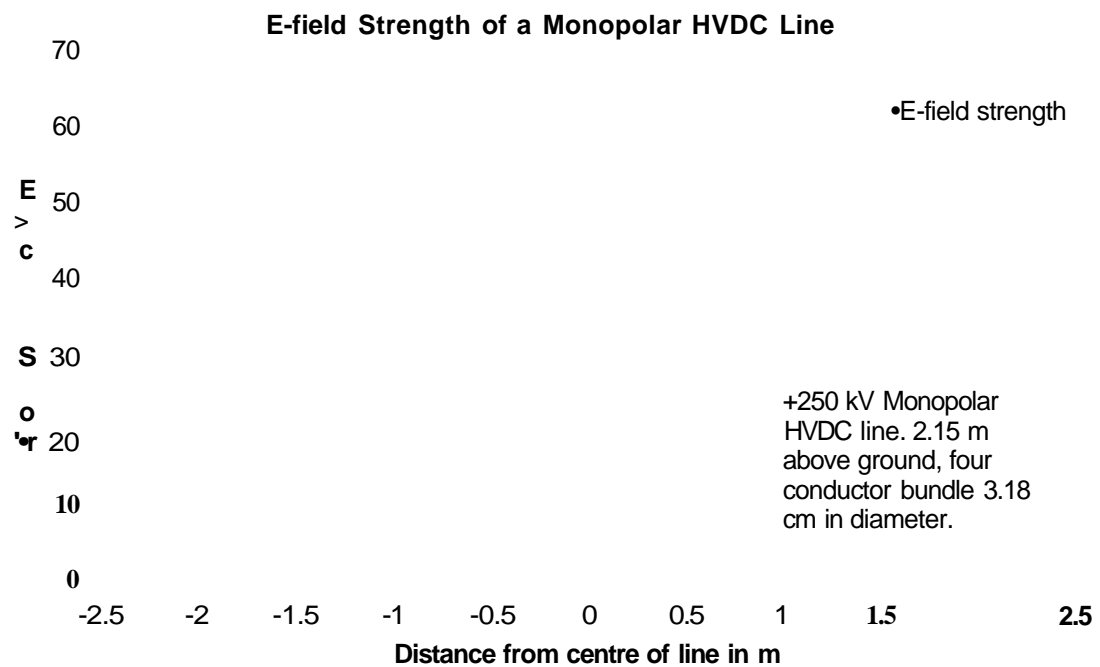
Figure 6.2: Calculated Electric Field Strength - Test Line (+ ve)

6.1.2 Cahora Bassa Line Dimensions:

Height of pole conductors above ground, H = 25.8 m
Height of shield wire above ground, H_s = 36.7 m
Vertical distance between shield wire and pole conductor, h = 10.9 m
Diameter of pole conductors, d = 3.18 cm
Conductor type - Zambezi
Diameter of shield wire conductor, d_s= 1.76 cm
Shield wire type - Oden
Spacing between sub-conductors, S = 0.45 m
Number of sub-conductors = 4
Sag = 13.6 m (used for EPRI simulations)

*GMR   =   1.09^1^*

Where: r = conductor radius (1.59cm), d = sub-conductor spacing (45cm), n = 4

Therefore, *GMR* = $1.09^1.59 \times 45^3$ = 21.266 cm

And the Electric field strength above ground level;

$$E = \frac{2V}{\# \ln\left(\frac{}{r}\right)} T^{-x} \quad \overline{((H\text{-}h)^2+x^2))x((H + h)^2+x^2))} \quad \frac{H^2}{} \quad i \quad ^\wedge \tag{6-4}$$

Where: h = height above ground (1.8m), *x* = lateral distance away from the line

Using the geometric mean radius (GMR) obtained and equation 6.4, the electric field strength below the Cahora Bassa line was calculated using Microsoft Excel. The results for the Cahora Bassa line are shown in tables 6.2 and 6.3.

Table 6.2: Calculated Electric Field Strength - Cahora Bassa Line (-ve)

Voltage	Height of pole (m)	GMR 4 conductor	y d t s ance	x distance	E-Fwld 1.8m above ground (kV.m)	Ground level E-fieW (kV.m)
-533	25.5	5.21388	1 &	-Sfl	-2.295	-2.25o
-555	25.5	0.21255	1 8	-3ft	-2.575	-2.374
-533	25.8	5.21335	1 5	-5?	-2.456	-5.461
-353	25.5	Oil 556	1 8	-35	-y.552	-2.555
-533	25.5	0.212M	1 5	-35	-5.548	-2.649
-533	25.8	0.21356	1 a	-54	-2.74s	-2.749
-535	55.5	5.51385	i	53	-5.855	-2.854
-533	25.s	5.21588	1 a	-32	-2.555	-2.054
-533	25.8	fl.21385	1 a	-51	-3.875	
-533	25.fi	5.21555	i 8	-55	-3.16s	-9.155
-533	25.8	0.21255	1 8	-28	-3.325	-5.354
-533	25.8	0.21265	1 8	-28	-3.454	-3.455
-533	25.8	0.21355	1 8	-27	-3.581	-9.581
-533	25.8	0.21285	1 a	-2S	-3.753	-3.733
-533	25.8	6.21555	1 tr	-25	-5.861	-3.830
-535	25.8	0.51386	1 a	-24	-4.094	-4.654
-533	25.8	0.21255	< a	-23	-4.195	-4.192
-533	25.8	0.21255	1 a	-22	-4.358	4.356
-533	25.5	0.21266	1 8	-21	-4.528	-4.526
-533	25.8	0.21555	1 8	-20	-4.705	-4.7flo
-533	25.8	0.21356	1 8	-10		
-533	25.8	0.21355	1 3	l&	5556	-5.551
-535	2'5	0.21355	1 8	-1?	-5.255	-5.246
-533	25.5	0.2)255	1 8	-IS	-5.442	-5.434
-533	25.8	0.21266	1 8	-15	-5.533	-5.653
-533	25.5	Oil 266	1 8	-14	-5.834	-5.812
-533	25.8	0.21266	1 a	-15	-S.oU	-5.000
-533	25.5	0.21355	1 a	-12		-6.155
-533	25.8	0.21265	1 a	-11		
-533	25.8	0.21355	1 a	-ld	-8.562	-6.541
-533	25.8"	0.21385	1 a	U	-0.790	-5.708
-533	25.8	0.2 IS*	1 a	-8		-5854
-533	25.5	0.21355	1 8	-i		
-533	551	OTTSSS	rT	5	TT77	rra 7.731
-533	25.8	5.21255	1 a	-5	-i'.283	
.539	55.8	0.21255	1 a	-4	-7.981	
-533	25.8	0.21266	1 a	-3	-7.458	-7.423
-533	25.8	0.51355	1 a	-2	-7.515	-7.479
-533	25.8	0.21355	1 a	-I	-7.548	-7.515
-535	25.8	0.21356	1 a	0	-7.5SI	-7.524
-533	25.5	0.21266	1 a	1	-/.549	-7.513
-553	25.5	6.21356	1 8	2	V.5I5	-7.475
-533	25.8	5.21266	1 8	3	-7.455	-7.423
-533	25.8	0.21355	1 a	4	-7.391	-7.347
-533	25.8	0.21266	1 a	5	-7.285	-7.251
-533	25.8	Oil 255	1 a	6	-7.157	-7.198
-533	25.8	0.21266	1 a	7	-7.035	-7.008
-533	25.8	5.21266	1 a	S	-S.88S	-8.864
-533	25.5	0.21355	1 a	9	-6.790	-6.708
-533	25.5	6.2(355	1 8	16	-6.562	-6.541
-533	25.5	6.21256	1 8	1!	-5.595	-6.357
-533	25.5	6.21256	1 8	12	-5.202	-S.le5
-535	25.5	0.21256	1 8	13	-8.0U	-6.M0
-533	25.8	0.21266	1 a	14	-5.834	-5.912
-533			a	15	-5.633	-5.623
-535	25.8	0.21255	1 a	lE	-5.442	-5.434
-595	25.8	6.21255	1 a	l7	-5.253	-5.246
-553	25.fi	5.21 Ss5	I a	19	-5.066	-5.061
-533	25.8	6.21355	) a	lS		
-533		6.21255	1 a	28	-4.709	
-533	25.8	0.21356	1 a	21	-4.528	4.526
-533			8	22	-4.558	
-533	25.8	0.21336	1 a	23	-4.193	-4.192
-533	25.8	0.21355	1 •5"	24	-4.034	-4.034
-533	25.5	6.21355	1 a	23	-3.981	-3.880
-533		6.21356	1 a	25	-5.739	-3.733
-535	25.8	6.21355	1 T™'		-3.591	-3.591
-533	25.8	0.21256	1 a	25	-3.454	-3.455
-535	251	OTTSSS	a ·•	2 5	7555	-3.324
-533	25.8	oilSBS	1 &	98	-3.18s	-5.159
-593	25.8	0.2)265	1 a	51	-5.075	
-535	25.8	0.21256	1 a	55	-5.953	-2.964
-533	25.8	0.51266	1 a	55	-5.955	-2854
-533	25.8	0.21355	1 a	34	-5.74s	-2.749
-533	25.8	0.21266	1 a	35	-2.S4S	-2.649
-533	25.8	5.21 aSS	1 a	36	-2.552	-2.555
-533	25.8	6.21268	1 a	37	-5.450	-2.451
-533	25.5	0.21256	1 a	98		-2.374

Table 6.3: Calculated Electric Field Strength - Cahora Bassa Line (+ve)

Voltage	Height of pole (m)	GMR 4 conductor	y distance	x distance	E- Field 1.8m above ground (kV. m)	Ground level E-fieW (KV.m)
553	255	0.21255	1 a~~"	-95	2.288	2.586
593	25.3	021356	1 5	-55	5.573	2.374
533	55.3	0.21265	\ &	-57	2.465	2.451
593	25.5	5.21258	1 &	-36	2.552	2.553
593	25.8	5.21255	1 3	-55	2.546	2.545
553	25.3	0.21355	1 8	-34	2.748	2.748
553	25.8	Oil 255	1 8	-93	2.553	2.854
533	25.8	0.21255	1 8	-32	5.863	5.954
533	25.5	0.212S5	1 &	-31	5.675	3.575
533	25.S	0.21255	1 8	-55	3.13a	5.(88
533	25.8	0.21555	1 B	-20	5.523	3.324
553	25.8	0.21266	1 S	-25	3.454	3.455
533	25.8	0.21355	1 a	-27	5.551	3.551
533	25.8	0.21266	1 8	-26	5.753	3.753
533	25.8	'.'21*6	I 8	-25	3.551	3.990
553	25.5	0.21266	1 8	-24	4.094	4.034
553	25.5	0.21266	1 8	-23	4.193	4.192
533	55.5	0.21255	l a	-22	4.955	4.555
553	25.5	0.21255	1 a	-21	4.525	4.528
533	25.8	0.21556	1 8	-20	4.703	4.7M
553	25.5	0.21266	1 8	-15	4.583	4.878
553	JJ.fi	0.21365	1 a	-la	5.066	5.061
533	25.8	8.21266	1 a	-17	5.253	5.2*5
593	25.8	0.21286	1 a	-15	5.442	5.434
533	25.8	0.21355	1 a	-is	5.893	5.623
553	25.3	0.21356	1 a	-14	5.524	5.812
553	25.8	6.21385	1 T~		6.014	6.000
553	25.8	0.21355	1 8	-12	6.202	6.186
553	25.8	6.21355	1 T " 1		6.385	6.367
555	25.8	5.21266	1 V~		6.562	6.541
553	25.5	0.21266	1 a	-9		6.70S
553	25.8	0.21266	1 T~	-8	6.889	6.864
553	25.8	0.51255	1 T ~		7.035	7.008
593	253	o-Sm T~		3	7.167	i.m
593	25.8	5.21356	1 a	-5	7.283	7.25)
593	25.5	6.21366	1 t''	-4	7.381	7.347
553	25.5	5.21356	1 T	-3	7.458	7.423
533	2s.5	0.21356	1 a	-2	7.515	7.479
553	25.5	0.5 IKS	1 a	-1	7.543	7.513
593	25.8	0.21266	1 a	0	7.561	7.524
533	25.5	0.21268	1 8	1	7.545	7.513
553	25.5	5.21265	1 8	2	7.515	7.479
553	25.8	3.J!l2o5	1 8	3	7.458	7.429
533	25.5	0.21256	1 8	4	7.981	7.347
553	25.8	0.21255	1 •B—	5	7.283	7.251
533	25.3	0.21256	1 8	6	7.167	7.138
533	25.8	oaias 0.21266	j a	/	7.035	7.00S
553	25.5	0.21266	1 a	8	6.889	6.864
553	25.5	0.21256	1 8	9	6.750	6.765
533	25.3	0.212S6	1 a	15	6.552	8.541
593	25.5	0.21266	1 a	11	6.985	6.367
553	25.8	0.21266	1 a	12	6.202	5.196
553	25.5	0.21555	1 5	13	6.014	5.000
593	25.8	0.21335	1 a	14	5.524	5.812
533	25.8	0.21356	1 a	15	5.593	5.6Z3
593	25.8	6.21266	1 a	15	5.442	5.454
553	25.5	0.21356	1 8	17	5.253	5.246
553	25.5	0.21556	1 a	19	5.066	5.061
593	25.5	0.21266	1 a	18	4.583	4.878
593	25.5	0.21585	1 a	20	4.709	4.700
595	25.8	tviiiase	j a	21	4.52a	4.526
593	25.8	oilSSS	1 8	22	4.35a	4.3S6
533	25.8	5.21255	1 B~~	29	4.193	4.192
553	25.8	6.21356	1 8	24	4.034	4.034
553	25.8	0.21266	1 8	25	5.S81	
593	25.8	6.21255	1 8	26		5.799
553	25.8	0.21336	1 a	2/	3.591	3.501
533	25.8	oil ass	i a	28	3.454	3.455
555	551	051355	r a	5 5	sm	3524
553	25.8	0.21266	I a	30	9.19a	3.199
MS	55.8	0.21266	1 8	31	5.07a	3.075
593	25.8	Oil 256	1 T''	32	2.963	2.364
553	25.8	0.21356	1 a	39	2.853	Z854
553	SS.8	0.21266	1 a	54	2.748	2.749
533	55.8	0.21356	1 a	35	2.646	2.649
553	25.8	0.21266	r E		2.552	2.553
533	25.8	511566	1 a	37	2.460	2.451
		0.21266	1 1H"	38	2.373	2.374

E-field Strength of **a Monopolar** HVDC Line

——E-field strength 1 .8 m above ground - - E-field strength at ground level

J

E -3 -
>

-5 -

/

\

/ - 533 kV HVDC line, 25.8 m above
/   ground with a 4 conductor
          bundle, 3.18 cm diameter.

Distance away from centre of tower in m

Figure 6.3: Calculated Electric Field Strength - Cahora Bassa Line (- ve)

E-field Strength of a Monopolar HVDC Line

• 533 kV HVDC line. 25.8 m above
ground with a 4 conductor bundle.
3.18 diameter.

•E-field strength 1.8 m above ground - - E-field strength at ground level

Distance away from centre of tower in m
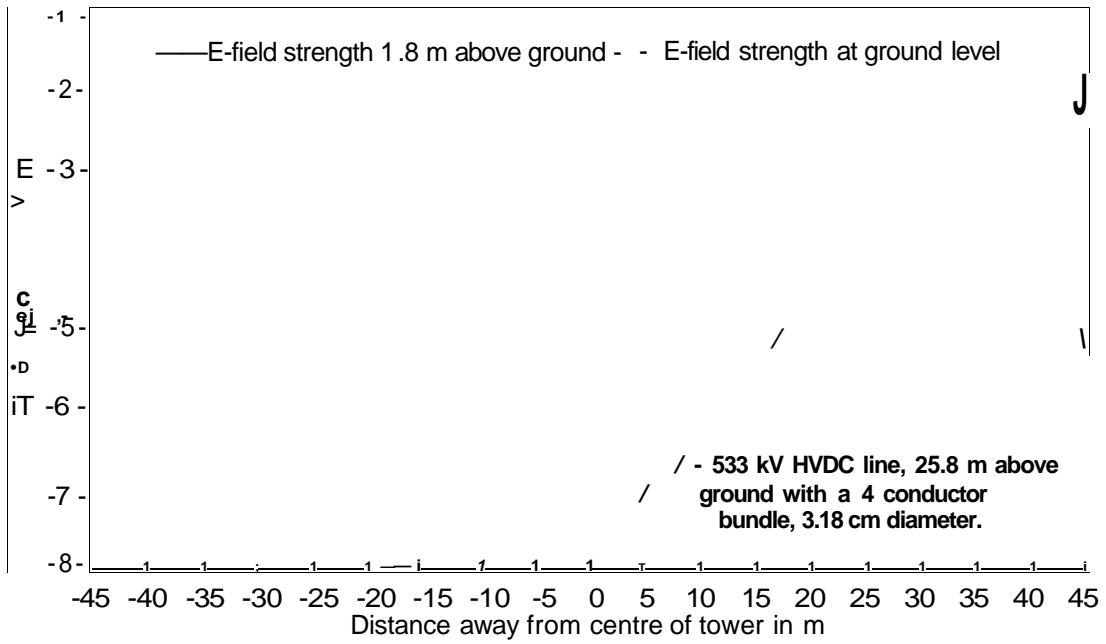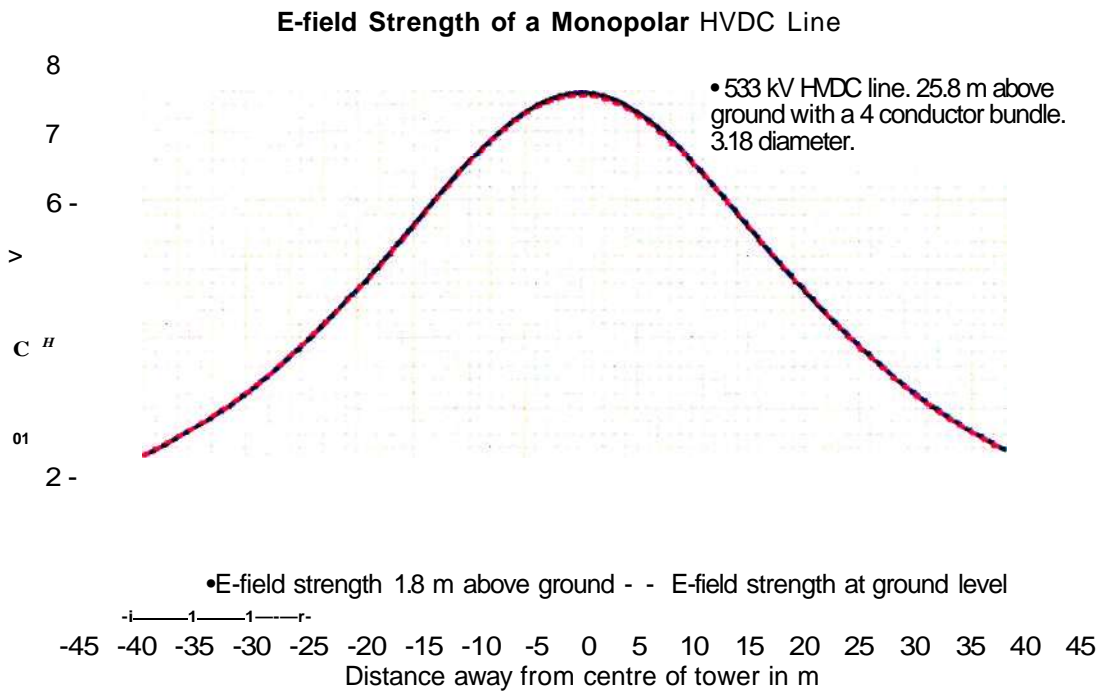
Figure 6.4: Calculated Electric Field Strength - Cahora Bassa Line (+ ve)

6.1.3 Discussion and Findings:

The electric field of the test line and the Cahora Bassa line were both simulated using Microsoft excel software. The dimensions that were used for the simulations on the test line are the as built dimensions. The calculated GMR for the four conductor bundle of the test line was found to be 11.58 cm. Using equation 6.2, the electric field at ground level was calculated for applied voltages of + 250 kV. The electric field on either side of the test line, up to 2.5 m, was calculated. The results of these calculations can be seen in table 6.1. The electric field strength is at its peak directly below the line at 64.34 kV/m.

The electric field strength of the Cahora Bassa line was calculated using equation 6.4. The GMR of the Cahora Bassa conductor bundle was calculated to be 21.27 cm. Using this GMR in equation 6.4; the electric field strength was calculated, up to 40 meters away. The voltage used in the calculations is the operating voltage of the Cahora Bassa line, i.e., + 533 kV DC. The electric field strength 1.8 meters above ground and at ground level was calculated. This was used to verify the electric field that a human being of average height is exposed to. Comparing the electric field at ground level to the electric field 1.8 meters above ground shows that the difference is marginal. The results from tables 6.2 & 6.3 show that the highest level of electric fields will be directly below the line and up to 2 meters on either side of the line. The electric field directly under the line is calculated as 7.524 kV/m.

It is important to note that the ground level electric field furthest away from the line is slightly higher than the electric field 1.8 meters above ground. This gives a clear picture of how the field lines radiate outwards and away from the energised pole conductors. This is seen for both positive and negative applied voltages. The results of the Microsoft Excel simulations will be used as a guide for the laboratory measurements and the field measurements taken on the Cahora Bassa line. A comparison of the Microsoft Excel simulations to the EPRI TL Workstation simulations is done in section 6.2.

6.2 EPRI TL WORKSTATION SIMULATIONS:

The laboratory test line dimensions were also used for the simulations with the EPRI TL Workstation software. The results for the test line are shown below:

6.2.1 Test Line Simulation Results:

Table 6.4: Test Line (+250kV) - Maximum Surface Gradient

```
* * * * v * * * * * * * * * * * * * * * * * * Jr * * * * * * * * * * * * *
*                                                                    *
*  MAXIMUM SURFACE GRADIENT (kV/cm)  *
*                                                                    *
* * * * * * * * * * * * * * * * A * * * * ». * * ir * * * *.**.* * * * A *
```

BNDL #	Type	DC	PEAK(+)	PEAK(-)
1	DC	16.69	16.69	16.69
2	Ground Wire	-24.05	-24.05	-24.05

Table 6.5: Test Line (+250kV) - E-Field, Current Density & Ion Density

LATERAL DISTANCE (feet)	(meters)	<— DC ELECTRIC FIELD —> ELECTROSTATIC (kV/m)	SATURATED (kV/m)	CURRENT DENSITY (nA/m2)	ION DENSITY (1/cm3)
-16.4	-5.00	7.75	39.66	252.6	346112.
-14.8	-4.50	9.35	45.00	359.6	434222.
-13.1	-4.00	11.45	51.39	522.0	552026.
-11.5	-3.50	14.24	59.11	774.1	711638.
-9.8	-3.00	18.00	68.42	1169.0	928605.
-8.2	-2.50	23.10	80.81	18 47.0	1242124.
−6.6	-2.00	29.90	95.78	2941.7	1669145.
-4.9	-1.50	38.52	113.33	4646.8	2228472.
-3.3	-1.00	48.21	130.92	6893.2	2861580.
-1.6	-.50	56.58	146.45	9300.7	3451600.
0	.00	6 0.01	152.44	10361.1	3693936.
1.6	.50	56.58	146.45	9300.7	3451600.
3.3	1.00	48.21	130.92	6893.2	2861580.
4.9	1.50	38.52	113.33	4646.8	2228472.
6.6	2.00	29.90	95.78	2941.7	1669145.
8.2	2.50	23.10	80.81	1847.0	1242124.
9.8	3.00	18.00	68.42	1169.0	928605.
11.5	3.50	14.24	59.11	774.1	711638.
13.1	4.00	11.45	51.39	522.0	552026.
14.8	4.50	9.35	45.00	359.6	434222.
16.4	5.00	7.75	39.66	252.6	346112.

Electric Field Profile

125r

-~ VERT60Hz
-o 95% FAIR
- 50% FAIR

100

75-

a'   /

50-

*   \

v

25.

-5.0   -2.5   2.5   5.0

Distance (meters)

Figure 6.5: Test Line (+250kV) - E-Field Profile

Ion Density Profile

3000

i
i
n   n 0^0/ FAIR
*   * ^0^0/ FAIR

p   •

2000

\

/

/   b   J

1000   _ ^ _   ——y -   K   —

•

...Cf' | y   * .   I
.n'"   i   ^ x
r'"   1   .•.   D-

−5.0   -2.5   2.5   5.0

Distance (meters)
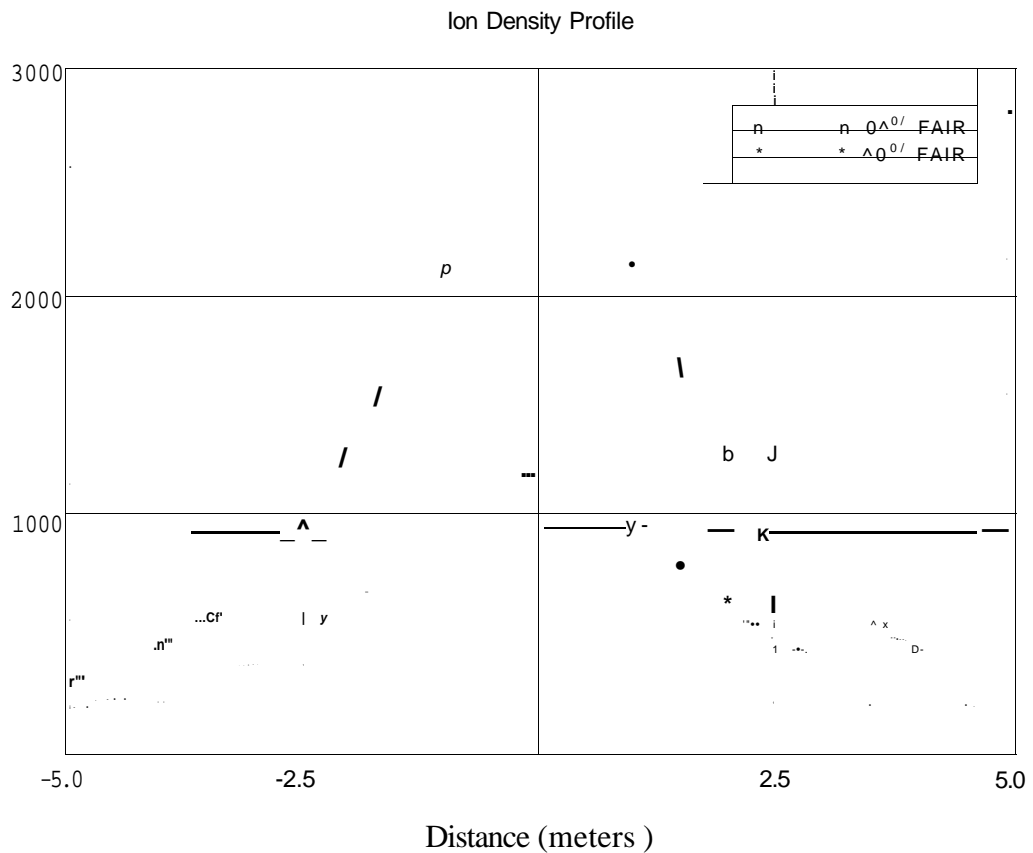
Figure 6.6: Test Line (+250kV) - Ion Density Profile

Ion Current Profile
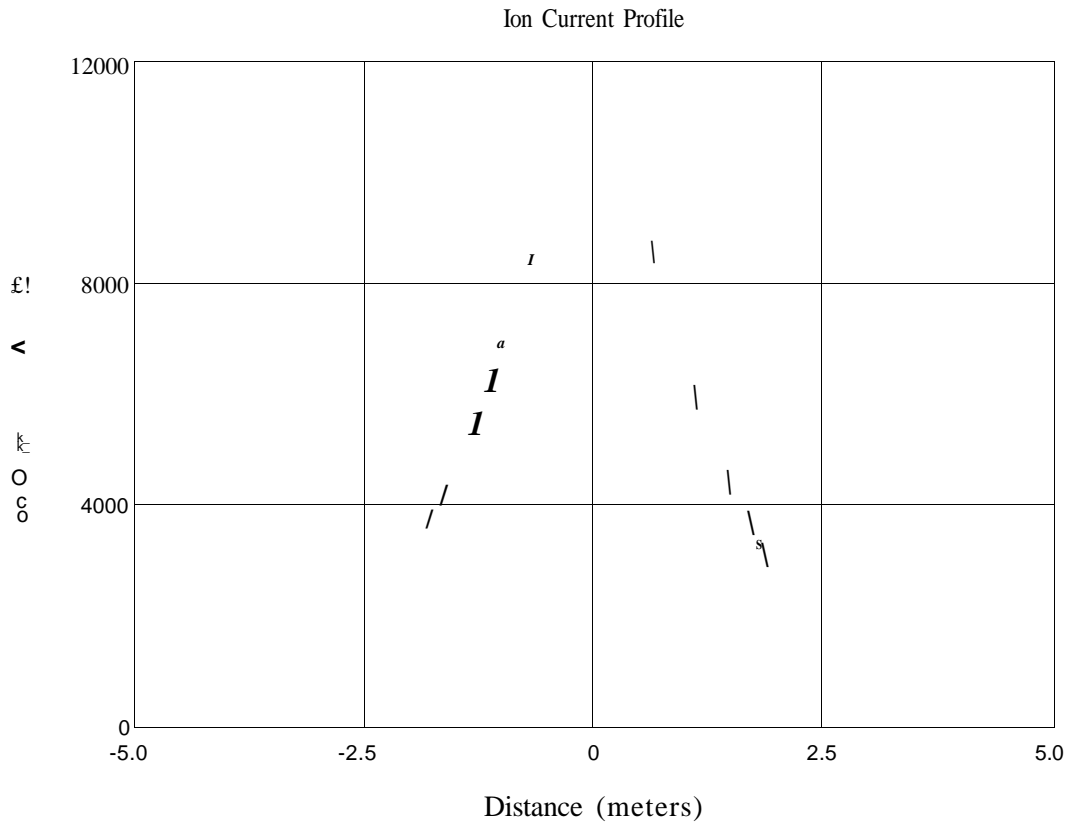
Figure 6.7: Test Line (+250kV) - Ion Current Profile

Table 6.6: Test Line (-250kV) - Maximum Surface Gradient

```
 . . . . . . . . . . . . . . . . . . . . .. . . . . . . . . .
 *                                                    *
 * MAXIMUM SURFACE GRADIENT (kV/cm)  *
 *                                                    *
 * * * * * * * * * * * * * * * * * * * * * * * * * * * * * * * *

BNDL #    Type         DC       PEAK(+)   PEAK(-)

  1         DC      -16.6 9    -16.69    -16.69
  2 Ground wire    2 4.05      24.05      24.05
```

Table 6.7: Test Line (-250kV) - E-Field, Current Density & Ion Density

LATERAL DISTANCE (feet)	(meters)	DC ELECTRIC FIELD ELECTROSTATIC (kV/m)	SATURATED (kV/m)	CURRENT DENSITY (nA/m2)	ION DENSITY (l/cm3)
-16.4	-5 00	-7.75	-39.66	-329.5	-346112.
-14.8	-4 50	-9.35	-45.00	-469.0	-434222.
-13.1	-4 00	-11.45	-51.39	-680.9	-552026.
-11.5	50	-14.24	-59.11	-1009.6	-711638.
-3.8	-3 00	-18.00	-68.42	-1524.8	-928605.
-8.2	-2 50	-23.10	-80.81	-2409.1	-1242124.
-6.6	-2 00	-29.90	-95.78	-3837.1	-1669145.
-4.9	-1 50	-38.52	-113.33	-6061.1	-2228472.
-3.3	-1 00	-48.21	-130.92	-8991.1	-2861580.
-1.6	- 50	-56.58	-146.45	-12131.3	-3451600.
.0	00	-60.01	-152.44	-13514.4	-3693936.
1.6	50	-56.58	-146.45	-12131.3	-3451600.
3.3	1 00	-48.21	-130.92	-8991.1	-2861580.
4.9	1 50	-38.52	-113.33	-6061.1	-2228472.
6.6	z 00	-29.90	-95.78	-3837.1	-1669145.
8.2	2 50	-23.10	-80.81	-2409.1	-1242124.
9.8	3 00	-18.00	-68.42	-1524.8	-928605.
11.5	3 50	-14.24	-59.11	-1009.6	-711638.
13.1	4 00	-11.45	-51.39	-680.9	-5 52 026.
14.8	4 50	-9.35	-45.00	-46 9.0	-434222.
16.4	5 00	-7.75	-39.66	-329.5	-346112.

Electric Field Profile
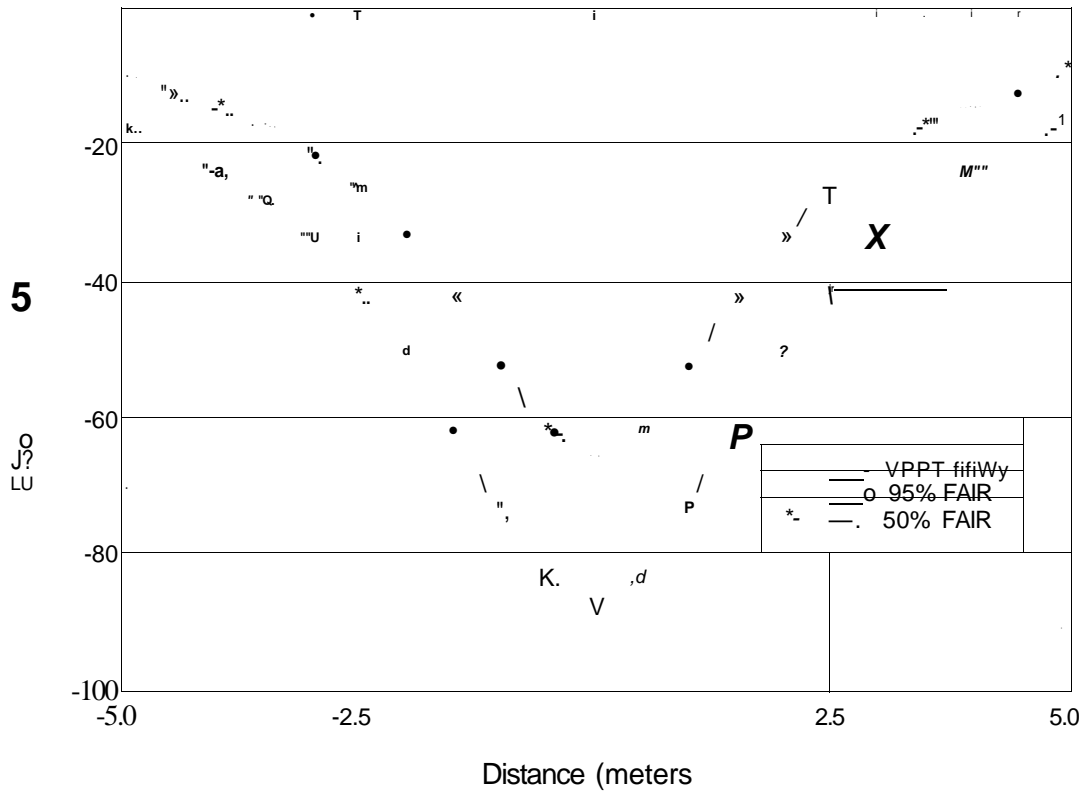
Figure 6.8: Test Line (-250kV) - E-Field Profile

Ion Density Profile
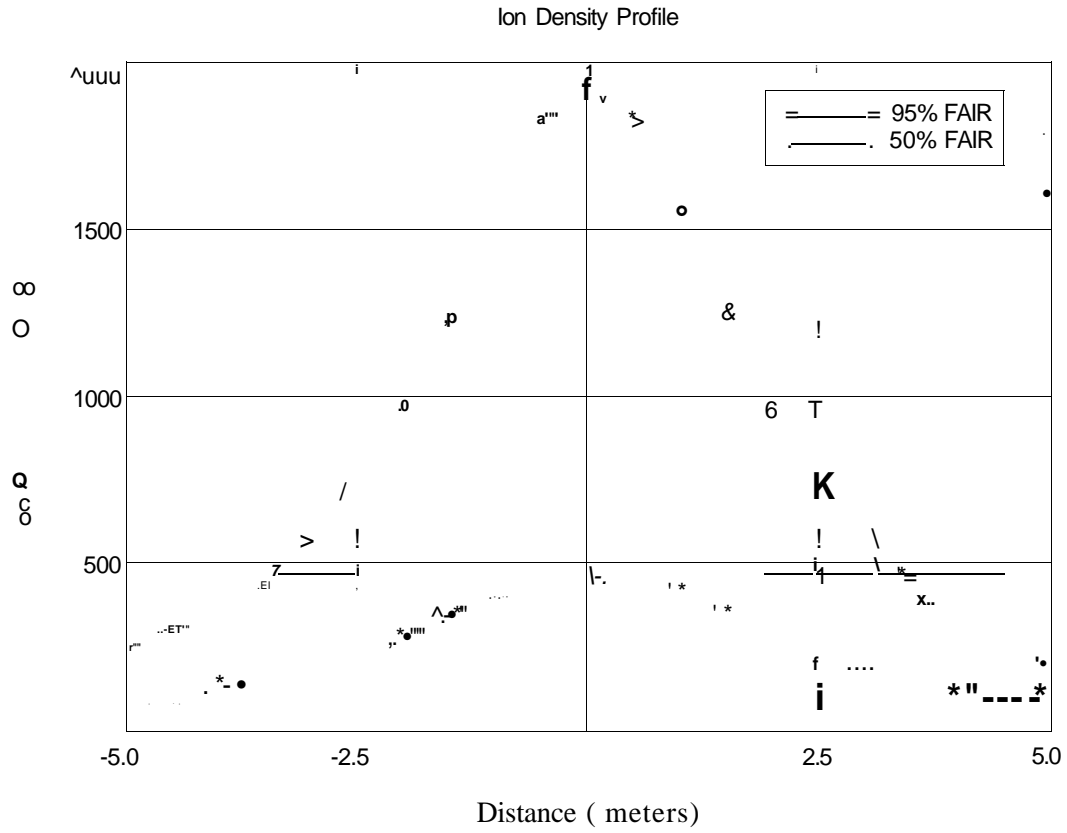
Figure 6.9: Test Line (-250kV) - Ion Density Profile

Ion Current Profile
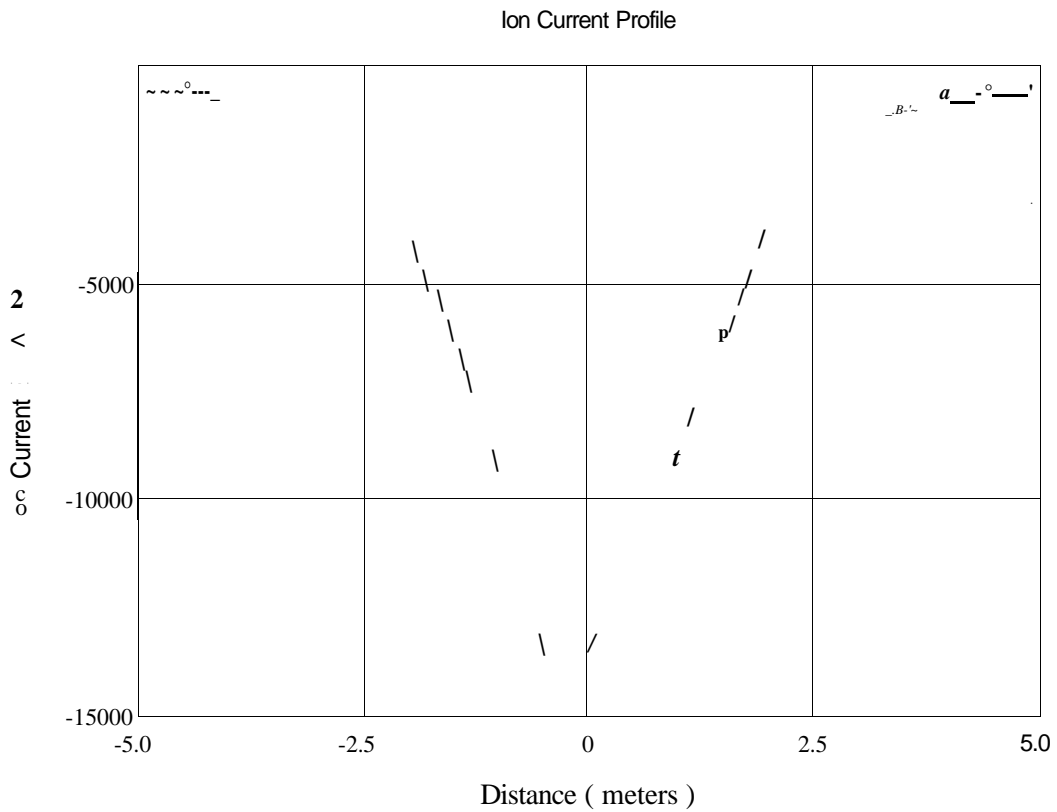
Figure 6.10: Test Line (-250kV) - Ion Current Profile

6.2.2 Cahora Bassa Line Simulation Results:

Table 6.8: Cahora Bassa Line (+533kV) - Maximum Surface Gradient

```
* * * * * * * * * * * * * * * * * * * * * * * * * * * * * * * * * *
*                                                                 *
*  MAXIMUM SURFACE GRADIENT (kV/cm)  *
*                                                                 *
* * * * * * * * * * * * * * * * * * * * * * * * * * * * * * * * *
```

BNDL #	Type	DC	PEAK(+)	PEAK(−)
1	DC	18.70	18.70	18.70
2	Ground Wire	−21.64	•21.64	−21.64

Table 6.9: Cahora Bassa Line (+533kV) - E-Field, Current Density & Ion Density

LATERAL DISTANCE		<— DC ELECTRIC FIELD —>		CURRENT DENSITY	ION DENSITY
		ELECTROSTATIC	SATURATED		
(feet)	(meters)	(kV/m)	(kV/m)	(nA/m2)	(1/cm3)
-32.8	-10.00	6.17	25.17	22.2	47876.
-26.2	-8.00	6.52	26.15	24.6	51155.
-19.7	-6.00	6.81	27.02	26.9	54081.
-13.1	-4.00	7.04	27.49	28.3	55950.
-6.6	-2.00	7.19	28.06	29.8	57706.
.0	.00	7.24	28.16	30.1	58128.
6.6	2.00	7.19	28.06	29.8	57706.
13.1	4.00	7.04	27.49	28.3	55950.
19.7	6.00	6.81	27.02	26.9	54081.
26.2	8.00	6.52	26.15	24.6	51155.
32.8	10.00	6.17	25.17	22.2	47876.

Table 6.10: Cahora Bassa Line (+533kV) - E-Field & Ion Density Profile

LATERAL DISTANCE		FIELD 50%	FIELD 95%	IONS 50%	IONS 95%	FIELD 50%	FIELD 95%	IONS 50%	IONS 95%
(feet)	(meters)	(kv/rn)	(kV/m)	(1/cc)	(1/cc)	(kV/m)	(kV/m)	(1/cc)	(1/cc)
-32.8	-10 00	10.4	16.7	25814.	40062.	16.4	19.2	39523.	43025.
-26.2	-8 00	10.9	17.4	27370.	4269 0.	17.1	20.0	42107.	45894.
-19.7	-6 00	11.3	18.1	28774.	45041.	17.7	20.7	44421.	48458.
-13.1	-4 00	11.6	18.4	29547.	46473.	18.0	21.0	45825.	50050.
-6.6	-2 00	11.8	18.8	30474.	47932.	18.4	21.5	47263.	51621.
.0	00	11.9	18.9	306 52.	48257.	18.5	21.6	47582.	51981.
6.6	2 00	11.8	18.8	30474.	47932.	18.4	21.5	47263.	51621.
13.1	4 00	11.6	18.4	29547.	46473.	18.0	21.0	45825.	50050.
19.7	6 00	11.3	18.1	28774.	45041.	17.7	20.7	44421.	48458.
26.2	8 00	10.9	17.4	27370.	42690.	17.1	20.0	42107.	45894.
32.8	10 00	10.4	16.7	25814.	40062.	16.4	19.2	39523.	43025.
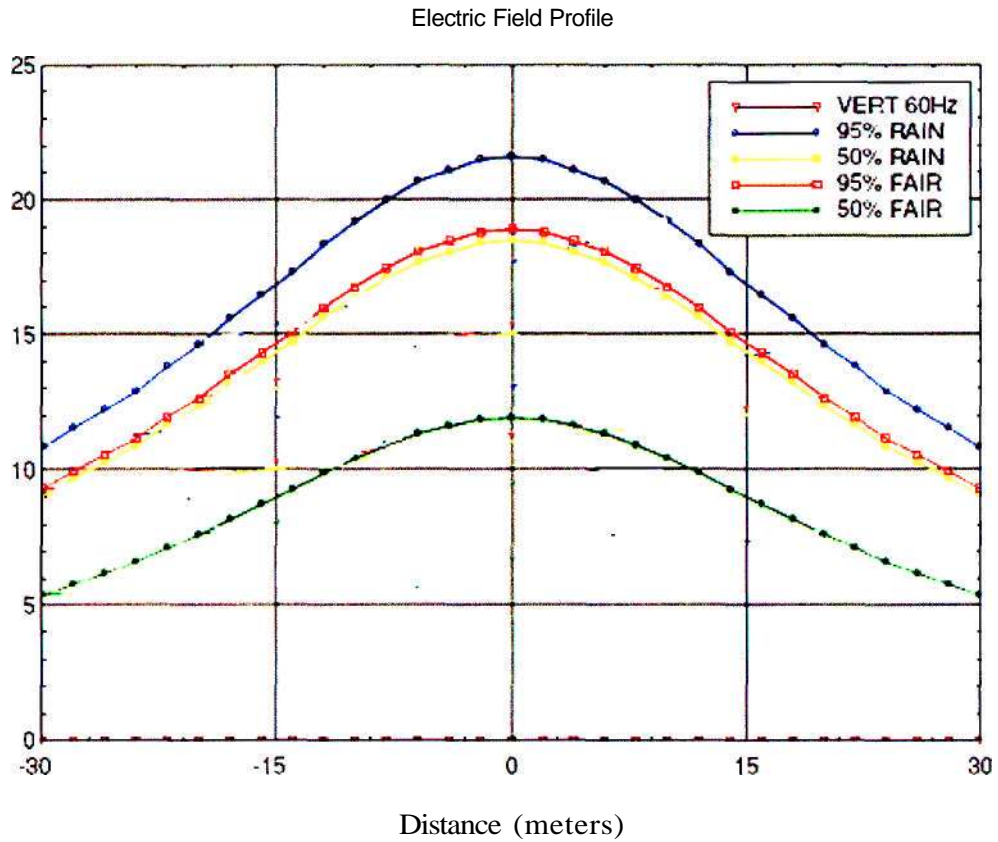
Electric Field Profile

Distance (meters)

Figure 6.11: Cahora Bassa Line (+533kV) - E-Field Profile

Ion Density Profile

Distance {meters)

Figure 6.12: Cahora Bassa Line (+533kV) - Ion Density Profile

Ion Currenl Profile

-30   -15   15   30

Distance (meters >
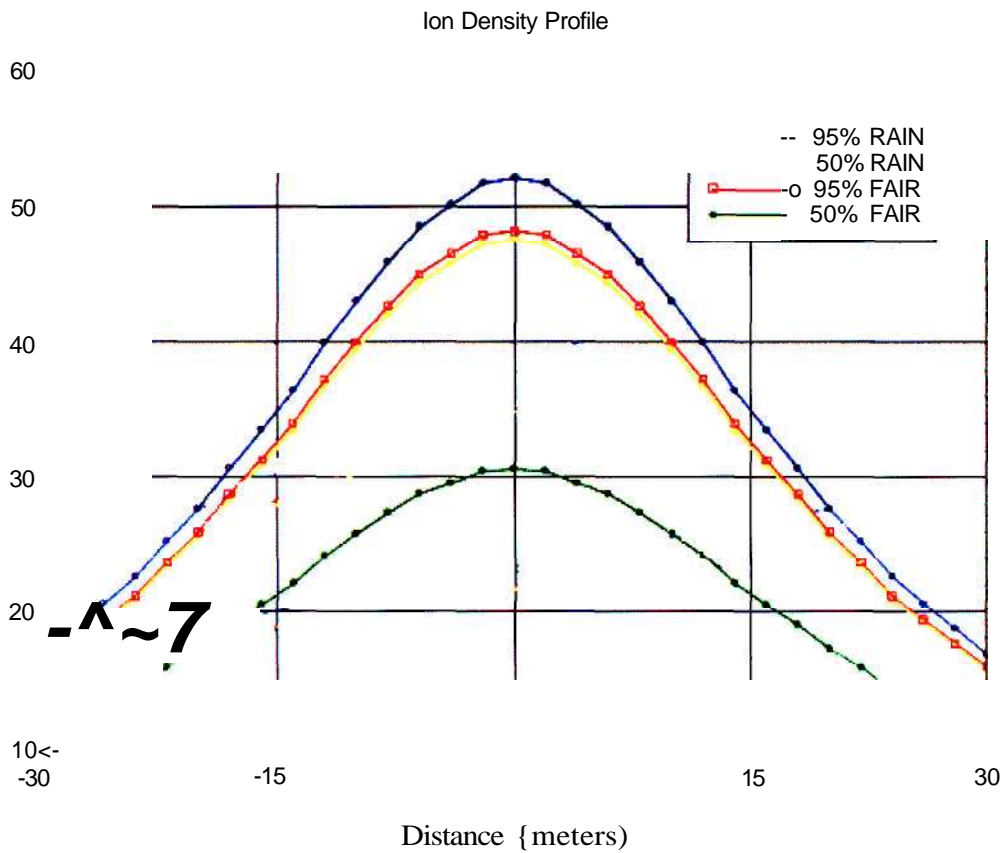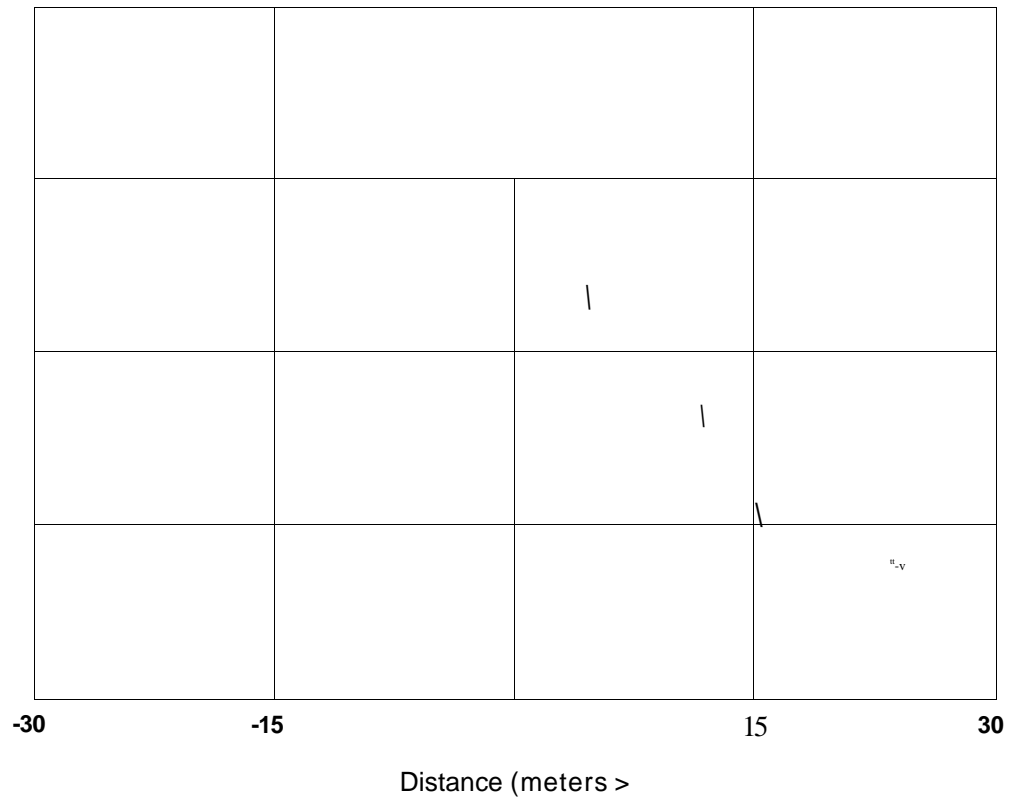
Figure 6.13: Cahora Bassa Line (+533kV) - Ion Current Profile

Table 6.11: Cahora Bassa Line (-533kV) - Maximum Surface Gradient

```
             * MAXIMUM SURFACE GRADIENT (kV/crn)  *


      BNDL #    Type        DC      PEAK(+)    PEAK(-)

        1        DC       -18.70    -18.70     -18.70
        2  Ground Wire    21.38     21.38      21.38
```

Table 6.12: Cahora Bassa Line (-533kV) -E-Field, Current Density & Ion Density

LATERAL DISTANCE		<— DC ELECTRIC FIELD —>		CURRENT DENSITY	ION DENSITY
(feet)	(meters)	ELECTROSTATIC (kv/m)	SATURATED (kV/m)	(nA/m2)	(1/cm3)
-98.4	-30.00	-2.77	-14.54	-6.4	-18447.
-91.9	-28.00	-3.02	-15.50	-7.6	-20546.
-85.3	-26.00	-3.29	-16.37	-8.9	-22680.
-78.7	-24.00	-3.59	-17.26	-10.4	-25001.
-72.2	-22.00	-3.91	-18.44	-12.3	-27900.
-65.6	-20.00	-4.26	-19.45	-14.4	-30744.
-59.1	-18.00	-4.64	-20.72	-17.0	-34177.
-52.5	-16.00	-5.03	-21.83	-19.6	-37507.
-45.9	-14.00	-5.43	-22.91	-22.5	-40932.
-39.4	-12.00	-5.83	-24.27	-26.2	-44968.
-32.8	-10.00	-6.22	-25.35	-29.5	-48525.
-26.2	-8.00	-6.58	-26.35	-32.8	-51892.
-19.7	-6.00	-6.88	-27.23	-35.9	-54897.
-13.1	-4.00	-7.12	-27.71	-37.8	-56829.
-6.6	-2.00	-7.27	-28.29	-39.8	-58630.
Q	.00	-7.32	-28.40	-40.3	-59065.
6.6	2.00	-7.27	-28.29	-39.8	-58630.
13.1	4.00	-7.12	-27.71	-37.8	-56829.
19.7	6.00	-6.88	-27.23	-35.9	-54897.
26.2	8.00	-6.58	-26.35	-32.8	-51892.
32.8	10.00	-6.22	-25.35	-29.5	-48525.
39.4	12.00	-5.83	-24.27	-26.2	-44968.
45.9	14.00	-5.43	-22.91	-22.5	-40932.
52.5	16.00	-5.03	-21.83	-19.6	-37507.
59.1	18.00	-4.64	-20.72	-17.0	-34177.
65.6	20.00	-4.26	-19.45	-14.4	-30744.
72.2	22.00	-3.91	-18.44	-12.3	-27900.
78.7	24.00	-3.59	-17.26	-10.4	-25001.
85.3	26.00	-3.29	-16.37	-8.9	-22680.
91.9	28.00	-3.02	-15.50	-7.6	-20546.
98.4	30.00	-2.77	-14.54	-6.4	-18447.

Table 6.13: Cahora Bassa Line (-533kV) - E-Field & Ion Density Profile

LATERAL DISTANCE (feet)	(meters)	FIELD 50% (kv/tn)	FIELD 95% (kv/m)	IONS 50% (1/cc)	IONS 95% (1/cc)	FIELD 50% (kv/m)	FIELD 95% (kV/m)	IONS 50% (1/cc)	IONS 95% (1/cc)
		<---------SUMMER FAIR							
-9 8 4	-30 00	-4 4	_7 4	8500	14265.	-9.1	-10.8	15842.	16959.
-91 9	-28 00	-4 8	-7 9	9356	15809.	-9.7	-11.6	17590.	18855.
-85 3	-26 00	-5 1	-8 4	10151	17324.	-10.3	-12.2	19328.	20760.
-78- 7	-24 00	-5 5	-9 0	10983	18944.	-10.9	-13.0	21200.	22818.
-72 2	-22 00	-5 9	-9 6	12114	2103 4.	-11.7	-13.9	23582.	25417.
-65 6	-20 00	-6 4	-10 2	13107	22993.	-12.4	-14.7	25856.	27927.
-59 1	-18 00	-6 9	-11 0	14399	25428.	-13.3	-15.7	28648.	30987.
-52 ₂	-16 00	-7 4	-11 6	15537	27696.	-14.0	-16.5	31291.	33913.
-45 9	-14 00	-/ 9	-12 3	16673	29998.	-14.8	-17.4	33985.	36907.
-39 4	-12 00	-8 4	-13 1	18167	32834.	-15 7	-18 5	37248.	40491.
-32 g	-10 00	-8 9	-13 8	19359	35230.	-16 5	-19 3	40048.	43602.
-26 2	-8 00	-9 3	-14 4	20492	37498.	-17 A	-20 1	42699.	46546.
-19 7	-6 00	-9 7	-14 9	21518	39534.	-17 8	-20 8	45073.	49179.
-13 1	-4 00	-10 0	-15 2	22057	40741.	-18 2	-21 2	46525.	50824.
-6 6	-2 00	-10 2	-15 6	22754	42030.	-18 6	-21 /	47997.	524 33.
0	00	-10 3	-15 6	22879	42304.	-18 6	-21 8	48326.	52805.
6 6	2 00	-10 2	-15 6	22754	42030.	-18 6	-21 /	47997.	52433.
13 1	4 00	-10 0	-15 2	22057	40741.	-18 2	-21 2	46525.	50824.
19 7	6 00	-9	-14 9	21518	39534.	-17 8	-20 8	45073.	49179.
26 2	8 00	-9 3	-14 4	20492	37498.	-17 °	-20 1	42699.	46546.
32 8	10 00	-8 9	-13 8	19359	35230.	-16 5	-19 3	40048.	43602.
39 4	12 00	-8 4	-13 1	18167	32834.	-15 ⁊	-18 5	37248.	40491.
45 9	14 00	-/ 9	-12 3	16673	29998.	-14 8	-17 4	33985.	36907.
52 ₆	16 00	-/ 4	-11 6	155 37	27696.	-14 0	-16 5	31291.	3 3913.
59 1	18 00	-6 9	-11 0	14399	25428.	-13 3	-15 7	28648.	30987.
65 6	20 00	-6 4	-10 2	13107	22993.	-12 4	-14 /	25856.	27927.
72 2	22 00	-5 9	-9 6	12114	21034.	-11 ⁊	-13 9	23582.	25417.
78 7	24 00	-5 5	-9 0	10983	18944.	-10 9	-13 0	21200.	22818.
8 5 3	26 00	-5 1	-8 4	10151	17324.	-10 3	-12 2	19328.	20760.
91 3	28 00	-4 8	—7 9	9356	15809.	-9	-11 6	17590.	188 55.
98 4	30 00	-4 4	-7 4	8500	14265.	-9 1	-10 8	15842.	16959.

Electric Field ProJile

Distance (meters)
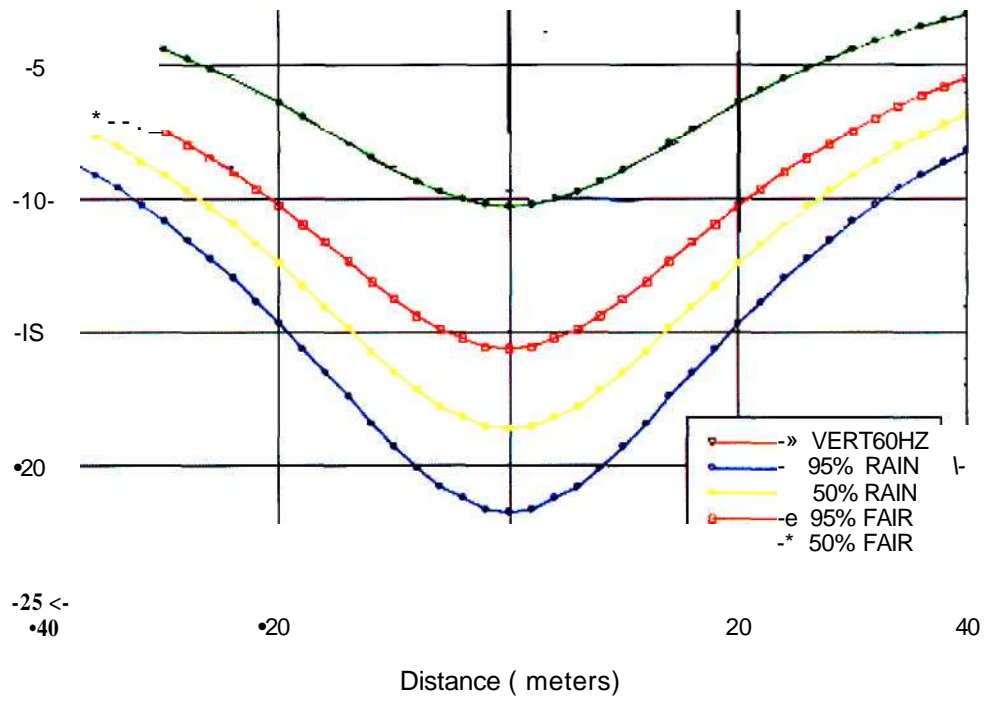
Figure 6.14: Cahora Bassa Line (-533kV) - E-Field Profile

Ion Density Profile

Distance {meters
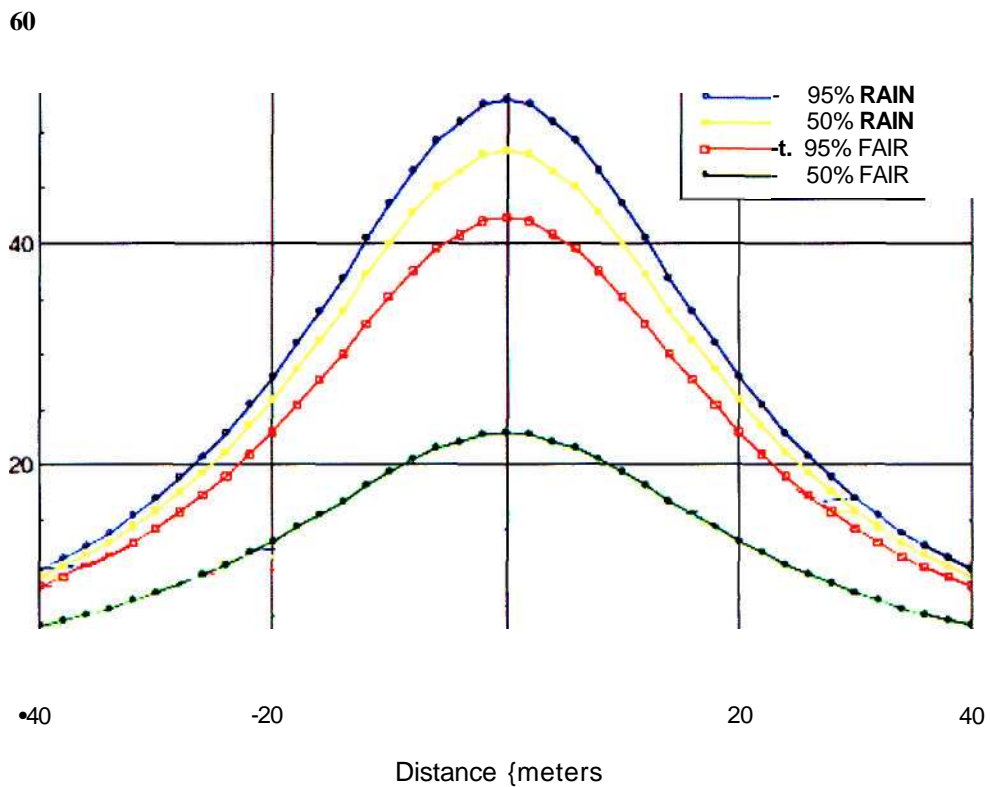
Figure 6.15: Cahora Bassa Line (-533kV) - Ion Density Profile

Ion Current Ptolile

Distance {meters}
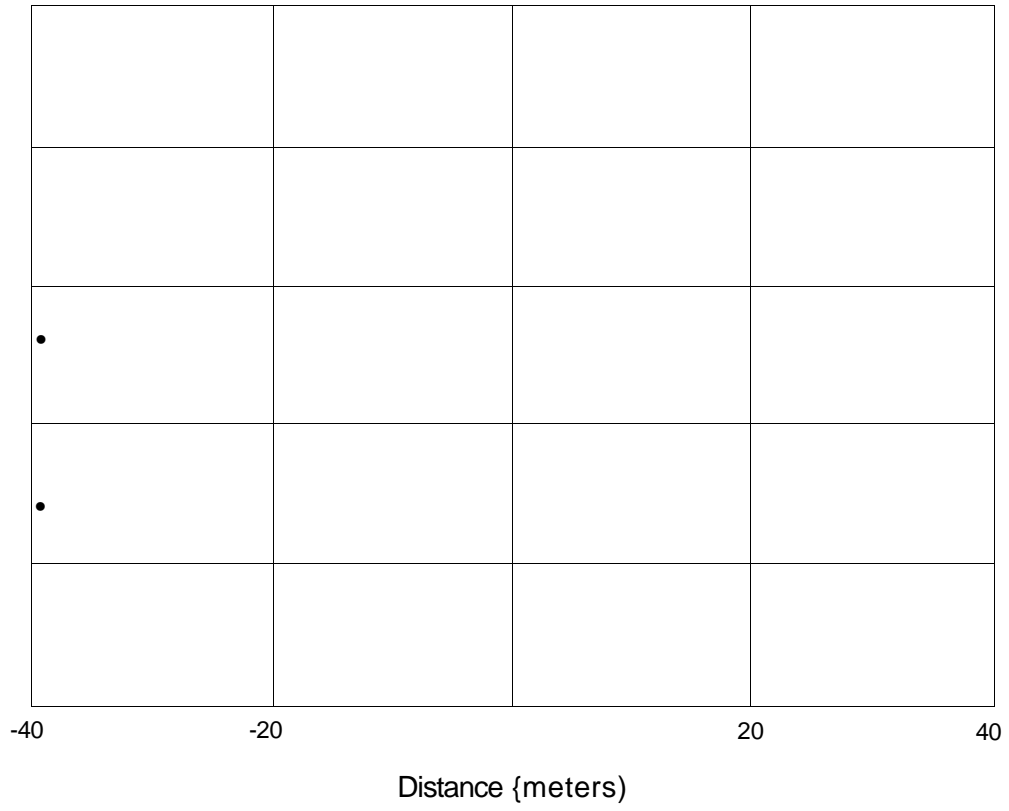
Figure 6.16: Cahora Bassa Line (-533kV) - Ion Current Profile

6.2.3 Discussion and Findings:

The EPRITL Workstation software was used for simulations on the laboratory test line and the Cahora Bassa line. The simulations were carried out for applied voltages of + 250kV on the test line and for + 533 kV for the Cahora Bassa line.

The simulations find the maximum conductor surface gradient to be 16.69 kV/cm for both positive and negative, on the laboratory test line. The peak value of the electric field is once again recorded directly below the line with a value of 60.01 kV/m. The current densities recorded were 10361.1 nA/m^2 and - 13514.4 nA/m^2 for the positive (+ 250kV) and negative (- 250kV) applied voltages respectively. This means that we can expect a higher ion current density for the negative pole as compared to the positive pole. Even though the electric fields for positive and negative are similar, laboratory measurements tend to indicate otherwise.

The EPRI simulations find the maximum surface gradient of the Cahora Bassa line to be 18.7 kV/cm for both positive and negative. Our calculation for the maximum surface gradient was 19.43 kV/cm. The electrostatic DC electric field was found to be 7.24 kV/m and - 7.32 kV/m for positive and negative respectively. The ion current density is 30.1 nA/m^2 for positive and - 40.3 nA/m^2 for negative. The ion density is 3.065 x 10^4 $ions/cm^3$ for positive and 2.288 x 10^4 $ions/cm^3$ for negative.

6.3 COMPARISON OF RESULTS: MICROSOFT EXCEL SIMULATIONS VERSUS EPRI TL WORKSTATION SIMULATIONS

6.3.1 Laboratory Test Line:

The Microsoft Excel simulations find the electric field directly below the test line to be 64.34 kV/m for both positive and negative polarity (at 250 kV). The electric field 1 metre away from the test line on either side is 52.9 kV/m for both positive and negative polarity. The reason for the electric fields being equal under the different polarities is because the Excel simulations use formulae (equation 6.2) to calculate the values. When using equation 6.2 to calculate the electric field below the test line, the only difference is the voltage polarity and hence we obtain the same electric field strength below the laboratory test line. It should also be noted that equation 6.2 does not take the effect of space charge into account.

The results from the EPRI simulations find the DC electrostatic field directly below the test line to be 60.01 kV/m for positive and negative polarity. The electric field 1 metre away from the line is 48.21 kV/m for both polarities.

By comparing the results from both simulations, it is found that they are very similar. There seems to be good comparison between the two results and the difference is also very marginal. When we move further away from the line, the results are still quite similar (52.9 kV/m for the Excel simulations compared to 48.21 kV/m for the EPRI simulations).

6.3.2 Cahora Bassa Line:

The Excel simulations for the Cahora Bassa line shows that the electric field directly below the line is 7.524 kV/m for both positive and negative poles. The electric field at ground level 10 metres away from the line is 6.541 kV/m.

The results of the EPRI simulations for the Cahora Bassa line find the electric field directly below the positive pole to be 7.24 kV/m and - 7.32 kV/m for the negative pole. The electric field at ground level 10 metres away from the line is 6.17 kV/m and - 6.22 kV/m for positive and negative poles respectively. The result shows that we can expect higher electric fields below the negative pole, but the difference is marginal

When we compare the results of the two simulation methods, we find that the correlation is much better for the Cahora Bassa line than the test line results. The Excel simulations find the electric field to be marginally higher (about 0.3 kV/m) directly below the line. The electric field 10 metres away, at ground level, also show excellent correlation between the Excel results and the EPRI simulations. This tends to tell us that the EPRI simulations are also based on calculations that use the same equations (equations 6.1 - 6.3). The Excel simulations use equations 6.1, 6.2 and 6.3 to calculate the electric fields and these equations do not take space charge into account. The EPRI simulation results and the Excel simulations show very good correlation for the "unsaturated electric field." The EPRI software seems to be taking the space charge effect into account however it shows that the EPRI software is under estimating the enhancement of the electric field at ground level. Long term statistical measurements at several different locations need to be conducted to make a proper comparison between the actual measurements and the EPRI simulations.

6.4 COMPARISON OF RESULTS: TEST LINE VERSUS CAHORA BASSA LINE

In this section we compare the simulation results of the test line against the simulation results for the Cahora Bassa line by considering the scaling factor. The scaling factor of the test line to the Cahora Bassa line is 1/12 (this only applies to the shield wire height, the pole conductor height and the distance between the shield wire and pole conductor). For the scaling factor to be correct for all criteria, the conductor dimensions (conductor diameter, conductor configuration) and voltage ratio also needs to be 1/12. The actual scaling ratio of the test line can be calculated using equation 6.3 (page 83).

$$\frac{E_x}{E_2} \quad \frac{\_V_{,y}H_2\underline{Jn(2H_2/r_2)}\_{Z55}}{V_2 \quad H_x \quad \backslash n\{2HJr_x)}$$

(Ei = Test Line Electric Field & E_2 = Cahora Bassa Electric Field)
(V! = 250 kV & V_2 = 533 kV)

By looking at the Excel results of both lines, we find that the ground level electric field is 64.2 kV/m for the test line and 7.524 kV/m for the Cahora Bassa line. From this we calculate a ratio of 8.53 for the electric fields as compared to the scaling factor of 8.55. This shows good correlation for the Excel simulation results for the electric field in the absence of space charge.

If we consider the results from the EPRI simulations, we find the ground level electric field is 60.01 kV/m for the test line and 7.24 kV/m below the Cahora Bassa line, under positive polarity. This equates to a ratio of 8.29 and correlates well with the 8.55 expected ratio.

When comparing the unsaturated electric fields for the test line and the Cahora Bassa line, the scaling factor seems to be quite accurate. This does not hold true when comparing the actual measurements (test line and Cahora Bassa line) to the simulated values as phenomenon such as corona and space charge are nonlinear and hence they cannot be accurately scaled.

CHAPTER 7

CONCLUSIONS

7.1 CONCLUSIONS:

- From the results of the laboratory measurements, it is clear that there is a difference in the levels of corona leakage currents and induced voltages that are measured under positive and negative polarity. For the same levels of applied voltage (150 kV), it is seen that the corona leakage current for negative polarity is about 16 % higher than the corona leakage current for the positive polarity (corona sources on shield wire and pole conductor). For similar levels of induced voltages (35 kV), we find that the negative applied voltage (- 145 kV) is about 9 % lower than the positive (+157.5 kV) applied voltage when there are corona sources on both the pole conductor and the shield wire. This suggests that the positive pole can be operated at a higher voltage than the negative pole for the same levels of coupling but it remains speculative whether this will work operationally. The results of the measurements under negative applied voltage show a lot more stability and linearity when compared to positive applied voltage.

- The results of the Microsoft Excel simulations and the EPRI simulations for the laboratory test line show good correlation for the electric field at ground level, directly below the pole conductor. The Excel simulations calculate the electric field below the pole conductor to be 64.34 kV/m while the EPRI simulation calculates the electric field to be 60.01 kV/m (for both positive and negative applied voltages). The Excel simulation results are marginally (7 %) higher than the EPRI results for the test line. The results of the Microsoft Excel simulations and the EPRI simulations for the Cahora Bassa line also show very good correlation for the electric field at ground level. The Excel simulation calculates the electric field to be + 7.524 kV/m as compared to the EPRI simulation which finds the electric fields to be 7.24 kV/m and - 7.32 kV/m for positive and negative polarity respectively. This equates to a difference of less than 4 % between the two methods.

- When comparing the actual measurements that were taken under the laboratory test line against the EPRI simulations (expected values), one can see that the EPRI simulations predict higher ionic currents and lower electric fields. The ion current measurements below the test line shows that the levels of ion currents below the negative polarity (-5.1 uA) at maximum applied voltage are almost twice the levels of ion currents below the positive polarity (2.7 uA). The EPRI simulations predict the ionic currents to be + 10.36 uA and - 13.5 uA for positive and negative polarity respectively. From this we can conclude that the path to ground under negative polarity is more conductive.

- The measured electric field below the laboratory test line shows that the electric field strength under negative polarity (- 109 kV/m) is about 17 % higher than the electric field strength for positive polarity (+ 93.5 kV/m) for + 250 kV of applied voltage. The EPRI simulations for the electric field under the laboratory test line are + 60.01 kV/m at + 250 kV applied voltage. By comparing the two results we see that the measured electric fields are higher than the EPRI simulations. The measured electric field under negative polarity is almost double the EPRI expected value. It seems that the EPRI simulation does not take into account the effect of the space charge enhancement on the electric field. The small scale geometry of the test line (a smaller air gap means that the space charge effect is more pronounced) could also be the reason for the higher measured values. The difference

between the positive and negative measured values could be attributed to the behaviour of the ions and further investigation into this behaviour pattern is required.

- For the actual measurements below the Cahora Bassa line, the measured results for ionic currents were lower than the EPRI simulated values. For the ionic currents under negative polarity, the measured value (- 150 nA) was about half the EPRI simulated (- 317.2 nA) value. The measured ionic current for the positive polarity was 5.11 nA as compared to the EPRI simulated value of 131.6 nA. The EPRI simulated values for ionic currents are higher than the actual measured currents, as was the case for the laboratory test line.

- When comparing the measured electric field values for the Cahora Bassa line against the EPRI simulated values for the actual conditions (Appendix C), one can see that the EPRI value (+ 12.5 kV/m) is higher than the measured value (+5 kV/m) for positive polarity and EPRI value (- 55.6 kV/m) is lower than the measured value (- 67 kV/m) for the negative polarity. There is no correlation between the measured values and the EPRI simulations for positive polarity and this is attributed to the higher wind speeds that were experienced during the measurements. The electric field under negative polarity shows good correlation between the two cases. The measured value is higher than the EPRI simulated value for the negative polarity and this was the same for the laboratory test line comparison.

- From the comparisons that were made (EPRI simulation versus actual measurements) for the test line and Cahora Bassa line, the EPRI simulations found higher ionic currents and lower electric fields while the measurements showed the opposite, i.e. higher electric fields and lower ionic currents. This could be attributed to the way the EPRI software calculates the values. When we compared the space charge density (section 5.8), we found that the EPRI simulated values were the same for both positive and negative space charge density. The measured values have shown that this is not practical (equal space charge densities for both polarities) and hence this could explain why the measured values are opposite of the simulated values. The EPRI simulation is under estimating the space charge enhancement of the electric field and it then uses this electric field to calculate the ionic currents, hence the higher ionic currents (equation 2.2).

- When comparing the laboratory measurements against the Cahora Bassa line measurements, considering a scaling factor design of 1/12, we find no correlation between the two. The actual ratio (section 6.4) of the electric fields is calculated to be 8.55. The laboratory measurements find the electric field for the test line to be twice that of the Cahora Bassa line (negative polarity). One possible reason for this could be the size constraints of the laboratory which could be concentrating the space charge within the laboratory and this is causing further enhancement of the measured electric fields. The line loading (current) is another factor that cannot be modelled into a scaled test line. The line current leads to higher conductor temperatures and we have seen from previous studies [11] that this can effect the electrical environment at ground level.

- The hypothesis is rejected based upon the results presented. The electric field environment below HVDC lines can be fundamentally studied under laboratory conditions although these results cannot be used directly to predict the performance of full-scale transmission lines. The highly non-linear nature of corona and space charge phenomena are not scalable and a more accurate method for correlating test line results against actual operating lines needs to be developed. An outdoor test line may be a better option than an indoor test line for this study. It will help simulate the actual line that is in the field, wind speeds can be accounted for, there will be no concentration of ions on the outdoor test line and the line sag can also be incorporated into the design. All dimensions (height, conductor configurations, voltage, sag and power loading) will need to be accurately scaled for an outdoor test line to be used for a study of this nature.

- The first study that can be carried out will be to look at the effect of different conductor configurations on the electric field and ion current density at ground level. We have already conducted measurements (ion current density, induced voltages, corona currents and electric field) using a 4 conductor bundle (3.18 cm sub-conductor diameter) and we should now conduct the same measurements using a 2 conductor bundle, 3 conductor bundle and a 6 conductor bundle.

- We should also conduct small scale bipolar line tests. For these tests, two DC generators will be required. A small scale variable test line needs to be designed and built. We should be able to vary the pole conductor height, pole conductor spacing (between positive and negative poles), sub-conductor diameter size and distance between the shield wire and pole conductor. It is recommended that a maximum of 2 conductors be used for the conductor bundles. This will help us verify the effect of pole height and pole spacing on the electrical environment below the line as well as how to reduce these effects.

- It is also believed that large clouds of space charge could be forming at conductor height, near the insulator strings thus affecting the insulation strength in that region. Tests on insulator strings need to be conducted to verify this effect by measuring the voltage distribution across the insulator string. We have already seen that the current path to ground becomes more conductive in the presence of space charge. The space charge could then affect the flash over distance between the live end of the insulator and the tower. The tests can be conducted under laboratory conditions by using two DC generators. The possible test set up is shown in figure 7.1.
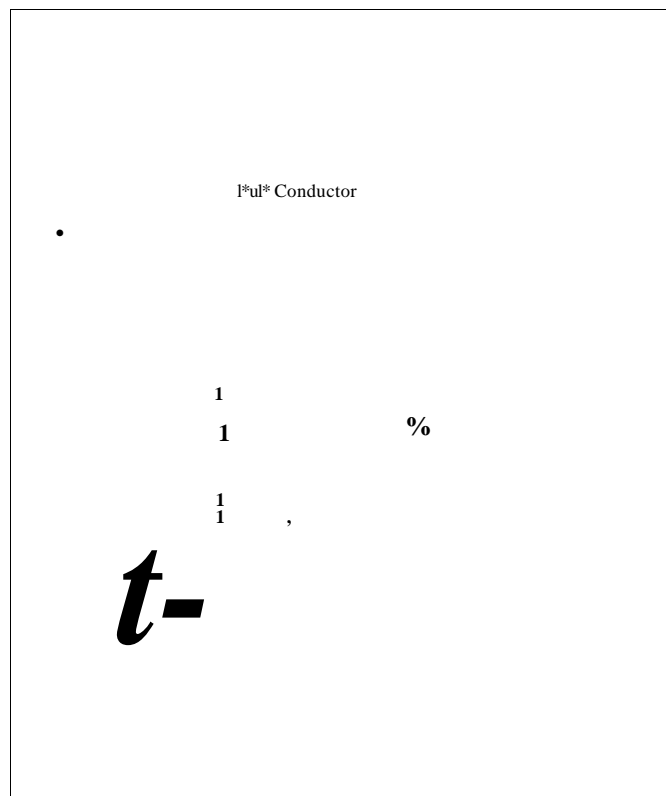
Figure 7.1: Insulator Test Set Up

REFERENCES

1. F.F Bologna, A.C Britten, R.E Kohlmeyer, H.F Vosloo. **Investigation into the cause of "Unknown Line Faults on a + 533 kV DC Line in South Africa".** IEEE HVDC Conference, University of KwaZulu-Natal, July 2006, pages 1-8.

2. IEEE Standard 1227 - **Guide for the Measurement of DC Electric Field Strength and Ion Related Quantities,** 1990, pages 1 - 50.

3. **HVDC Transmission Line Reference Book,** EPRI, White Book - Pages 4-37 & 4-38.

4. T. Suda, Y. Sunaga. **An Experimental Study of Large Ion Density under the Shiobara HVDC Test Line.** IEEE Transactions on Power Delivery, Vol. 5, No. 3, July 1990, pages 1426-1435.

5. P.S Maruvada. **Corona Generated Space Charge Environment in the Vicinity of HVDC Transmission Lines.** IEEE Transactions on Electrical Insulation, Vol. EI-17 No. 2, April 1982, p.p. 125-130.

6. B.L. Qin, J.N Sheng, Z. Yan, G. Gela. **Accurate Calculation of Ion Flow under HVDC Bipolar Transmission Lines.** IEEE Transactions on Power Delivery, Vol. 3, No. 1, January 1988, pages 368 - 376.

7. T. Suda, Y. Sunaga. **Small Ion Mobility Characteristics under the Shiobara HVDC Test Line.** IEEE Transactions on Power Delivery, Vol. 5, No. 1, January 1990, pages 247 -253.

8. T. Suda, Y. Sunaga. **An Experimental Study of Large Ion Density under the Shiobara HVDC Test Line.** IEEE Transactions on Power Delivery, Vol. 5, No. 3, July 1990, pages 1426-1435.

9. T. Suda, Y Sunaga. **Calculation of Large Ion Densities under HVDC Transmission Lines by Finite Difference Method.** IEEE Transactions on Power Delivery, Vol. 1, No. 4, October 1995.

10. V. Jaiswal, M.J Thomas. **Finite Element Modelling of Ionized Field Quantities around a Monopolar HVDC Transmission Line.** Indian Institute of Science, Journal of Physics, J. Phys. D: Applied Phys. 36 (2003), pages 3089 - 3094.

11. V.L Chartier, R.D Stearns. **Examination of Grizzly Mountain Data Base to Determine Effects of Relative Air Density and Conductor Temperature on HVDC Corona Phenomenon.** IEEE Transactions on Power Delivery, Vol. 5, No. 3, July 1990, pages 1575-1582.

12. Y. Amano, Y. Sunaga. **Study on Reduction in Electric Field, Charged Voltage, Ion Current and Ion Density under HVDC Transmission Lines by Parallel Shield Wires.** IEEE Transactions on Power Delivery, Vol. 4, No. 2, April 1989, pages 1351-1359.

13. P.J Carter, G.B Johnson. **Space Charge Measurements Downwind from a Monopolar 500 kV HVDC Test Line.** IEEE Transactions on Power Delivery, Vol. 3, No. 4, October 1988, pages 2056-2063.

14.   R.H McKnight, F.R Kotter, M. Misakian. **Measurement of Ion Current Density at Ground Level in the Vicinity of HVDC Transmission Lines.** IEEE Transactions on Power Apparatus and Systems, Vol. PAS-102, No. 4, April 1983, pages 934 - 941.

15.   Y. Sunaga, Y. Amano, T. Sugimoto. **Electric Field and Ion Current at the Ground and Voltage of Charged Objects under HVDC Lines.** IEEE Transactions on Power Apparatus and Systems, Vol. PAS-100, No. 4, April 1981, pages 2082 - 2091.

16.   M.G Comber, G.B Johnson. **HVDC Field and Ion Effects Research at Project UHV: Results of Electric Field and Ion Current Measurements.** IEEE Transactions on Power Apparatus and Systems, Vol. PAS-101, No. 7, July 1982, pages 1998 - 2006.

17.   P.S Maruvada, R.D Dallaire, P. Heroux, N. Rivest. **Long Term Statistical Study of the Corona Electric Field and Ion-Current Performance of a + 900 kV Bipolar HVDC Transmission Line Configuration.** IEEE Transactions on Power Apparatus and Systems, Vol. PAS-103, No. 1, January 1984, pages 77 - 83.

18.   P.S Maruvada, R.D Dallaire, O.C Norris-Elye, C.V Thio, J.S Goodman. **Environmental Effects of the Nelson River HVDC Transmission Lines - RI, AN, Electric Field, Induced Voltage, and Ion Current Distribution Tests.** IEEE Transactions on Power Apparatus and Systems, Vol. PAS-101, No. 4, April 1984, pages 951 - 959.

19.   P.S Maruvada. **Corona Performance of High Voltage Transmission Lines.** Research Studies Press Ltd, 2000.

20.   M. Grant, J.M Garrard, K.J Nixon. **Low Cost Electric-Field Mill: Design, Construction and Testing.** University of Witwatersrand, School of Electrical and Information Engineering, Johannesburg, South Africa, 2006.

21.   **Pico scope 3000 Series PC Oscilloscopes, User Guide.** Pico Technology Ltd. 2006.

22.   **Ferrite Kit Clip-on, Manual.** Hitek Electronic Materials Ltd. 15 Wentworth Road, Scunthorpe, North Lines, DN17 2AX.

23.   **Portable Electrostatic Fieldmeter Model 257D, Operator's Manual.** Monroe Electronics Inc. 2000

24.   G.C Sibilant, A.C Britten, D. Govender, R.W Wachal. **The Effect of Ions and Space Charge on the Performance of HVDC Lines - Literature Review and Case Study.** HVDC 2006 Congress, University of Kwa-zulu Natal, July 2006, pages 1 - 6.

25.   **EPRI TL 3.0 Workstation.** EPRI, Palo Alto, USA, 2003.

26.   MWB (India) LTD. **Instruction Manual, 500 kV - DC Test Set.**

27.   N.M Moyo. **Noise Generation Phenomena in the PLC System of the Cahora Bassa HVDC Transmission Line.** MSc Dissertation, University of Kwazulu Natal, April 2003.

BIBLIOGRAPHY

28.   R.E. Vosteen. **DC Electrostatic Voltmeters and Fieldmeters.** Monroe Electronics Inc, Lyndonville, New York, 14098, 1974, pages 799 - 810.

29.   E. Lubini. **The Westcor HVDC Project.** Energize, May 2006, pages 30 -32.

30.   A.C Britten, T. Pillay, P. Naidoo, D. Muftic, F.F Bologna, N.M Ijumba. **Eskom's Proposed Strategic Research into Long-Distance HVDC Transmission.** Eskom - Resources and Strategy Division. Lower Germiston Road, Rosherville, Johannesburg, South Africa, 2006, pages 1-10.

31.   A.C Britten, P. Naidoo, D. Muftic, N.M Ijumba, G.C Sibilant, A. Burger, W.L Vosloo, R. Stephen. **Investigations into Electrical and Corona Effects for the Upgrade of HVAC Transmission Lines to HVDC.** Eskom - Johannesburg, South Africa,2006, pages 1 - 6.

32.   G.B Johnson, L.E Zaffanella. **Techniques for Measurements of the Electrical Environment created by HVDC Transmission Lines.** Fourth International Symposium on High Voltage Engineering, Athens, Greece, 5-9 September, 1983, pages 1- 4.

33.   R.B Bent, H.L Collin, W.C.A Hutchinson, J.A Chalmers. **Space Charges Produced by Point Discharge from Trees during a Thunderstorm.** Journal of Atmospheric and Terrestrial Physics, Volume 27, 1965, page 67-72.

34.   V.L Chartier, L.D Dickson, L.Y Lee, R.D Stearns. **Performance of a Long-Term Unattended Station for Measuring DC Fields and Air Ions from an Operating HVDC Line.** IEEE Transactions on Power Delivery, Vol. 4, No. 2, April 1989, pages 1318-1328.

35.   M. Misakian, R.H McKnight, C. Fenimore. **Calibration of Aspirator-Type Ion Counters and Measurement of Unipolar Charge Densities.** Journal of Applied Physics, 61(4), 15 February 1987, pages 1276 - 1287.

36.   M. Hara, N. Hayashi, K. Shiotsuki, M. Akazaki. **Influence of Wind and Conductor Potential on Distributions of Electric Field and Ion Current Density at Ground Level in DC High Voltage Line to Plane Geometry.** IEEE Transactions on Power Apparatus and Systems, Vol. PAS-101, No. 4, April 1982, pages 803-813.

37.   P.S Maruvada, R.D Dallaire, R. Pedneault. **Development of Field-Mill Instruments for Ground-Level and Above-Ground Electric Field Measurement under HVDC Transmission Lines.** IEEE Transactions on Power Apparatus and Systems, Vol. PAS-102, No. 3, March 1983, pages 738 - 743.

38.   H. Jianfeng, G. Zhicheng, W. Liming. **Study on AC and DC Corona Inception Voltage at Different Air Pressure and Relative Humidity Conditions.** XlVth International Symposium on High Voltage Engineering, Beijing, China, 25-29 August, 2005, H-67, pages 1 - 4.

39.   T. Suda, Y. Hirayama, Y. Sunaga. **Aging Effects of Conductor Surface Conditions on DC Corona Characteristics.** IEEE Transactions on Power Apparatus and Systems, Vol. 3, No. 4, October 1988, pages 1903 - 1912.

40. A.P Fews, RJ Wilding, P.A Keitch, N.K Holden, D.L Henshaw. **Modification of Atmospheric DC Fields by Space Charge from High-Voltage Power Lines.** Atmospheric Research 63, 2002, pages 271-289.

41. T.D Bracken, S. Russell, W.H Bailey. **DC Electric Fields from Corona Generated Space Charge near AC Transmission Lines.** IEEE Transactions on Power Apparatus and Systems, Vol. 20, No. 2, April 2005, pages 1692 - 1699.

42. L. Ziyu, L. Rongsheng, W. Huiming, L. Wenbin. **Space Charges and Initiation of Electrical Trees.** IEEE Transactions on Electrical Insulation, Vol. 24, No. 1, February 1989, pages 83-90.

43. G.C Sibilant, U. Minnaar. **Anomalous Ionic Coupling between the Cahora Bassa HVDC Line and Adjacent Lines.** Research Report. Eskom - Resources and Strategy, RES/RR/04/23110, 21 February 2005.

44. A.A Burger. **Ion-Cloud Coupling between Cahora Bassa HVDC Line and Open Telephone Line at Apollo Converter Station.** Research Report. Eskom - Technology Group, TRR/E/98/EL115, October 1998.

45. G.B Johnson. **Electric Fields and Ion Currents of a + 400 kV HVDC Test Line.** IEEE Transactions on Power Apparatus and Systems, Vol. PAS-102, No. 8, August 1983, pages 2559-2568.

46. **JCI140 Static Monitor, Product Pamphlet.** John Chubb Instruments.

APPENDIX A

HVDC LABORATORY SET UP

THE HVDC TEST SET:

The High Voltage Direct Current laboratory has a test set that is used for carrying out testing in a laboratory environment. It is capable of delivering test voltages up to 500 kV DC for the positive polarity and 540 kV DC for the negative polarity. The specifications for the HVDC test set can be seen below in table A.1. The entire laboratory is fitted with a special shielding (metal grid) to ensure that the laboratory is grounded properly and to eliminate any coupling effects that may affect the readings of measurements taken.

Table A.1: HVDC Test Set Specifications [26]

AC VOLT.UiK	
Rated Voltage	lOOkV(rms)
Rated Output (Continuous)	5 kVA - Continuous 7.5 kVA-Short time
Frequency	50 Hz
Short Circuit impedance Voltage	5% approximately with respect to rated continuous kVA and rated voltage.
IKVOLTAGE	
No Load Rated Output, Positive Polarity	500 kV
Negative Polarity	540 kV
Rated Continuous Current	7.5 mA
Ripple Voltage	< *yje* at rated current and voltage

The HVDC Test Set consists of the following main components,

High voltage test transformer
Silicone rectifier
Smoothing capacitor
Isolating transformer
Control panel

Over and above the main components, the laboratory consists of other components that are required for taking measurements for different tests. There are measuring devices (voltmeters, ammeters, sound level meters), measuring resistors, insulators, a test line, earthing rods and a corona cage.

GENERATION OF HVDC - COCKCROFT WALTON CIRCUIT:

In order to generate direct voltages, a rectifier circuit is required. For voltages up to 50 kV DC, a simple half-wave rectifier circuit is recommended. When higher DC voltages are to be generated, a voltage doubler or cascaded voltage multiplier circuit is used. One of the most popular doubler circuits is known as the Greinacher doubler circuit. In 1932, an improvement to the Greinacher circuit was suggested by Cockcroft and Walton for generating high DC voltages.

The test set acquired by the University of Kwazulu Natal uses a half wave voltage doubler and half wave voltage multiplier Cockcroft Walton circuit, shown in figure A.l.
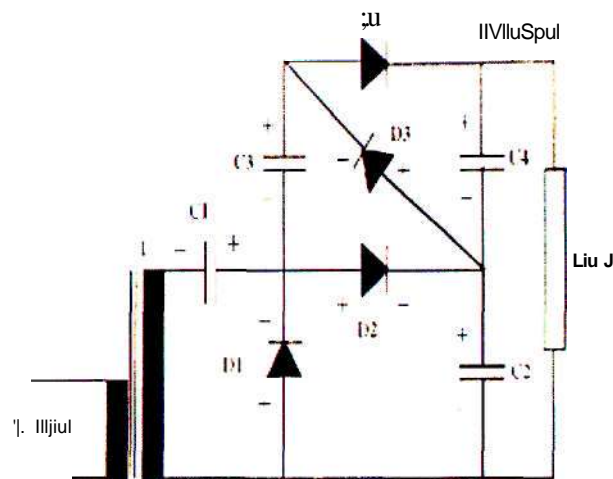
Figure A.l: HVDC Test Set - Cockcroft Walton Circuit [26]

CLEARANCES REQUIRED:

The clearance within the laboratory is another safety factor. For laboratories that are designed to operate up to 1 MV, the following minimum clearances must be maintained:

For AC and DC   50cm for every 1 OOkV

For Impulses   20cm for every 1 OOkV

Fibre glass insulation is utilised within the FTVDC laboratory where the clearances do not comply with the above minimum clearances stipulated. The HVDC test set used in the laboratory is shown in figure A.2.
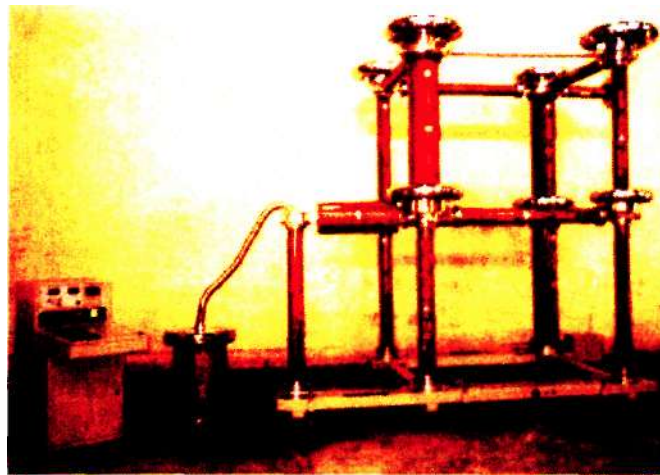
Figure A.2: HVDC Test Set [26]

APPENDIX B

HVDC TEST LINE DESIGN

The HVDC Centre already has a test line that was designed and constructed by a previous student working on his MSc project. The test line design is a scaled model of the Cahora Bassa HVDC line.

OPERATING LINE DESIGN - CAHORA BASSA HVDC SCHEME:

The dimensions of the Cahora Bassa HVDC scheme are known and these dimensions were used to design the scaled laboratory test line. The test line was designed and scaled in such a manner that we obtain the same electric field gradients as the operating transmission line [27].

Pole Conductor - Dimensions

- Conductor type - "Zambeze" (ACSR)
- Sub conductor diameter - $d = 3.18$ cm
- Number of bundle conductors - $n = 4$
- Conductor spacing - $S = 45$ cm

Shield Wire - Dimensions

- Conductor type - "Oden"
- Insulated earth wire - "Oden"
- Diameter - $d_s = 1.76$ cm

Line Configuration

- Shield wire height (from ground), $H_s = 36.7$ m
- Pole conductor height (from ground), $H = 25.8$ m
- Height between conductor and shield wire, $h = 10.9$ m
- Horizontal distance between conductor and shield wire, $s = 3.6$ m
- Tower structure height, 37.2 m
- Sag= 16 m

r
-•I
i

Figure B.l: Cahora Bassa Transmission Line Configuration [27]

LABORATORY TEST LINE DESIGN:

The laboratory test line design is based on the Cahora Bassa Transmission Line. The test line has a monopolar configuration, a 4 conductor bundle and shield wire. In order to carry out tests for different polarities (negative or positive), the polarity has to be changed on the Cockroft-Walton generator.

Based on the size of the HVDC laboratory, a scaling factor of 1/12 was used for the test line model. For a scaling factor of 1/12, the dimensions of the test line was calculated as follows [27]:

Height of pole conductors above ground, H = 2.15 m
Height of shield wire above ground, H_s = 3.06 m
Vertical distance between shield wire and pole conductor, h = 0.91 m
Diameter of pole conductors, d = 3.18 cm
Diameter of shield wire conductor, d_s= 1.76 cm
Spacing between sub-conductors, S = 0.2 m

Figure B.2: HVDC Laboratory Test Line

The configuration for the scaled model is shown in figure B.3.

Shield wire

h - O.'ylrr.

Pole conductors

O   O

1 1

i \

S - C i m

H =- *l.*\5m

Ground
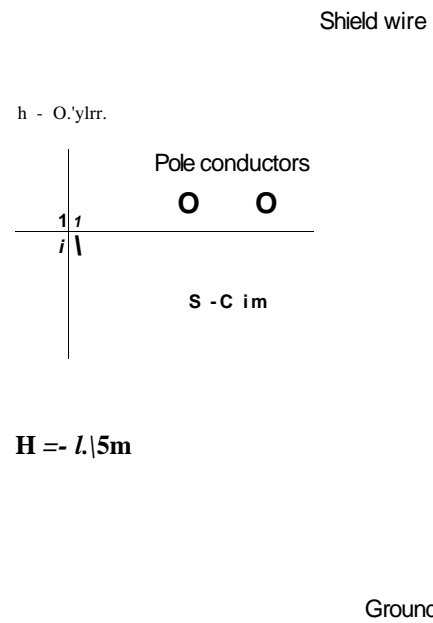
Figure B.3: Scaled Test Line Configuration [27]

Figure B.4: Test Line - Corona Sources Applied
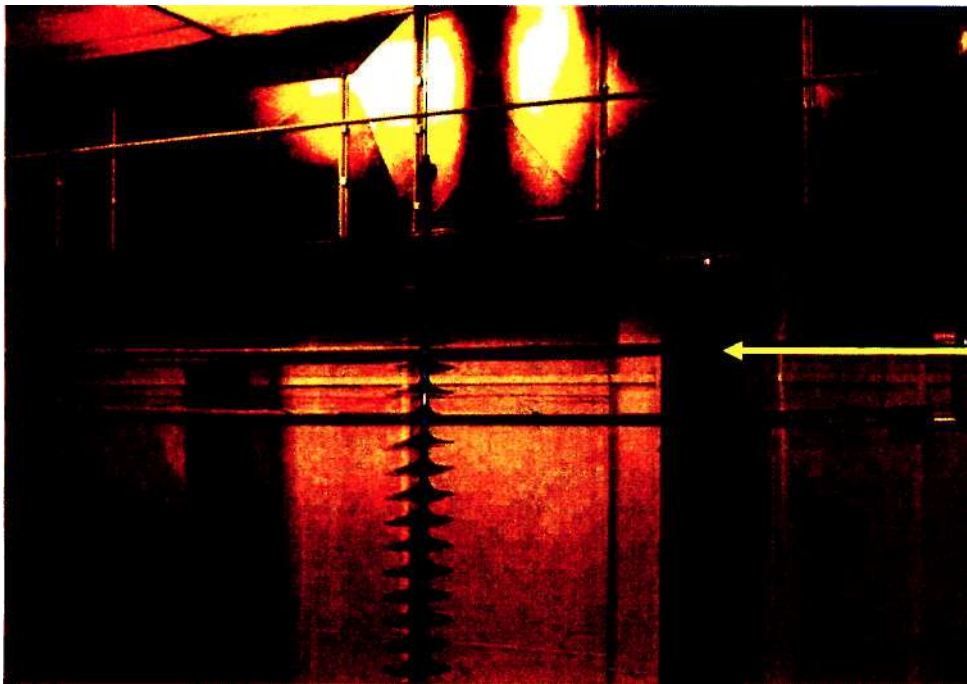
Corona Source
(nail)

Figure B.5: Test Line - Corona Sources Applied

POLE CONDUCTOR MAXIMUM GRADIENT;

The maximum gradients of the pole conductor and shield wire were calculated using the following formulae [27]:

Average **Conductor Gradient:**

$$\frac{2V}{(ndlnT)} \quad kV/cm \qquad\qquad (B.1)$$

$$= 2x533/(4x3.18x/«142.4)$$
$$= 16.9 kV/cm$$

Maximum Conductor Gradient:

$$E_{max} = Eav(\backslash + d(n-1)/D) \quad kV/cm \qquad\qquad (B.2)$$

$$16.9 (1 + 3.18(4-l)/63.64) \quad kV/cm$$
$$19.43 \ kV/cm$$

Shield Wire Gradient:

$$Eav(nd/d_s).(\frac{}{\backslash n(AH_s d_s)}) \quad kV/cm \qquad\qquad (B.3)$$

$$16.9(4x3.18/1.76).(\frac{ln5 - 743}{ln(4x\ 2603x1.76)})$$
$$21.73 \ kV/cm$$

APPENDIX C

CAHORA BASSA - FIELD TESTS

The results of the simulations using the actual operating line conditions (positive pole at +370 kV, 1800 A and negative pole at - 503 kV, 1743 A) are shown in table C.l and C.2.

Table C.l: Positive Pole - E-Field, Current Density & Ion Density

LATERAL DISTANCE (feet)	(meters)	<— DC ELECTRIC FIELD —> ELECTROSTATIC (kV/m)	SATURATED (kV/m)	CURRENT DENSITY (nA/ra2)	ION DENSITY (l/cm3)
-98.4	-30.00	1.56	9.56	2.4	13916.
-88.6	-27.00	1.89	10.83	3.5	17343.
-78.7	-24.00	2.31	12.48	5.1	22150.
-68.9	-21.00	2.88	14.48	7.7	28720.
-59 .1	-18.00	3.65	17.11	12.0	38217.
-49.2	-15.00	4.69	20.37	19.4	51647.
-39.4	-12.00	6.09	24.36	31.6	70599.
-29.5	-9.00	7.90	29.35	52.6	97342.
-19.7	-6.00	9.97	34.53	82.4	129696.
-9.8	-3.00	11.80	38.82	114.2	159903.
.0	.00	12.54	40.92	131.6	174798.
9.8	3.00	11.73	38.63	113.6	159859.
19.7	6.00	9.83	34.25	81.9	129926.
29.5	9.00	7.72	29.00	52.2	97768.
39.4	12.00	5.89	24.18	31.9	71705.
49.2	15.00	4.49	20.14	19.5	52511.
59.1	18.00	3 .46	16.87	12.1	38836.
6 8.9	21.00	2 .72	14.42	7.8	29455.
78.7	24.00	2.17	12.44	5.2	22681.
88.6	27.00	1.76	10.84	3.5	17728.
98.4	30.00	1.45	9.50	2.5	14030.

Table C.2: Negative Pole - E-Field, Current Density & Ion Density

LATERAL DISTANCE (feet)	(meters)	<— DC ELECTRIC FIELD —> ELECTROSTATIC (kV/m)	SATURATED ():V/m)	CURRENT DENSITY (nA/m2)	ION DENSITY (l/cm3)
-98.4	-30.00	-2.12	-13.00	-5.9	-18918.
-88 .6	-27.00	-2.56	-14.72	-8.3	-23577.
-78.7	-24.00	-3.14	-16.96	-12.3	-30112.
-68.9	-21.00	-3.92	-19.69	-18.4	-39044.
-59.1	-18.00	-4.96	-23.26	-29.0	-51954.
-49.2	-15.00	-6 .38	-27.69	-46 .7	-70211.
-39.4	-12.00	-8.28	-33.12	-76.3	-95976.
-29.5	-9.00	-10.73	-39.90	-126.7	-132332.
-19.7	-6.00	-13.56	-46.95	-198.7	-176317.
-9.8	-3.00	-16.04	-52.77	-275.3	-217382.
.0	.00	-17.05	-55.62	-317.2	-237631.
9.8	3 .00	-15.94	-52.52	-273.9	-217321.
19.7	6.00	-13.37	-46.57	-197.4	-176629.
29.5	9.00	-10.49	-39.42	-125.7	-132911.
39.4	12.00	-8.01	-32.87	-76.9	-97480.
49.2	15.00	-6.11	-27.38	-46.9	-71387.
59.1	18.00	-4.71	-22.94	-29.1	-52796.
68.9	21.00	-3.69	-19.60	-18.8	-40042.
78.7	2 4.00	-2.95	-16.92	-12.5	-30833.
88.6	27 .00	-2.39	-14.74	-8.5	-24100.
98.4	30.00	-1.98	-12.92	-5.9	-19074.